SC71066.FR

Physics and Applications of Coherently Coupled Phase Conjugators

Final Report
March 01, 1992 thru December 31 1995
Contract No. F49620-92-C-0023
Project No. 2301/AS

Prepared for:
Air Force Office of Scientific Research
Directorate of Physics and Electronics
110 Duncan Ave. Suite B115
Bolling, AFB, DC 20332-0001
Attn: Dr. Howard Schlossberg

Prepared by:
I. McMichael
Principal Investigator

Rockwell Science Center
1049 Camino Dos Rios
Thousand Oaks, CA 91360
May 1996

Rockwell

Science Center

Copy # 6

REPORT DOCUMENTATION PAGE

Form Approved OMB No. 0704-0188

1. AGENCY USE ONLY *(Leave Blank)*	2. REPORT DATE	3. REPORT TYPE AND DATES COVERED
	May 1996	Final Report 03/01/92 through 12/31/95

4. TITLE AND SUBTITLE

Physics and Applications of Coherently Coupled Phase Conjugators

5. FUNDING NUMBERS

61102F
2301/CS

4. AUTHOR(S)

I. McMichael

AFOSR-TR-96

0286

7. PERFORMING ORGANIZATION NAME(S) AND ADDRESS(ES)

Rockwell Science Center
P.O. Box 1085
Thousand Oaks, CA 91358

9. SPONSORING / MONITORING AGENCY NAME(S) AND ADDRESS(ES)

AFOSR/NE
Directorate of Physics & Electronics
Building 410
Bolling AFB, DC 20332-6448

9. SPONSORING / MONITORING AGENCY REPORT NUMBER

F49620-92-C-0023

11. SUPPLEMENTARY NOTES

19960618 028

12a. DISTRIBUTING/AVAILABILITY STATEMENT

Approved for public release; distribution is unlimited.

13. ABSTRACT *(Maximum 200 Words)*

This contract focused on the physics and applications of coherently coupled phase conjugators. Of particular interest is the physics of mutually pumped phase conjugation (MPPC) and its application to wavefront matched heterodyne communications. This application requires a nonlinear optical Kerr media that is capable of high gain. Under this contract we demonstrated a beam coupling gain of 22 times by the process of nondegenerate two-wave mixing in a crystal of chromium doped yttrium orthoaluminate. This is currently the largest continuous wave gain obtained in a solid state non-photorefractive material, and it is within a factor of two of that required for MPPC. We used this gain to demonstrate "self-oscillation" in which an oscillation spontaneously builds up between the opposing surfaces of a crystal, when a single beam is incident. Calculations show that significantly higher gain should be possible. This result should be of general interest to the nonlinear optics community since it will allow researchers to study continuous wave oscillators and self-pumped conjugators, with properties different from those using photorefractives. In addition, a theoretical study of Brillouin induced mutually pumped phase conjugation in the reflection geometry was completed, and we present the first solutions to the transcendental equation that illustrate the potential of large dynamic range that is required in applications such as wavefront matched heterodyne communications.

14. SUBJECT TERMS

phase conjugation, Kerr, two-wave mixing, beam coupling

15. NUMBER OF PAGES
17

16. PRICE CODE

17. SECURITY CLASSIFICATION OF REPORT	18. SECURITY CLASSIFICATION OF THIS PAGE	19. SECURITY CLASSIFICATION OF ABSTRACT	20. LIMITATION OF ABSTRACT
UNCLASSIFIED	UNCLASSIFIED	UNCLASSIFIED	UL

DISCLAIMER NOTICE

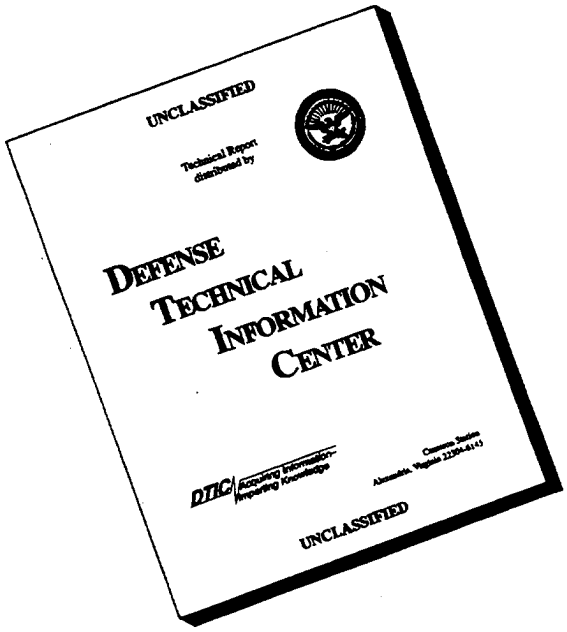

THIS DOCUMENT IS BEST QUALITY AVAILABLE. THE COPY FURNISHED TO DTIC CONTAINED A SIGNIFICANT NUMBER OF PAGES WHICH DO NOT REPRODUCE LEGIBLY.

Table of Contents

List of Figures

1.0 SUMMARY

1.1 Contract Description

This contract focused on the physics and applications of coherently coupled phase conjugators. Of particular interest is the physics of mutually pumped phase conjugation (MPPC) and its application to wavefront matched heterodyne communications. These studies involve theoretical investigations of Brillouin induced MPPC in both transmission and reflection geometries, and experimental investigations of high gain nondegenerate two-wave mixing in Cr:$YAlO_3$.

1.2 Scientific Problem

One limitation for MPPC is the limited dynamic range over which photorefractive materials will operate in MPPC mode. This is a problem, for example, in a wavefront matched heterodyne receiver application, where the power in an aberated incoming signal wave may be very weak as compared with the power required for the local oscillator plane wave. To alleviate this problem we studied alternatives such as using a Kerr media as a replacement for photorefractive media in MPPC.

It would be desirable to do MPPC experiments, and many other nonlinear optical experiments, using a convenient solid state Kerr media with low power cw lasers. CW lasers are often easier to work with than high power pulse lasers, and they often provide better quantitative data due to the lack of any need to characterize pulses and their pulse-to-pulse fluctuations. When this is possible, it often brings about rapid progress in experimental research, as was the case with photorefractives. Unfortunately, to our knowledge, no one has demonstrated the required gain of $e^4 \sim 55$ in a solid state bulk (as opposed to guided wave) Kerr material using a cw source. In this program we demonstrated the largest cw nonlinear optical gain in a bulk solid-state nonphotorefractive material. Although the net gain was less than that required for MPPC, theoretical calculations indicate that larger gain is possible.

The same optical nonlinearity that gives rise to nonlinear optical gain in Cr:$YAlO_3$ also gives rise to self-focusing. To obtain an accurate description of nonlinear optical gain in Cr:$YAlO_3$,

it is necessary to include the effects of self-focusing in the theoretical model. One theoretical effort was focused on an analysis of the effects of self-focusing on nonlinear optical gain in Cr:$YAlO_3$.

1.3 Progress Summary

There were many areas of significant progress achieved under this contract in the development of a solid state Kerr media for MPPC and in the theory of MPPC. These include:

- Completion of a study of metal-ion-doped insulators as nonlinear optical materials, and identification of the potential of Cr:$YAlO_3$ to achieve high nonlinear optical gain using cw lasers.

- Conclusively demonstrated the potential for large dynamic range in Brillouin induced mutually pumped phase conjugation in reflection geometry by obtaining the first solutions to the transcendental equation giving the phase-conjugate reflectivity.

- First accurate determination of the nonlinear refractive index and saturation intensity of Cr:$YAlO_3$.

- Procurement, processing and fabrication of several cubes from a highly doped boule of Cr:$YAlO_3$ to be used in experiments for obtaining large nonlinear optical gain.

- A gain of 22 times was obtained by nondegenerate two-wave mixing in Cr:$YAlO_3$. This is currently the largest cw two-wave mixing gain obtained in a bulk solid state nonphotorefractive material, and within a factor of two of that required for MPPC.

- Observation of a nonlinear optical beam break-up phenomena that is the result of the interaction between spatial inhomogeneities and the optical nonlinearity in a crystal of Cr:$YAlO_3$.

- Theoretical prediction that significantly higher gain, in excess of 200, is possible in a homogeneous crystal of Cr:$YAlO_3$.

- Conclusive demonstration of the near equal strengths of transmission and reflection gratings in metal-ion-doped insulators like Cr:$YAlO_3$, for which there currently exists a disagreement in the literature. This indicates that there is very little spatial migration of the excitation on time scales corresponding to the excited state lifetime of 33 ms.

- Analysis of transverse effects on nonlinear optical gain in Kerr media indicating that a significant enhancement in nondegenerate two-wave mixing gain is possible due to self-focusing phenomena.

Details of this progress are presented in Section 2.0, and in the publications listed below that are included in this report as Appendices.

1.4 Publications

1. I. McMichael, T. Chang, M. Noginov, M. Curley, P. Venkateswarlu and H. Tuller, "Application of Laser and Related Materials to Demonstrate Large Nonlinear Optical Effects and Diffraction Efficiency," to be published by the Optical Society of America in the Trends in Optics and Photonics Series volume on Advanced Solid State Lasers, 1996.

2. I. McMichael and T. Chang, "Self-Oscillation and Self-Pumped Phase Conjugation in Cr:YALO3," paper CFF7 to be presented at the Conference on Lasers and Electro-Optics, Anaheim, CA, June 2-7, 1996.

3. I. McMichael, T. Chang, M. Noginov and H. Tuller, "Application of Laser and Related Materials to Demonstrate Large Nonlinear Optical Effects and Diffraction Efficiency," presented at the conference on Advanced Solid State Lasers, San Francisco, CA, January 31-February 3, 1996.

4. I. McMichael, M. Ewbank and F. Vachss, "Efficiency of Phase Conjugation for Highly Scattered Light," Optics Comm. 119, **13** (1995).

5. I. McMichael, T. Chang and H. Tuller, "Optical Nonlinearity of Cr:$YAlO_3$ and Other Metal-Ion Doped Insulators," presented at the Annual Meeting of the Optical Society of America, Portland, OR, September 10-15, 1995.

6. I. McMichael, R. Saxena, T. Chang, Q. Shu, S. Rand, J. Chen and H. Tuller, "High Gain Nondegenerate Two-Wave Mixing in Cr:$YAlO_3$," Opt. Lett. **19**, 1511 (1994).

7. I. McMichael, M. Ewbank and F. Vachss, "Efficiency of Phase Conjugation for Highly Scattered Light," presented at the Annual Meeting of the Optical Society of America, Dallas, TX, October 2 - 7, 1994.

8. R. Saxena, T. Chang and I. McMichael, "Effects of Self-Focusing on Nondegenerate Two-Wave Mixing in Kerr Media," presented at the Annual Meeting of the Optical Society of America, Dallas, TX (1994).

9. R. Saxena and I. McMichael, "Brillouin Induced Mutually Pumped Phase Conjugation in Reflection Geometry," presented at the Conference on Nonlinear Optics, Waikoloa, Hawaii (1994).

10. I. McMichael, R. Saxena, T. Chang, Q. Shu, S. Rand, J. Chen and H. Tuller, "High Gain Nondegenerate Two-Wave Mixing in Cr:$YAlO_3$," presented at the Conference on Nonlinear Optics, Waikoloa, Hawaii (1994).

11. I. McMichael, R. Saxena, T. Chang, R. Neurgoankar, and S. Rand, High Gain Nondegenerate Two-Wave Mixing in Cr:$YAlO_3$," in *Conference on Lasers and Electro-Optics,* Vol. 11 of 1993 OSA Technical Digest Series (Optical Society of America, Washington, D.C., 1993), paper CThS34, pp. 514-515.

12. R. Saxena and I. McMichael, "Brillouin Induced Mutually Pumped Phase Conjugation in Reflection Geometry," submitted to the Journal of the Optical Society of America B.

13. R. Saxena and P. Yeh, "Nonlinear Optical Phase Conjugation by Four-Wave Mixing in Kerr Media," in *Phase Conjugation*, M. Gower and D. Proch, eds., (Springer-Verlag, Berlin, 1994), Chap. 2.

14. R. Saxena, "Diffraction Properties of Photorefractive Gratings," in *Photorefractive Materials, Effects and Applications; Critical Reviews*, P. Yeh and C. Gu, eds., (Society of Photo-Optical Instrumentation Engineers, Bellingham, Washington, 1993).

2.0 PROGRESS

2.1 Identification of the Potential of Cr:$YALO_3$

As noted in the summary, a convenient solid state Kerr media with large cw nonlinear optical gain is required in experiments on MPPC for applications such as wavefront matched heterodyne communications. We had previously demonstrated that nonlinear optical gain could be achieved in ruby by the process of nondegenerate two-wave mixing of two beams from a cw argon laser.[1] However, calculations indicated that it would be difficult to achieve the gain required for MPPC using ruby. We therefore initiated a search of the literature to see if some other metal-ion-doped insulator might work, and found that, of the materials previously investigated, Cr:$YAlO_3$ was the most promising for achieving the high gain required in MPPC.[2]

2.2 First Demonstration of High Nonlinear Optical Gain in Cr:$YAlO_3$

After identifying Cr:$YAlO_3$ as a promising candidate material for future investigations of MPPC in Kerr media, we then focused our attention on demonstrating the potential for obtaining high nonlinear optical gain. Using a borrowed sample of Cr:$YAlO_3$, we demonstrated a beam coupling gain of 6 times.[3] At that time, this was the largest cw nonlinear optical gain obtained in a bulk solid state nonphotorefractive material. Details of this experiment are presented in the paper entitled "High Gain Nondegenerate Two-Wave Mixing in Cr:$YAlO_3$," that was presented at the Conference on Lasers and Electro-Optics and is included in the Appendix. The important data are shown in Fig. 1, where gain for a weak probe beam is plotted as a function of the pump intensity. A fit to this data yields the nonlinear refractive index $n_2 = 1.4 \times 10^{-7}$ cm^2/W and the saturation intensity $I_S = 1.5$ kW/cm^2. For comparison, we find that $n_2/\alpha = 3 \times 10^{-7}$ cm^2/W for Cr:$YAlO_3$, is more than one order of magnitude larger than the value for ruby, $n_2/\alpha = 1.7 \times 10^{-8}$ cm^2/W. It is also satisfying that the value of the saturation intensity is consistent with calculations using the expression $I_S = h\nu/\sigma\tau$ together with values of the cross section σ and the decay time τ reported in the literature.

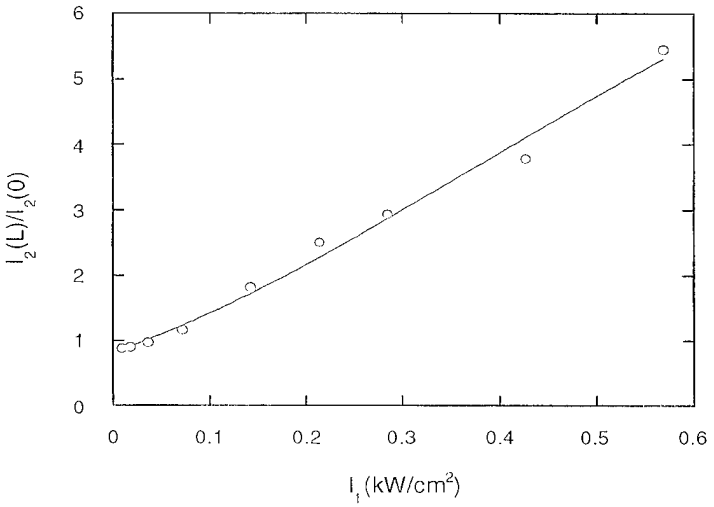

Fig. 1 Nonlinear optical gain in Cr:$YAlO_3$ as a function of the pump intensity.

2.3 Procurement, Processing and Fabrication of Highly Doped Cr:$YAlO_3$

We recognized that it should be possible to obtain higher gain than reported above by using higher Cr doping and a longer interaction length. We procured a crystal boule with which we later obtained significantly higher gain, and allowed us to continue our claim of demonstrating the largest cw nonlinear optical coupling in a non-photorefractive media. A survey of several potential vendors and several individuals indicates that this crystal, sitting on a shelf to be sold as "gem" material, may have been the only crystal available in the US at that time.

As grown Cr:$YAlO_3$ has a color center absorption that competes with the absorption responsible for the optical nonlinearity. A collaboration was established with Harry Tuller at MIT who removed the color centers by heating the as grown material in a forming gas atmosphere.[4] Figure 2 shows absorption spectra for the 12 mm thick end of the boule of Cr:$YAlO_3$, as grown (dotted line), after a first anneal (dashed line) in 95% N_2/5% H_2 at 1050° C for 8 hours with a flow rate of 250 cc/min and a ramp rate of 1 °C/min, and after a second anneal (solid line) at 1300° C for 24 hours with the same atmosphere, flow and ramp rates as used in the first anneal. After the second anneal, the boule was fabricated into several crystallographic cut cubes, one of which was used in the following experiments. Microprobe measurements indicated that the Cr concentration was 0.12 weight percent.

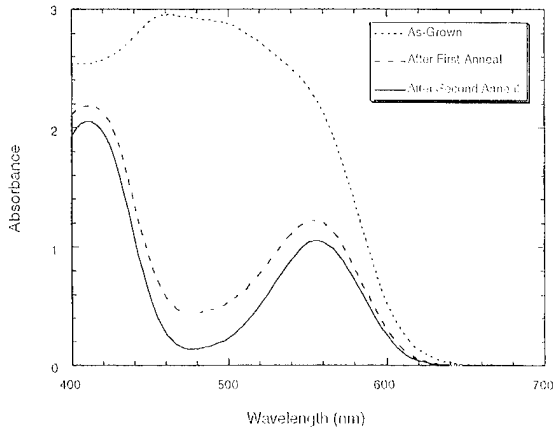

Fig. 2 Cr:$YAlO_3$ absorption spectra showing the removal of color centers by processing.

Following the heat treatment a strategy was developed to obtain one large cube and several smaller cubes from the boule, specifications were established, and the boule was sent out for x-ray orientation and fabrication. Estimates of the potential gain in the larger cube are of the order of 400 times, when one ignores transverse effects such as self-focusing. The total cost of materials, processing and fabrication of the cubes will be less than the cost of a single $BaTiO_3$ crystal.

2.4 Demonstration of High Nonlinear Optical Gain in Highly Doped Cr:$YAlO_3$

Based on the measured value of n_2/α, calculations indicated that one could obtain significantly higher gain by increasing the doping and interaction length. A crystal with higher doping was procured, processed and fabricated, and then used in experiments to demonstrate higher gain. Details of these experiment are presented in the papers entitled, "High Gain Nondegenerate Two-Wave Mixing in Cr:$YAlO_3$," that were published in Optics Letters[5] and presented at the Conference on Nonlinear Optics,[6] and are included in the Appendix. The important data are shown in Fig. 3, where gain for a weak probe beam is plotted as a function of the pump intensity. Figure 3 (a) shows a plot of the gain as a function of the intensity of the pump for the range from 0 to 80 W/cm^2. The circles are the experimental measurements, and the line is a fit of the theoretical form,

$$\frac{I_2(L)}{I_2(0)} = e^{-\alpha L} \exp\left\{\left(\frac{1-e^{-\alpha L}}{\alpha L}\right)\left[\frac{2\pi n_2 I_1(0) L/\lambda}{\left(1+I_1(0)/I_S\right)^2}\right]\right\} \quad (1)$$

with $\alpha L = 0.69$, L = 9.1 mm, $\lambda = 514.5$ nm and $I_S = h\nu/\sigma\tau = 1.27$ kW/cm^2, where h is Planck's constant, ν is the optical frequency, σ is the absorption cross-section and τ is the metastable state lifetime. Using n_2 as the only adjustable parameter, the fit yields $n_2 = 3.2 \times 10^{-7}$ cm^2/W. For comparison, we find that $n_2/\alpha = 4.2 \times 10^{-7}$ cm^2/W for Cr:YAlO$_3$, is more than one order of magnitude larger than the value for ruby, $n_2/\alpha = 1.7 \times 10^{-8}$ cm^2/W.

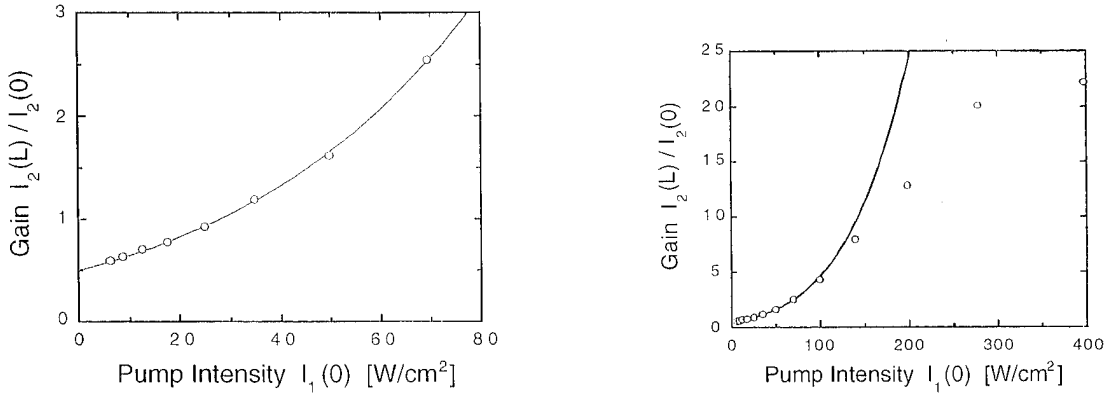

Fig. 3 Nonlinear optical gain in Cr:YAlO$_3$ as a function of the pump intensity. (a) from 0 to 70 W/cm^2, and (b) from 0 to 400 W/cm^2.

Figure 3 (b) shows the gain for the range from 0 to 400 W/cm^2. Using the previously stated parameters and n_2 as determined from the fit for the lower intensity range of Fig. 3(a), the line in Fig. 3(b) represents projections based on the theoretical form expressed by Eq. (1). A gain of 22 times was obtained at approximately 400 W/cm^2, but the measured gain does not increase with intensity as much as theory predicts. (Theory predicts a gain of 200 at 400 W/cm^2.) As described in the following section, at first we believed this was due to "beam break-up" resulting from spatial nonuniformities of the nonlinear refractive index change in the interaction region. However, as we discuss in later in Section 2.6, measurements of the luminescence as a function of pumping intensity indicate that the reduction in beam coupling gain is due mostly to a reduction of the metastable state population, which is greater than that predicted by depletion of the ground state, as expressed in Eq. (1), when using the usual expression for the saturation intensity, $I_S = h\nu/\sigma\tau$.

2.5 Nonlinear Optical Beam Breakup

In our experiments on high gain nondegenerate two-wave mixing in Cr:$YAlO_3$, we observed a nonlinear optical beam break-up phenomena that is the result of the interaction between spatial inhomogeneities and the optical nonlinearity in the crystal. This phenomena is illustrated in Fig. 4. The figure shows a transmitted pump beam, (a) at low intensity and normal exposure, indicating the transmitted beam size, (b) at low intensity and long exposure, showing an "X" shaped pattern of linear scattering that is believed to be the result of scattering by crystal striae and (c) at high intensity and exposure equivalent to case (b), showing the nonlinear scattering phenomena due to nonuniformities in the nonlinear refractive index change.

Spatial nonuniformities of the nonlinear refractive index change in the interaction region can be the result of shadows or distortions from surface or bulk defects, or from spatial variations in the Cr-ion concentration. Photographs of the crystal illuminated by a low intensity collimated beam show radial and concentric patterns are thought to be Cr striae. Images of a low intensity pump beam inside the crystal also indicate that the striae have a significant effect on the beam profile. Beam break-up can result from both variations in Cr concentration, yielding a variation in n_2, and also from intensity variations, yielding variations in the induced nonlinear index change.

(a) (b) (c)

Fig. 4 Photographs of a beam transmitted through Cr:$YAlO_3$ illustrating the nonlinear optical beam breakup phenomena, (a) Gaussian beam size, (b) "X" shaped pattern resulting from linear scattering, and (c) nonlinear scattering.

Qualitative behavior indicated that the scattering at high intensity was nonlinear, but to confirm this we measured the intensity of a small region of the scattering as a function of the pump intensity. An aperture was closed down to a diameter such that, at low intensity, it would pass one half of the pump that transmitted through the crystal, and then it was placed in the "speckle" of the scatter indicated by the arrow in Fig. 2 (c). Figure 5 shows the scattered power divided by the pump power as a function of the pump power. The circles are the data, and the line is a quadratic fit, indicating that the nonlinear portion of the scatter has a cubic dependence on the pump intensity.

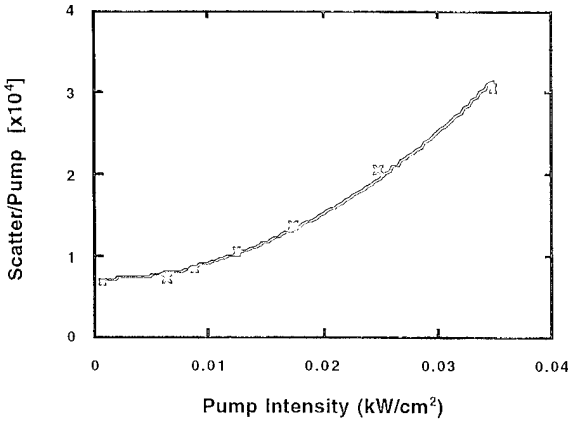

Fig. 5 Measurements showing the nonlinear scattering in Cr:$YAlO_3$.

We made the following observations concerning the scattering: first, the strength of the nonlinear scattering depended on feedback into the crystal, and second, a threshold existed above which the speckle pattern of the scattering was dynamic. An experiment looking at the interference between a portion of the transmitted pump and a "speckle" did not detect any frequency shift. This indicated that the dynamic scattering at high intensities was not due to beating between frequency-shifted stimulated scattering resulting from NDTWM gain, and some linear scattering from crystal inhomogeneities. When the crystal was oriented to retroreflect the pump, or when an external mirror was used, the strength of the nonlinear scattering increased and the threshold of dynamic scattering decreased. To obtain the highest gains in the NDTWM measurements, we rotated the crystal away from normal to reduce the nonlinear scattering. An angle of incidence for the pump of 0.03 radians yielded the largest gains. Further reductions in the feedback resulting from the rear

surface reflection might improve the gain. This could be achieved by an antireflection coating or by index matching, but increasing the angle further may not help if it reduces phase matching.

2.6 Luminescence Measurements

Figure 6 shows measurements of the luminescence intensity from the highly doped crystal of Cr:$YAlO_3$ as a function of the pump beam intensity. The crosses are the measurements, and the solid line is a fit of

$$P_L \approx \ln\left(1 + 2\frac{I_1}{I_S}\right). \tag{2}$$

This functional form describes the saturation of the luminescence due to depletion of the ground state for pumping by a beam with a Gaussian spatial profile. The fit gives I_S = 870 W/cm^2, which is less than the value of 1,270 W/cm^2 calculated using $I_S = h\nu/\sigma\tau$. The nonlinearity of the luminescence vs. pumping can be due to a number of factors including not only depopulation of the ground state, but also up-conversion, excited state absorption (ESA), and possibly other effects. However, for the purpose of subsequent calculations these effects are conveniently expressed in terms of an effective saturation intensity that results from the fit of the above equation. The subsequent calculations using this effective saturation intensity should be correct to first order.

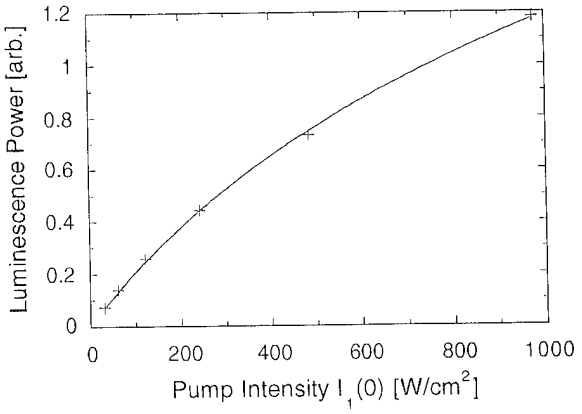

Fig. 6 Luminescence vs. pump intensity in the highly doped crystal of Cr:$YAlO_3$.

Using the value for I_S from the fit in Fig. 6, we can refit the beam coupling gain as shown in Fig. 3. The line is a fit to the range from 0 to 80 W/cm^2 that gives $n_2/\alpha = 4.0 \times 10^{-7}$ cm^3/W. The new fit is much better than the previous one shown in Fig. 3. Most of the remaining discrepancy at high pump intensity can be explained by the nonexponential decay of the luminescence that takes place at high intensity (see section on spectroscopy and kinetics). The fit in Fig. 3 assumed that the pump and probe beams were plane waves of infinite extent. The fit in Fig. 5 includes the effects of a Gaussian beam profile. Although the effect is relatively small, it does yield a slightly better fit to the data.

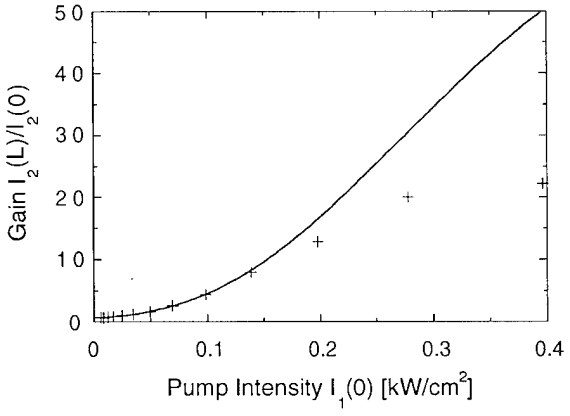

Fig. 7 New fit to the beam coupling measurements of Fig. 3, using I_S as determined from a fit to Fig. 6.

2.7 A New Sample of Cr:YAlO$_3$ Exhibits Different Saturation

We had a new crystal of Cr:YAlO$_3$ grown by Preciosa Crytur, Ltd., which we refer to as sample 2 (we refer to the previous crystal as sample 1) Since the Cr concentration in this crystal (0.028 wt.%) was less than we specified (0.1 wt.%), it did not exhibit as high a gain as the previous crystal (0.12 wt.%), but it also did not exhibit the premature saturation behavior. Figure 8 shows measurements of the luminescence vs. pump intensity for sample 2. The fit gives I_S = 1640 W/cm^2, which is greater than 870 W/cm^2 obtained for sample 1. Thus, sample 2 does not show premature saturation, and in fact the saturation appears to be less than that predicted by $I_S = h\nu/\sigma\tau$. One possible explanation for the measured value being greater than the predicted

value is that the cross section may contain terms due to residual color center absorption that do not contribute to the metastable state population.

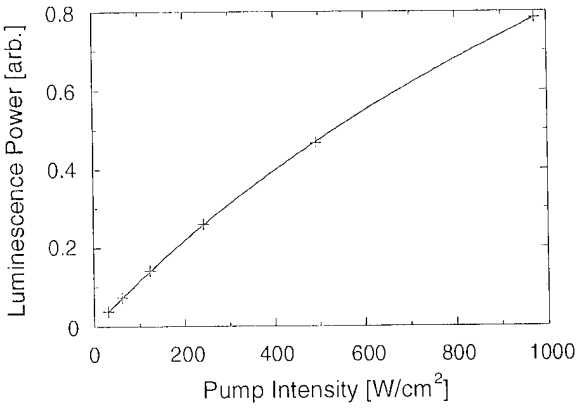

Fig. 8 Luminescence vs. pump intensity in sample 2.

Figure 9 shows measurements of the beam coupling gain in sample 2. The dashed line is a fit using the value of n_2/α from sample 1, and I_S=1,270 W/cm^2. It fits well at low intensity, but it greatly underestimates the gain obtained at high intensity. The solid line is a fit that gives n_2/α = 4.1 x 10^{-7} cm^3/W and I_S = 1,630 W/cm^2. These values are in excellent agreement with the value of n_2/α from sample 1, and the value of I_S from the fit of the luminescence for sample 2.

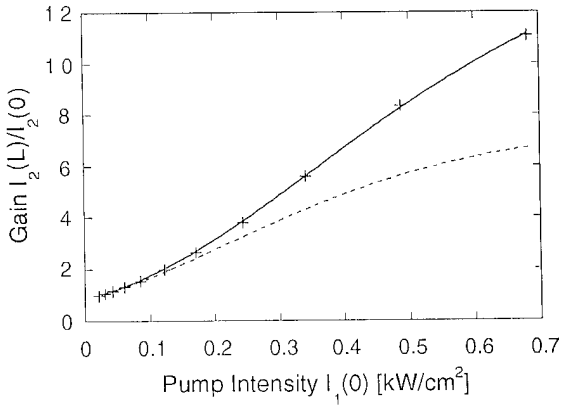

Fig. 9 Gain vs. pump intensity in the new sample of Cr:$YAlO_3$.

To conclude this section, by fitting the luminescence vs. pump intensity, we obtain an effective saturation intensity that lumps together the effects of ground state depletion, up-conversion, ESA, etc. Using this effective saturation intensity, we obtain a better fit to the beam coupling gain than is possible using the expression $I_S = h\nu/\sigma\tau$. Thus, the processes that give rise to saturation of the luminescence and the metastable state population, rather than the beam breakup that we had previously proposed, are the major factors responsible for the premature saturation of the beam coupling gain in sample 1.

2.8 Self-Oscillation in Cr:$YAlO_3$

At normal incidence, the reflectivity of Cr:$YAlO_3$ is 11%, and the absorption loss in sample 2 is 17%. Thus, the round-trip gain ($12^2 = 144$) is sufficient to overcome the losses ($(0.11 \times 0.83)^2 = 1/120$) of a resonator formed by the opposing surfaces of the crystal. (We previously demonstrated that the gain for a reflection grating is comparable to that for a transmission grating.) With the probe off and the crystal normal oriented at a small angle with respect to the incident pump beam, an oscillation builds up between the opposing surfaces of the crystal. Figure 10 shows far field patterns of the oscillating mode. As shown in the figure, it is possible to change the oscillating mode by translating the crystal perpendicular to the pumping beam. Using a microscope, we observe a moving fringe pattern in the fluorescence from the interaction region of the crystal that is formed by the interference between the beam incident on the crystal and the frequency shifted self-oscillation. By beating the oscillation with a portion of the incident beam, we measure a frequency shift of 6 Hz. This is consistent both with our measurements of the frequency shift at which the nondegenerate two-wave mixing gain was maximum, and with the theoretical expression, $1/2\pi\tau$, where τ is the response time of the nonlinearity (the lifetime of the metastable state, 33 ms).

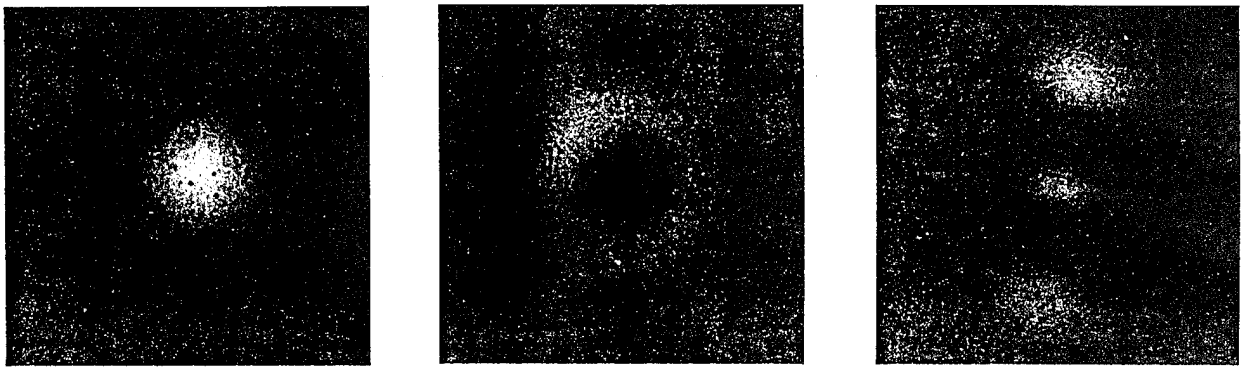

Fig. 10 Far field patterns of the oscillating mode from a self-pumped linear oscillator that is formed in a crystal of Cr:$YAlO_3$.

The bidirectional oscillation acts as pumping beams and the beam incident on the crystal acts as a probe beam in a four-wave mixing process to generate what we believe is the self-pumped phase-conjugate of the beam incident on the crystal. Figure 11 shows the resulting phase-conjugate return. We verified that the return was along a direction consistent with a retroreflection of the incident beam and that it built up with the oscillation. This is consistent with the interpretation of a phase-conjugate return. However, we have not yet verified the phase-conjugate nature of the wavefront by, for example, demonstrating distortion correction. Note that the return is elongated in the direction perpendicular to the plane of incidence defined by the pump and probe beams. A similar effect was previously observed in photorefractive ring conjugators.

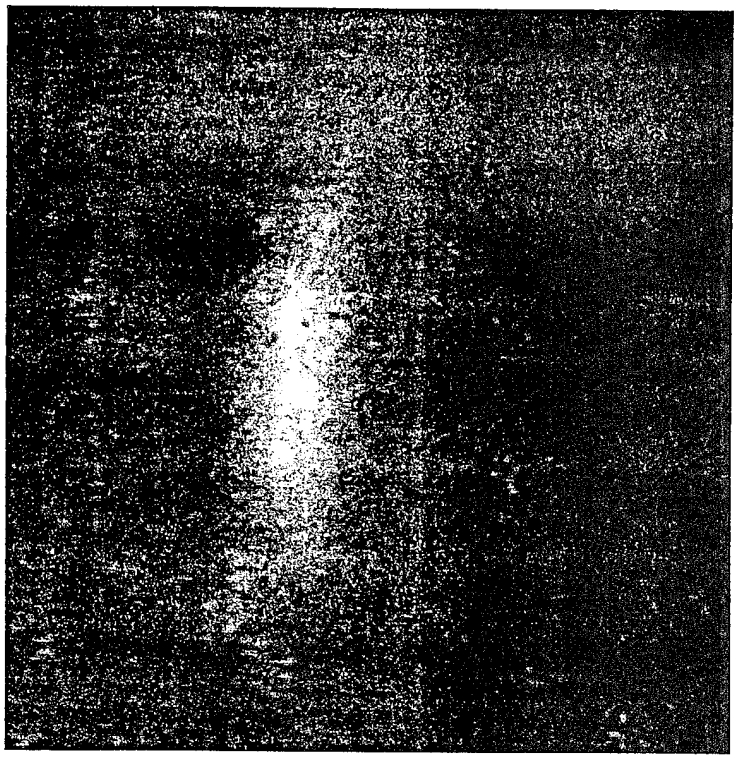

Fig. 11 Phase-conjugate return from the self-pumped linear oscillator that is formed in a crystal of Cr:$YAlO_3$.

3.0 References

1. I. McMichael, P. Yeh, and P. Beckwith, Opt. Lett. **13**, 500 (1988).

2. D. Steel, S. Rand, and J. Liu, *J. Opt. Soc. Am.* **B 4**, 1794 (1987).

3. I. McMichael, R. Saxena, T. Chang, R. Neurgoankar, and S. Rand, in *Conference on Lasers and Electro-Optics, 1993* (Optical Society of America, Washington, D.C., 1993), paper CThS34, pp. 514-515.

4. M. J. Weber and T. E. Varitimos, *J. Appl. Phys.* **45**, 810 (1974).

5. I. McMichael, R. Saxena, T. Chang, Q. Shu, S. Rand, J. Chen and H. Tuller, "High Gain Nondegenerate Two-Wave Mixing in Cr:$YAlO_3$," Opt. Lett. **19**, 1511 (1994).

6. I. McMichael, R. Saxena, T. Chang, Q. Shu, S. Rand, J. Chen and H. Tuller, "High Gain Nondegenerate Two-Wave Mixing in Cr:$YAlO_3$," paper WA5, presented at the Conference on Nonlinear Optics, Waikoloa, Hawaii, July 25 - 29, 1994.

4.0 APPENDICES

A.1

Application of Laser and Related Materials to Demonstrate Large Nonlinear Optical Effects and Diffraction Efficiency

Application of Laser and Related Materials to Demonstrate Large Nonlinear Optical Effects and Diffraction Efficiency

Ian McMichael and Tallis Y. Chang
Science Center, Rockwell International Corporation, 1049 Camino Dos Rios, Thousand Oaks, CA 91360

Mikhail A. Noginov, M. Curley and P. Venkateswarlu
Center for Nonlinear Optics and Materials, Department of Physics, Alabama A&M University, Normal, AL 35762

Harry Tuller
Materials Sci. & Eng. Dept, Massachusetts Institute of Technology, 77 Massachusetts Ave., Cambridge, MA 02139

Abstract

Long metastable lifetimes in laser and related materials combined with a large index change makes possible large nonlinear optical effects using cw lasers. We describe experiments demonstrating such effects using the solid state laser material Cr:$YAlO_3$, and we show how studies of the spectroscopy and kinetics can be used to understand the results. Since the same optical nonlinearity will affect the propagation of beams, it should be considered in the design of lasers.

Keywords

nonlinear optics, nonlinear optical materials, laser materials, rare earth and transition metal solid state lasers

Introduction

Laser and related materials can be used to demonstrate large nonlinear optical effects using cw lasers. For example, using Cr:$YAlO_3$ we have demonstrated an optical gain of 22 for a weak probe beam by using a moving grating technique [1]. Furthermore, we have used this gain to demonstrate "self-oscillation" in which an oscillation spontaneously builds up between the opposing surfaces of a crystal, when a single beam is incident [2]. Since these materials are solid state, they are much easier to use than the metal-vapors that also have large optical nonlinearities. Photorefractives are solid state materials that can be used to demonstrate large nonlinear optical effects using cw lasers, but their nonlinear optical response is typically nonlocal and not proportional to intensity. Thus, laser and related materials may play an important role in nonlinear optics by providing convenient solid state materials, with a local nonlinear optical response proportional to intensity, that will allow researchers to demonstrate large nonlinear optical effects using cw lasers. Furthermore, since the same optical nonlinearity will affect the propagation of beams, it should be considered in the design of lasers.

In this paper we first present results of a simple model of the optical nonlinearity in laser materials. These results can be used to find rules of thumb for developing materials with large refractive index changes. As an example of such a material, the second section describes our experiments demonstrating large nonlinear optical gain using chromium-doped yttrium aluminate (Cr:$YAlO_3$). We study two crystals from different growers that we refer to as sample 1 and sample 2, with Cr concentrations of 0.12 and 0.028 wt.% respectively. From measurements of the luminescence vs. pumping intensity, we obtain an effective saturation intensity that lumps together the effects of various mechanisms causing saturation of the metastable state population. Using this effective saturation intensity, we are able to account for most of the premature saturation of the beam coupling gain that is observed in sample 1. The final section of our paper describes studies of the spectroscopy and kinetics that yield clues as to the mechanisms behind the effective saturation intensity. We hope that this work will stimulate others to help us find better materials and greater understanding.

Results of a Simple Model of the Optical Nonlinearity of Laser Materials

The optical nonlinearity in laser materials results from the light induced population of a metastable state and the accompanying change of the refractive index. Long

metastable state lifetimes make it possible to achieve a large population of the metastable state, and thus a large change in refractive index, using relatively low power cw lasers. At least as long ago as 1977, the dominant contribution to the light induced change of the refractive index in ruby was explained [3] by considering just the strong charge-transfer (CT) transitions [4-6]. In ruby, the CT transitions are allowed transitions in which an electron is transferred from a nonbonding orbital, localized predominantly on the O^- ligands, to an antibonding orbital on the metal ion, and it results in a very strong absorption in the UV at approximately 180 nm. This suggestion continues to be used in the literature to explain the nonlinear refractive index of laser materials. If we follow this suggestion, then we can show that the maximum index change Δn_{max} is given by,

$$\Delta n_{\max} = n_2 I_s = \frac{\left(n_0^2+2\right)^2}{18 n_0} N \frac{e^2}{\varepsilon_0 m}\left(\frac{f_1}{\omega_1^2-\omega^2} - \frac{f_0}{\omega_0^2-\omega^2}\right) \quad (1)$$

where n_2 is the nonlinear refractive index, $I_S = h\nu/\sigma\tau$ is the saturation intensity, h is Planck's constant, ν is the frequency of the light interacting with the material, σ is the absorption cross-section, τ is the metastable state lifetime, n_0 is the linear refractive index, N is the number density of the active species (i.e., Cr for the case of ruby), e is the elementary charge, ε_0 is the permit-tivity of vacuum, m is the electron mass, f_1 and ω_1 are the oscillator strength and angular (i.e. $\omega = 2\ \nu$) frequency for the transition from the metastable state to the CT state, respectively; f_0 and ω_0 are the oscillator strength and angular frequency for the transition from the ground state to the CT state, respectively; ω is the angular frequency of the light interacting with the material. This expression is closely related to that for the polarizability used by Powell and Payne [7].

Assuming we can detune the light frequency to reduce absorption, and that τ is long enough that we can reach I_S with a cw laser, then this equation gives the figure-of-merit for obtaining a large refractive index change. It indicates the desirability of a large linear refractive index, a large doping, large oscillator strength for the transition from the metastable state to the CT state, small oscillator strength for the transition from the ground state to the CT state, a CT state that is closer to the metastable state, and a metastable state energy that is close to the laser photon energy. However, when a CT state closer to the metastable state is considered, at some point the resulting absorption must be included. Also note that under these conditions the two frequency dependent terms in this equation can have the same negative sign and combine to yield an even larger effect.

Although we have discussed only the CT transition, since historically this has been considered as the dominant contribution in ruby, the above equation for the maximum index change has a more general validity. That is, the above discussion also applies as an approximation if the CT transition is simply replaced with the appropriate dominant transition for a given material, and to a better approximation if a sum is taken over all possible transitions.

Demonstration of Large Nonlinearity

Figure 1 is a simplified schematic of a setup we have used to measure gain for a weak probe in a moving grating experiment [1]. This powerful technique can be used to determine both the real and imaginary parts of the nonlinear refractive index and the decay time for the metastable state [8]. Light from an argon laser is split into a weak probe beam $I_2(0)$ and a strong pump $I_1(0)$, with a fixed ratio $I_2(0)/I_1(0) = 1/1000$. The frequency of the pump is shifted by approximately 5 Hz with respect to the probe by reflecting it from a mirror mounted to a piezoelectric transducer and driven by a triangle-wave voltage source. The grating resulting from the interaction of the pump and probe in the crystal of $Cr:YAlO_3$ results in amplification for the probe when the mirror is moving in one direction, and attenuation when the mirror moves in the opposite direction.

For sample 1, Fig. 2 shows the gain for the probe beam as a function of the pump beam intensity for the range from 0 to 80 W/cm^2. The crosses are the measurements, and the line is a fit of a theoretical equation for the beam coupling gain [1],

$$\frac{I_2(L)}{I_2(0)} = e^{-\alpha L}\exp\left\{\left(\frac{1-e^{-\alpha L}}{\alpha L}\right)\left[\frac{2\pi n_2 I_1(0) L/\lambda}{\left(1+I_1(0)/I_S\right)^2}\right]\right\} \quad (2)$$

with $\alpha L = 0.69$, L = 9.1 mm, $\lambda = 514.5$ nm and $I_S = h\nu/\sigma\tau = 1.27\ kW/cm^2$. Using n_2 as the only adjustable parameter, the fit yields $n_2/\alpha = 4.2 \times 10^{-7}\ cm^3/W$.

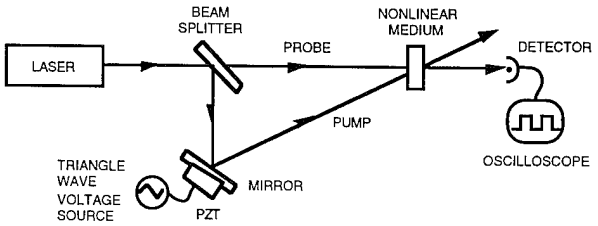

Figure 1. Schematic of the setup to measure gain for a weak probe in a moving grating experiment.

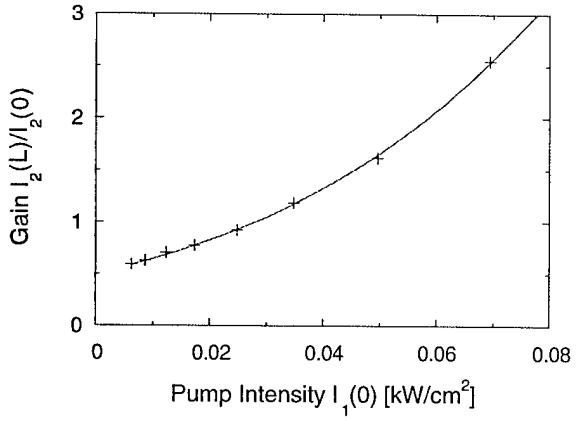

Figure 2. Gain vs. pump intensity from 0 to 80 W/cm^2.

Figure 3 shows the gain for the range from 0 to 400 W/cm^2. Using n_2 as determined from the fit for the lower intensity range of Fig. 2, the line in Fig. 3 represents projections based on Eq. (2). A gain of 22 was obtained at approximately 400 W/cm^2, but the measured gain does not increase with intensity as much as the simple theory predicts (a gain of 200 at 400 W/cm^2). Previously [1] we suggested that this might be due to a "beam break-up" phenomenon we observed and attributed to spatial nonuniformities of the nonlinear refractive index change in the interaction region. However, as we discuss in the following section, measurements of the luminescence as a function of pumping intensity indicate that the reduction in beam coupling gain is due mostly to a reduction of the metastable state population, which is greater than that predicted by depletion of the ground state, as expressed in Eq. (1), when using the usual expression for the saturation intensity, $I_S = h\nu/\sigma\tau$.

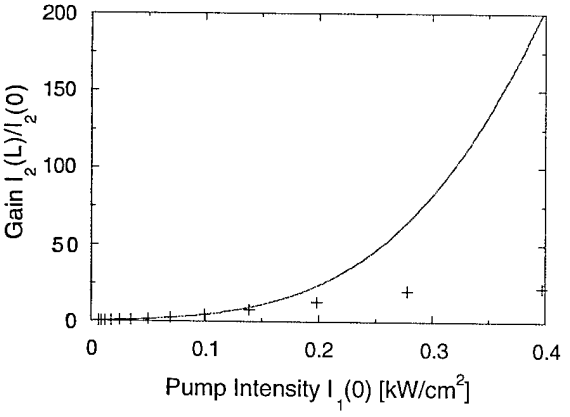

Fig. 3. Gain vs. pump intensity from 0 to 400 W/cm^2.

Luminescence Measurements

Figure 4 shows measurements of the luminescence intensity from sample 1 as a function of the pump beam intensity. The crosses are the measurements, and the solid line is a fit of

$$P_L \approx \ln\left(1+2\frac{I_1}{I_S}\right). \qquad (3)$$

This functional form describes the saturation of the luminescence due to depletion of the ground state for pumping by a beam with a Gaussian spatial profile. The fit gives I_S = 870 W/cm^2, which is less than the value of 1,270 W/cm^2 calculated using $I_S = h\nu/\sigma\tau$. The nonlinearity of the luminescence vs. pumping can be due to a number of factors including not only depopulation of the ground state, but also upconversion, excited state absorption (ESA), and possibly other effects. However, for the purpose of subsequent calculations these effects are conveniently expressed in terms of an effective saturation intensity that results from the fit of the above equation. The subsequent calculations using this effective saturation intensity should be correct to first order.

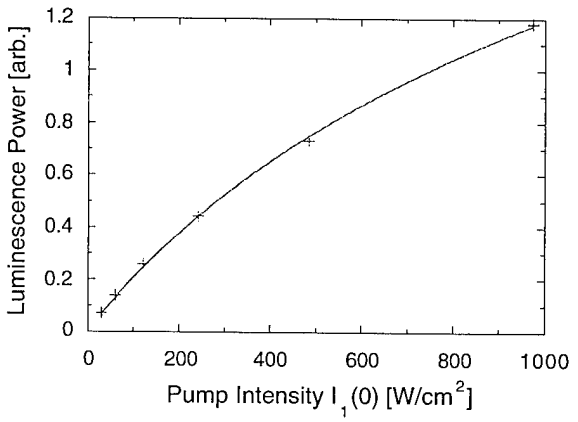

Figure 4. Luminescence vs. pump intensity in sample 1.

Using the value for I_S from the fit in Fig. 4, we can refit the beam coupling gain as shown in Fig. 5. The line is a fit to the range from 0 to 80 W/cm^2 that gives n_2/α = 4.0 x 10^{-7} cm^3/W. The new fit is much better than the previous one shown in Fig. 3. Most of the remaining discrepancy at high pump intensity can be explained by the nonexponential decay of the luminescence that takes place at high intensity (see section on spectroscopy and kinetics). The fit in Figs. 2 and 3 assumed that the pump and probe beams were plane waves of infinite extent. The fit in Fig. 5 includes the effects of a Gaussian beam profile. Although the effect is relatively small, it does yield a slightly better fit to the data.

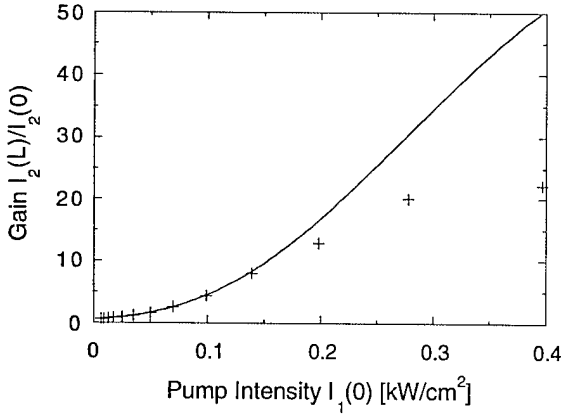

Figure 5. New fit to the beam coupling measurements of Fig. 3, using I_S as determined from a fit to Fig. 4.

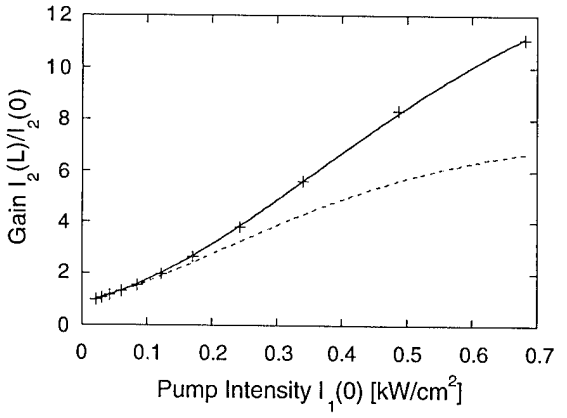

Figure 7. Gain vs. pump intensity in sample 2.

Sample 2 Exhibits Different Saturation

Figure 6 shows measurements of the luminescence vs. pump intensity for sample 2. The fit gives I_S = 1640 W/cm^2, which is greater than 870 W/cm^2 obtained for sample 1. Thus, sample 2 does not show premature saturation, and in fact the saturation appears to be less than that predicted by $I_S = h\nu/\sigma\tau$. One possible explanation for the measured value being greater than the predicted value is that the cross section may contain terms due to residual color center absorption that do not contribute to the metastable state population.

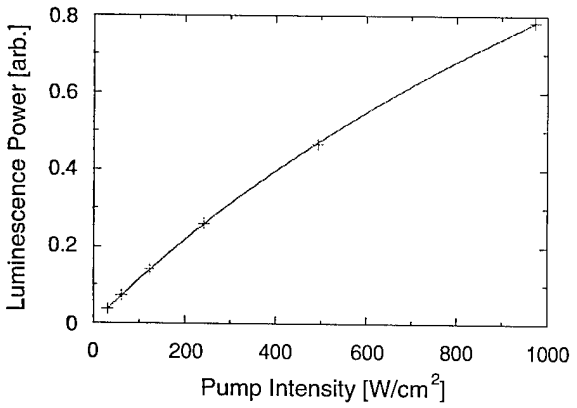

Figure 6. Luminescence vs. pump intensity in sample 2.

Figure 7 shows measurements of the beam coupling gain in sample 2. The dashed line is a fit using the value of n_2/α from the previous crystal, and I_S=1,270 W/cm^2. It fits well at low intensity, but it greatly underestimates the gain obtained at high intensity. The solid line is a fit that gives $n_2/\alpha = 4.1 \times 10^{-7}$ cm^3/W and I_S = 1,630 W/cm^2. These values are in excellent agreement with the value of n_2/α from the previous crystal, and the value of I_S from the fit of the luminescence for sample 2.

To conclude this first section, by fitting the luminescence vs. pump intensity, we obtain an effective saturation intensity that lumps together the effects of ground state depletion, upconversion, ESA, etc. Using this effective saturation intensity, we obtain a better fit to the beam coupling gain than is possible using the expression $I_S = h\nu/\sigma\tau$. Thus, the processes that give rise to saturation of the luminescence and the metastable state population, rather than the beam breakup that we had previously proposed [1], are the major factors responsible for the premature saturation of the beam coupling gain in sample 1.

Spectroscopy and Kinetics

We studied the spectroscopic and kinetics properties of sample 1 (the sample exhibiting premature saturation

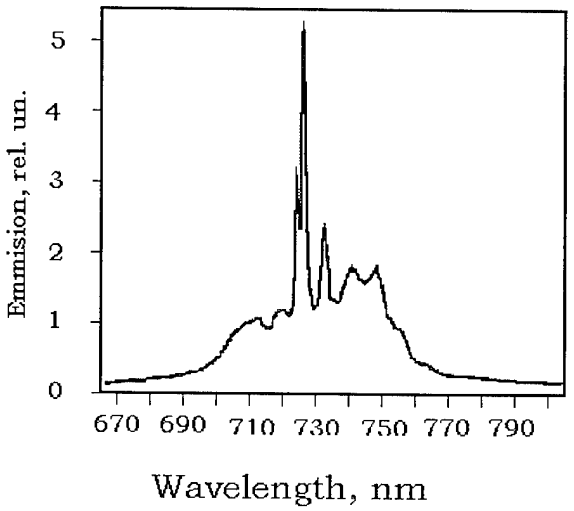

Figure 8. Luminescence spectra for strong pumping.

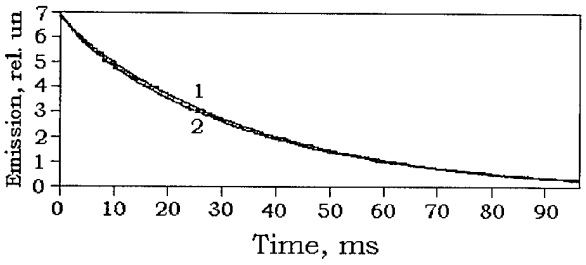

Figure 9. Luminescence kinetics taken at λ=750 nm. 1 - weak pumping, 2 - strong pumping (409 W/cm^2).

behavior). The room temperature luminescence spectra taken at high (10^4 W/cm^2) pumping density is presented in Fig. 8 for a pump wavelength of 514.5 nm. According to Ref. [9], two narrow lines at ~723 nm and 725.5 nm are attributed to the transition from the ^2E level to the ground state $^4A_2$ (R lines), and the irregular shaped broad luminescence band centered at ~740-750 nm is due to vibronic transitions.

Using long (200 ms) pulsed excitation of the sample with 488 nm or 514.5 nm light from an Ar laser, we studied the luminescence decay kinetics for each wavelength at which there was a significant peak in the luminescence spectrum. For long pulse excitation, the decay-kinetics taken at most of the peaks in the luminescence spectra were nearly exponential with a time constant of 36 ms (Fig. 9 trace 1). This value is equal to the room temperature lifetime of Cr ions in $YAlO_3$ reported in Ref. [9].

As shown in Fig. 10, the decay-kinetics taken at 732 nm were strongly nonexponential, and the time taken to reach the 1/e level was equal to 24 ms.

Although the decay kinetics at 725.5 nm and 750 nm were very similar for long pulsed excitation, they were different for short (2 ms) pulse excitation. For short pulsed excitation, all the kinetics studied were nonexponential to some degree. This nonexponential behavior was almost negligible at 750 nm, but significant at 725.5 nm.

These spectroscopic and kinetics studies imply the presence of at least three Cr luminescence centers in Cr:$YAlO_3$, that are responsible for the dominant

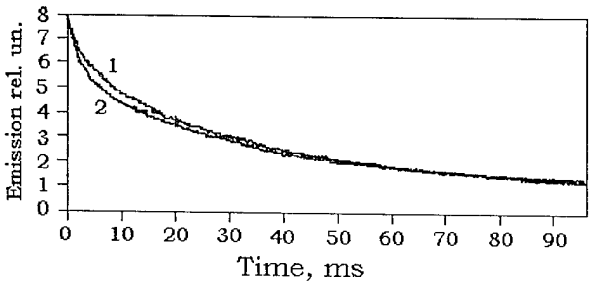

Figure 10. Luminescence kinetics taken at λ=732 nm. 1 - weak pumping, 2 - strong pumping (409 W/cm^2).

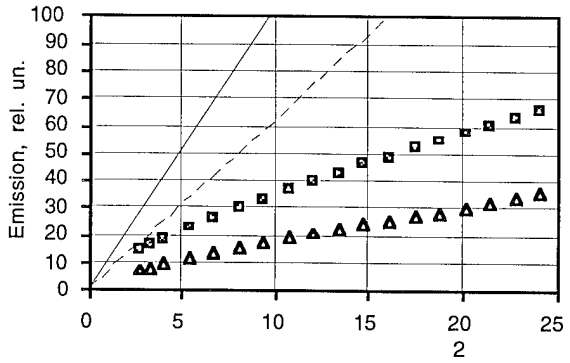

Figure 11. Luminescence intensity at λ=725.5 nm (squares) and λ=750 nm (triangles) as a function of pumping density; λpump=488 nm. The solid line represents the slope of the 725.5 nm luminescence curve obtained from separate measurements taken at low pumping, and the dashed line represents the same for 750 nm.

features of the luminescence spectra at 725.5 nm, 732 nm, and 750 nm. The presence of three types of Cr centers in $YAlO_3$ was also reported in Ref. [10]. According to Ref. [9], Cr decay curves are nonexponential due to the quenching of the luminescence of single Cr ions on Cr pairs [11]. However, in the presence of several types of Cr centers, we cannot exclude the possibility of energy transfer between them, which can also lead to nonexponential luminescence kinetics.

The dependence of the luminescence intensity on the pumping density is shown in Fig. 11. Similar nonlinear dependencies were obtained at 725.5 nm and 750 nm, as well as for the spectrally integrated emission that was shown in Fig. 4. In general, the nonlinear dependence can be explained by depletion of the ground state, excited state absorption (ESA), or energy transfer upconversion that shortens the effective life-time of the Cr metastable level. In Fig. 11, as was the case for the spectrally integrated emission shown in Fig. 4, the nonlinearity of the luminescence intensity is stronger than predicted by a model neglecting ESA and upconversion.

The study of Cr luminescence kinetics have shown that at λ 750 nm and many other wavelengths except 725.5 nm and 732 nm, upconversion is weak (the effective decay-time changes by no more than for 5%) for pumping densities as high as I/S 5x10 ^{3} W/cm^2. At λ 725.5 nm, upconversion is significant for I/S 5x10 ^{3} W/cm^2, but negligible for I/S 10 ^{3} W/cm^2. The strongest upconversion was found at 732 nm. As shown in Fig. 10, at this wavelength, the initial decay-time of the luminescence changed from 9 ms to 6.5 ms at I/S =410 W/cm^2. At all wavelengths studied, a higher rate of quenching at weak pumping corresponded to stronger upconversion at intense pumping.

Assuming that different types of Cr centers in the crystal behave independently, the strong nonlinearity of the luminescence intensity (at 725.5 nm and λ 750 nm as well as the spectral integrated luminescence intensity) *vs*. pumping density at I/S<1000 W/cm^2 cannot be explained by upconversion.

We obtained an unexpected result from the luminescence spectral measurements at high pumping intensity. Accounting for the upconversion kinetics measurements, we expected the relative intensity of the luminescence peak at 732 nm to be smaller at high pumping density than at weak pumping. On the contrary, in the experiment, the relative height of the 732 nm peak was greater at strong pumping than at weak excitation. This result cannot be explained under the assumption of independent behavior of different types of centers as well.

In principle, the last experimental result can be explained if we assume that one type of centers (manifesting itself at 732 nm) absorbs most pump power and then transfers it to the other types of centers. In this case, the reduction in the excited state concentration of 732 nm centers due to upconversion will cause the reduction in the energy transferred to the other centers. To explain the growth of the relative height of 732 nm peak at intense pumping, we should also assume that some additional upconversion (that can be rather weak) reduces the effective decay times of luminescence at 725.5 nm, 750 nm, *etc*. If we accept this model, then at I/S 400 W/cm^2, upconversion can explain up to a 30% reduction of Cr excited state concentration. This model also is consistent with the strong quenching of 732 nm luminescence at weak pumping. However, at the present moment we do not have enough experimental data to prove or reject this hypothesis.

Conclusion

Laser and related materials play an important role in nonlinear optics by providing convenient solid state materials with a local response proportional to intensity, which allows researchers to demonstrate large local nonlinear optical effects using cw lasers. For example, using Cr:$YAlO_3$ we demonstrated a beam coupling gain of 22, and self-oscillation based on this gain [2]. Since the same optical nonlinearity will affect the propagation of beams, it should be considered in the design of lasers.

One of the two crystals of Cr:$YAlO_3$ we studied shows a saturation in both beam coupling gain and luminescence as a function of pump intensity that is greater than that predicted using $I_S = h\nu/\sigma\tau$ and known values of the parameters. In this crystal, although the luminescence decay kinetics at most wavelengths were nearly exponential, they were strongly non-exponential and intensity dependent at 732 nm. The second crystal we studied did not exhibit the premature saturation behavior. If the premature saturation behavior of the first crystal is not linked to its higher concentration, then crystals like the second one, but of higher concentration, may provide very large beam coupling gain.

This research was sponsored by the U.S. Air Force Office of Scientific Research under contract F49620-92-C-0023, with partial support from grant AFOSR-91-0369.

References

1. I. McMichael, R. Saxena, T. Chang, Q. Shu, S. Rand, J. Chen and H. Tuller, "High gain nondegenerate two-wave mixing in Cr:$YAlO_3$," Opt. Lett. **19**, 1511 (1994).
2. I. McMichael and T. Chang, "Self-oscillation and self-pumped phase conjugation in Cr:$YAlO_3$," to appear in Technical Digest of *Conference on Lasers and Electro-Optics* (Optical Society of America, Washington, DC, 1996), paper CFF7.
3. T. Venkatesan and S. McCall, "Optical bistability and differential gain between 85 and 296°K in a Fabry-Perot containing ruby," Appl. Phys. Lett. **30**, 282 (1977).
4. D. McClure, "Optical spectra of transition-metal ions in corundum,"J. Chem. Phys. **36**, 2757 (1962).
5. T. Kushida, "Absorption and emission properties of optically pumped ruby," IEEE J. Quantum. Electron. **QE-2**, 524 (1966).
6. H. Tippins, "Charge-transfer spectra of transition-metal ions in corundum," Phys. Rev. **B 1**, 126 (1970).
7. R. Powell and S. Payne, "Dispersion effects in four-wave mixing measurements of ions in solids," Opt. Lett. **15**, 1233 (1990).
8. I. McMichael, P. Yeh, and P. Beckwith, "Non-degenerate two-wave mixing in ruby," Opt. Lett. **13**, 500 (1988).
9. M. J. Weber, T. E. Varitimos, "Optical spectra and relaxation of Cr^{3+} ions in Cr:$YAlO_3$", J Appl. Physics **45**, pp. 810-816 (1974).
10. J. A. Marles, G. Boulon, L. Lou, S. R. Rotman, H. Luria, "Cr^{3+},Nd^{3+} multisites, pairs and energy transfer processes in laser crystal $YAlO_3$", Journal de Physique IV, Colloque C4, supplement au Journal de Physique III, Volume **4**, pp. C4-385 - C4-388.
11. J. P. van der Ziel, "Spectrum of exchange coupled Cr^{3+} pairs in $YAlO_3$", J Chem. Phys. **57**, pp. 2442-2450 (1972).

A.2

Self-Oscillation and Self-Pumped Phase Conjunction in Cr:$YAlO_3$

Self-Oscillation and Self-Pumped Phase Conjugation in Cr:$YAlO_3$

Ian McMichael and Tallis Y. Chang

Rockwell International Science Center

1049 Camino Dos Rios

Thousand Oaks, CA 91360

Phone: (805) 373-4508

Fax: (805) 373-4423

e-mail: icmcmich@scimail.remnet.rockwell.com

Abstract

Continuous self-oscillation and self-pumped phase conjugation via nondegenerate two-wave mixing gain are demonstrated in Cr:$YAlO_3$. To our knowledge, this is the first demonstration of these effects in a solid state, non-photorefractive material.

Self-Oscillation and Self-Pumped Phase Conjugation in Cr:$YAlO_3$

Ian McMichael and Tallis Y. Chang

Rockwell International Science Center

1049 Camino Dos Rios

Thousand Oaks, CA 91360

Phone: (805) 373-4508

Fax: (805) 373-4423

e-mail: icmcmich@scimail.remnet.rockwell.com

Summary

When two beams of different frequency interact in a medium with a local nonlinear optical response, one beam experiences gain at the expense of the other. We refer to this process as nondegenerate two-wave mixing. Figure 1 shows measurements of the nondegenerate two-wave mixing gain for a weak probe beam interacting with a strong pump beam in a crystal of Cr:$YAlO_3$. The laser wavelength is 515 nm and the probe is downshifted with respect to the pump by approximately 5 Hz. Gain in excess of 12 times is obtained.

At normal incidence, the reflectivity of Cr:$YAlO_3$ is 11%, and the absorption loss for this crystal is 17%. Thus, the roundtrip gain ($12^2 = 144$) is sufficient to overcome the losses ($(0.11x0.83)^2 = 1/120$) of a resonator formed by the opposing surfaces of the crystal. (We previously demonstrated that the gain for a reflection grating is comparable to that for a transmission grating.) With the probe off and the crystal normal oriented at a small angle with respect to the incident pump beam, an oscillation builds up between the opposing surfaces of the crystal. Figure 2 shows far field patterns of the oscillating mode. As shown in Fig. 2, it is

possible to change the oscillating mode by translating the crystal perpendicular to the pumping beam. Using a microscope, we observe a moving fringe pattern in the fluorescence from the interaction region of the crystal that is formed by the interference between the beam incident on the crystal and the frequency shifted self-oscillation. By beating the oscillation with a portion of the incident beam, we measure a frequency shift of 6 Hz. This is consistent both with our measurements of the frequency shift at which the nondegenerate two-wave mixing gain was maximum, and with the theoretical expression, $1/2\,\tau$, where τ is the response time of the nonlinearity (the lifetime of the metastable state, 33 ms).

The bidirectional oscillation acts as pumping beams and the beam incident on the crystal acts as a probe beam in a four-wave mixing process to generate what we believe is the self-pumped phase-conjugate of the beam incident on the crystal. Figure 3 shows the resulting phase-conjugate return. We verified that the return was along a direction consistent with a retroreflection of the incident beam and that it built up with the oscillation. This is consistent with the interpretation of a phase-conjugate return. However, we have not yet verified the phase-conjugate nature of the wavefront by, for example, demonstrating distortion correction. Note that the return is elongated in the direction perpendicular to the plane of incidence defined by the pump and probe beams. A similar effect was previously observed in photorefractive ring conjugators. This research was sponsored by the U.S. Air Force Office of Scientific Research under contract F49620-92-C-0023.

Figure Captions

Fig. 1 Nondegenerate two-wave mixing gain for a weak probe beam interacting with a strong pump beam in a crystal of Cr:$YAlO_3$.

Fig. 2 Far-field patterns corresponding to the spatial modes of a self-oscillation in Cr:$YAlO_3$. The different modes result for different translational positions of the crystal.

Fig. 3 The elliptical spot on top of the speckle pattern of scattered light is the far-field pattern of the phase-conjugate return generated by the four-wave mixing interaction with the incident beam and the counterpropagating beams of the self-oscillation.

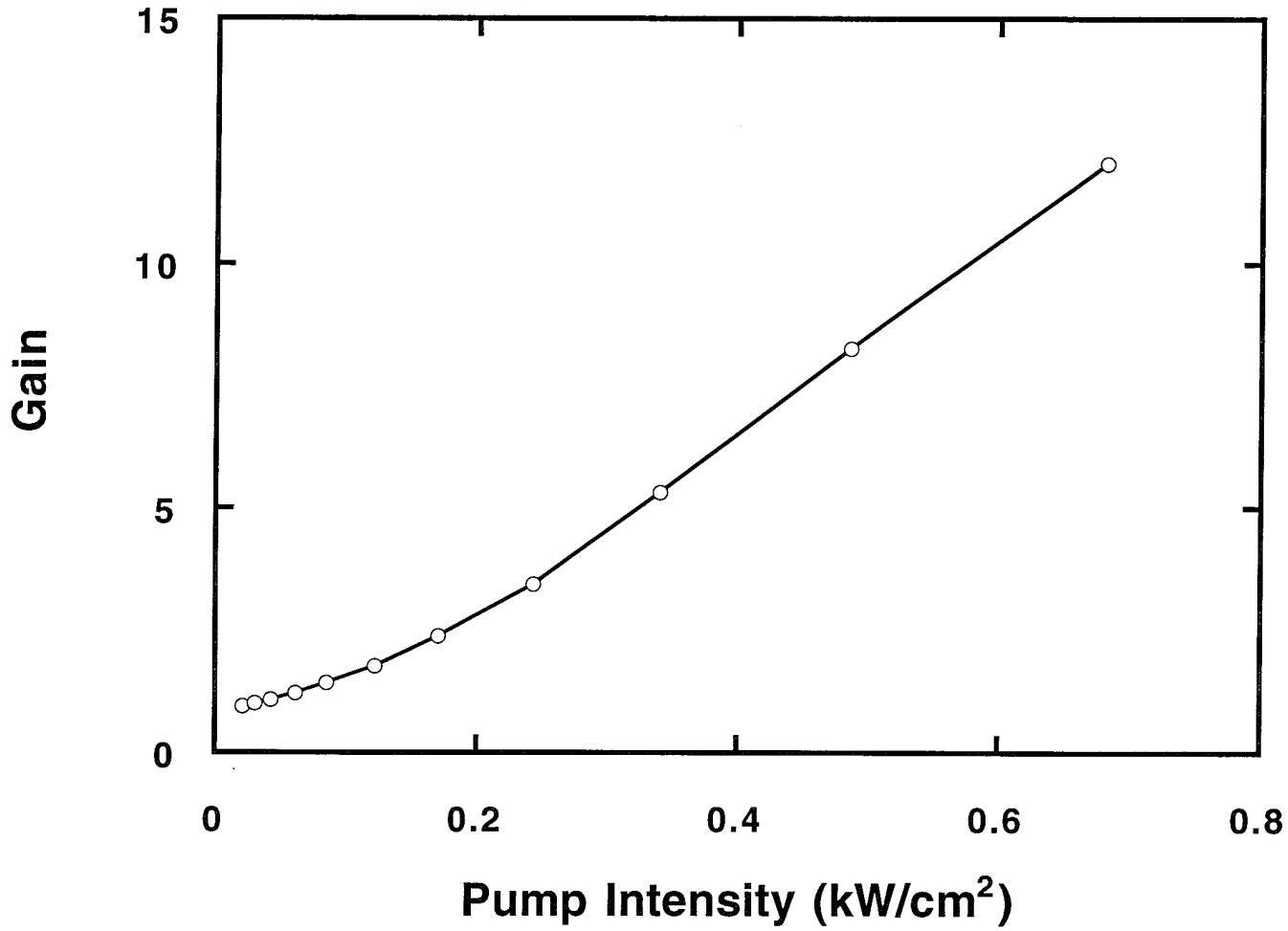
15
10
5
0
Gain
0
0.2
0.4
0.6
0.8
Pump Intensity (kW/cm^2)

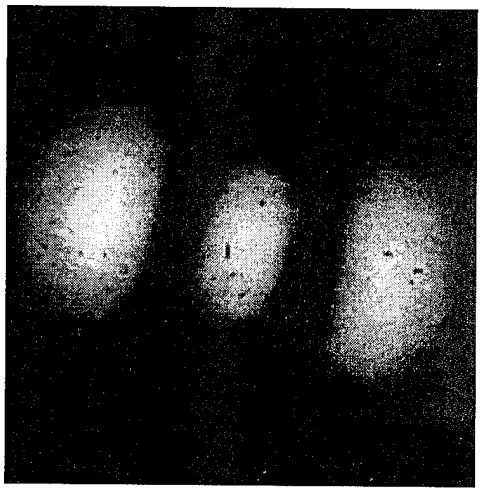

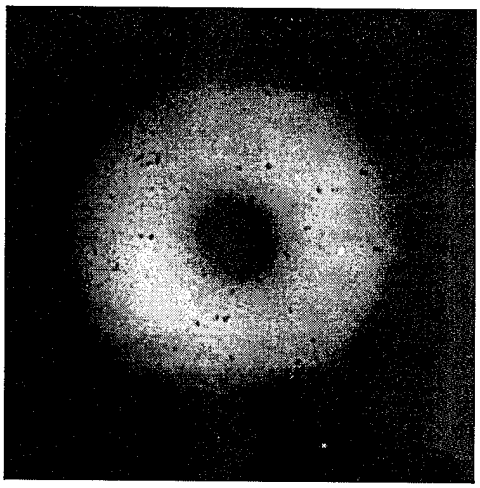

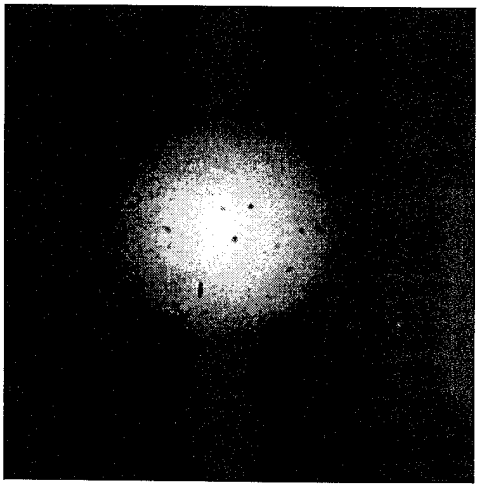

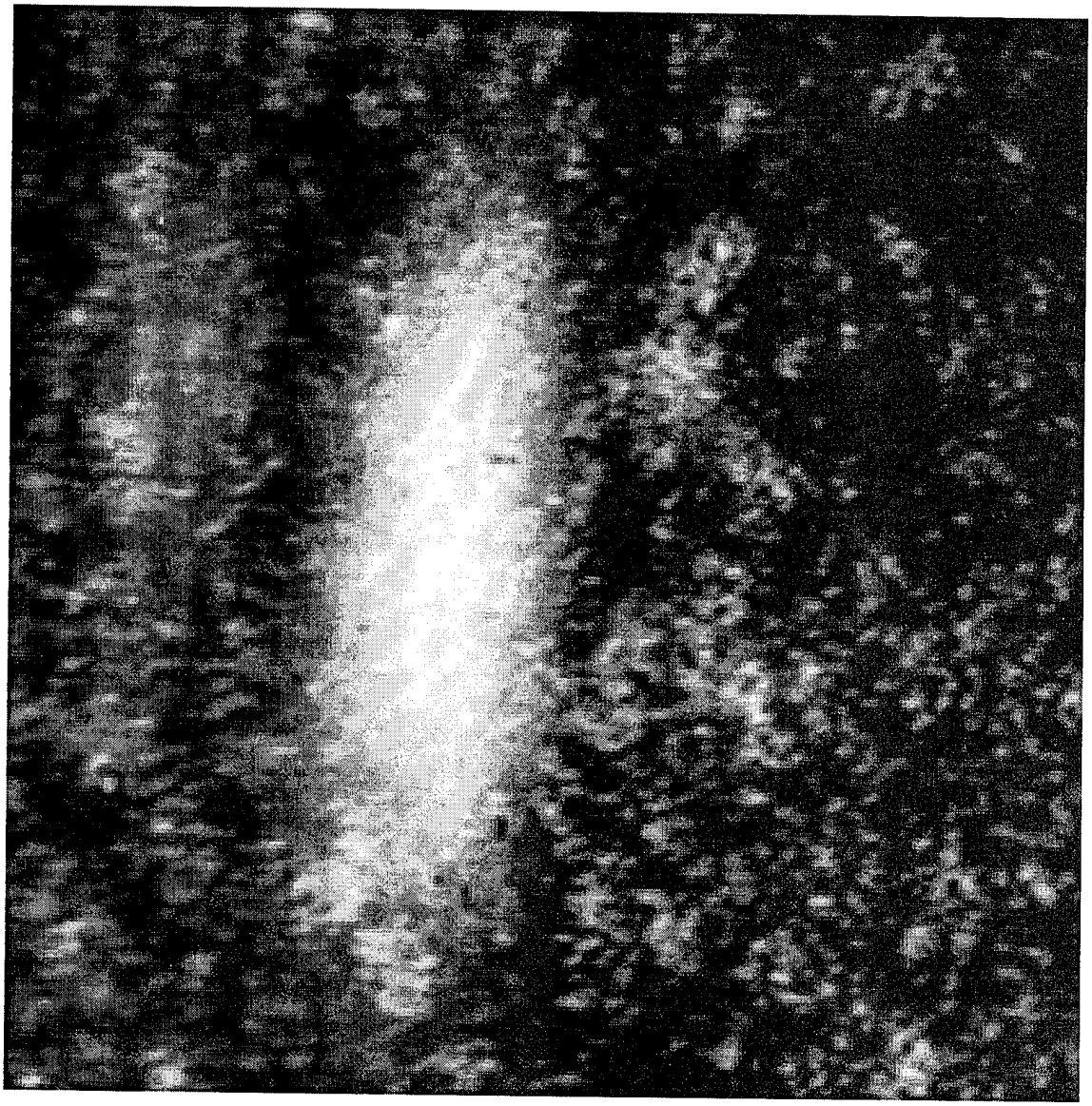

A.3

Efficiency of phase conjugation for highly scattered light

Reprinted from

OPTICS COMMUNICATIONS

Optics Communications 119 (1995) 13–16

Efficiency of phase conjugation for highly scattered light

Ian McMichael, M.D. Ewbank, Frederick Vachss

Science Center, Rockwell International Corporation, 1049 Camino Dos Rios, Thousand Oaks, CA 91360, USA

Received 1 February 1995; revised version received 10 May 1995

ELSEVIER

OPTICS COMMUNICATIONS

Aims and Scope
Optics Communications ensures the rapid publication of contributions in the field of optics and interactions of light with matter.

Abstracted/indexed in:
Chemical Abstracts; EI Compendex Plus; Engineering Index; INSPEC; Physics Briefs.

Subscription Information 1995
Volumes 112–121 (60 issues) of Optics Communications (ISSN 0030-4018) are scheduled for publication.

Prices are available from the publisher upon request. Subscriptions are accepted on a prepaid basis only. Issues are sent by SAL (Surface Air Lifted) mail wherever this service is available. Please address all enquiries regarding orders and subscriptions to:
Elsevier Science B.V.
Order Fulfilment Department
P.O. Box 211, 1000 AE Amsterdam
The Netherlands
Tel. +31 20 4853642, Fax: +31 20 4853598

Claims for issues not received should be made within six months of our publication (mailing) date.

US mailing notice – Optics Communications (ISSN 0030-4018) is published semi-monthly by Elsevier Science B.V., Molenwerf 1, P.O. Box 211, 1000 AE Amsterdam, The Netherlands. Annual subscription price in the USA is US$ 2384 (valid in North, Central and South America only), including air speed delivery. Second class postage paid at Jamaica, NY 11431.
USA Postmasters: Send changes to Optics Communications, Publications Expediting, Inc., 200 Meacham Avenue, Elmont, NY 11003. Airfreight and mailing in the USA by Publications Expediting.

⊗ The paper used in this publication meets the requirements of ANSI/NISO 239.48-1992 (Permanence of Paper).

Printed in The Netherlands

ELSEVIER

ELSEVIER

15 August 1995

Optics Communications 119 (1995) 13–16

OPTICS COMMUNICATIONS

Efficiency of phase conjugation for highly scattered light

Ian McMichael, M.D. Ewbank, Frederick Vachss

Science Center, Rockwell International Corporation, 1049 Camino Dos Rios, Thousand Oaks, CA 91360, USA

Received 1 February 1995; revised version received 10 May 1995

Abstract

We present experiments demonstrating reciprocity for conjugation of highly scattered light; if a fraction η of the total scattered light is incident on a phase-conjugate mirror having reflectivity ρ, then a fraction $\rho\,\eta^2$ returns back through the scatterer as a phase-conjugate wave, with the remaining fraction $\rho\,(\eta-\eta^2)$ being lost due to scattering. Low efficiency results from inability to gather a large fraction of scattering, but the efficiency is higher than is possible without conjugation.

Consider the case of light incident on a lossless, highly scattering media. As shown in Fig. 1a, if a phase conjugator could gather and reflect all of the scattered light, then by the principle of time reversal, all of the reflected light would return as the conjugate [1–4]. However, in practice it is difficult for an optical system to gather a large fraction of highly scattered light. What is the efficiency in this case of partial phase conjugation? According to the reciprocity theorem, if a fraction η of the total scattered light is incident on a phase-conjugate mirror having reflectivity ρ, then a fraction $\rho\,\eta^2$ returns back through the scatterer as a phase-conjugate wave, with the remaining fraction $\rho\,(\eta-\eta^2)$ being lost due to scattering [5]. This case is shown in Fig. 1b. We previously demonstrated the principle of reciprocity as it applies to non-polarization preserving phase conjugation of light from multimode fibers, where when a fraction 1/2 of the incident light (one polarization component) is reflected from a phase-conjugate mirror with a reflectivity ρ, a fraction $\rho/4$ returns as the conjugate [6]. New experimental results demonstrating the principle of reciprocity for the case where a varying fraction of the fiber modes are conjugated are to be published [7]. For multimode fibers, we had also

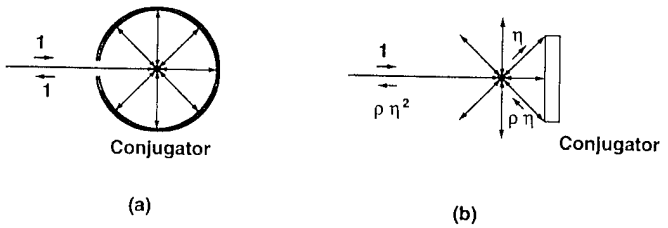

Fig. 1. (a) Light incident on a lossless, highly scattering media is scattered into all directions. An ideal conjugator gathers and reflects all of the scattered light with unity reflectivity to reproduce the incident beam with perfect efficiency. In this case all of the reflected light would return as the conjugate. (b) In practice, a conjugator gathers a finite fraction η of the scattered light. According to the reciprocity theorem, if a fraction η of the total scattered light is incident on a phase-conjugate mirror having reflectivity ρ, then a fraction $\rho\,\eta^2$ returns back through the scatterer as a phase-conjugate wave, with the remaining fraction $\rho\,(\eta-\eta^2)$ lost due to scattering.

Elsevier Science B.V.
SSDI 0030-4018(95)00318-5

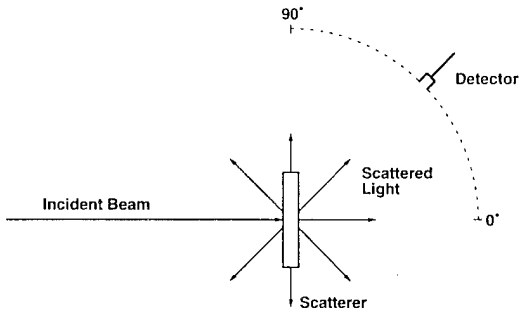

Fig. 2. Setup used to measure scattered power density as a function of angle.

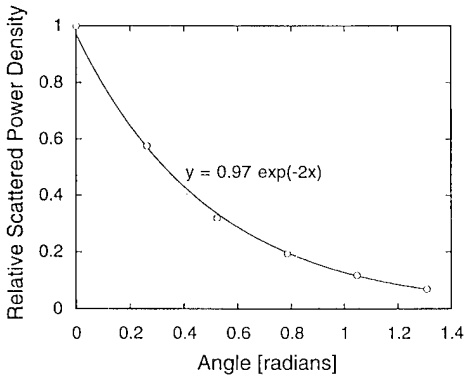

Fig. 3. Scattered power density as a function of angle for the thick (3/16″ polypropylene) scatterer used in our experiments. The measurements indicated by the circles are normalized to the on-axis power and the solid line is a fit of an exponential dependence.

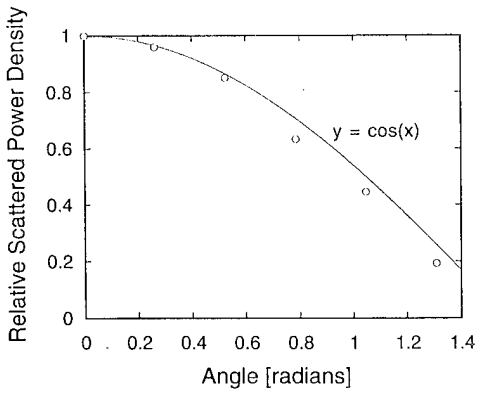

Fig. 4. Scattered power density as a function of angle for the thin (20 μm polypropylene) scatterer used in our experiments. The scatter for the thin scatterer is nearly isotropic, except for the cosine dependence resulting from the area projection of a flat surface.

previously demonstrated that all of the fiber modes can be gathered and conjugated, such that all of the light reflected by a phase-conjugate mirror will return as the conjugate [6]. Here, however, we describe the first experiments, to our knowledge, demonstrating the principle of reciprocity as it applies to the case of highly scattered light, where all of the scattered light cannot be gathered and conjugated.

In our experiments we used both a thick (3/16″ polypropylene) and a thin (20 μm polyethylene) scattering media to show that the principle of reciprocity applies to at least two scatterers with different properties, and therefore to lend credibility to the general application of reciprocity to other scattering media. To characterize the two scatterers we measured the scattered power density as a function of angle using the setup shown in Fig. 2. The beam incident on the scatterer was 100 mW of unfocused light from an argon laser operating at 515 nm. Measurements of the scattered light at various angles were taken using a detector of 1 cm^2 area, placed at 74 cm from the scatterer. These measurements are shown as circles in Fig. 3 and Fig. 4, and the solid lines are fits to the data. The scatter for the thick scatterer has an exponential dependence on angle with a fwhm of approximately 40°. The scatter for the thin scatterer is nearly isotropic, except for the cosine dependence resulting from the area projection of a flat surface. For both scatters, calculations of the integrated scatter indicate that losses are negligible.

Fig. 5 shows the experimental setup used to measure the efficiency for phase conjugation of scattered light.

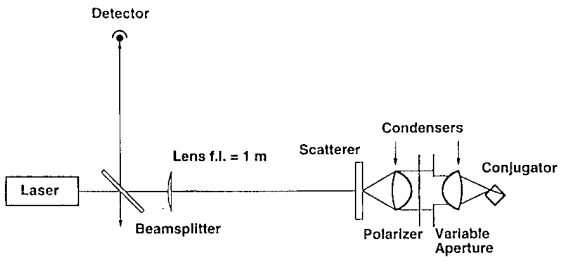

Fig. 5. Experimental setup used to measure the efficiency for phase conjugation of scattered light. Light from a laser is focused by a lens onto the surface of the scatterer. A pair of condensers gathers and focuses scattered light into a self-pumped conjugator. A polarizer placed between the condensers selects the proper polarization for operation of the conjugator. The conjugate return is measured by a detector as a function of the amount of light incident on the conjugator, which is adjusted with a variable aperture.

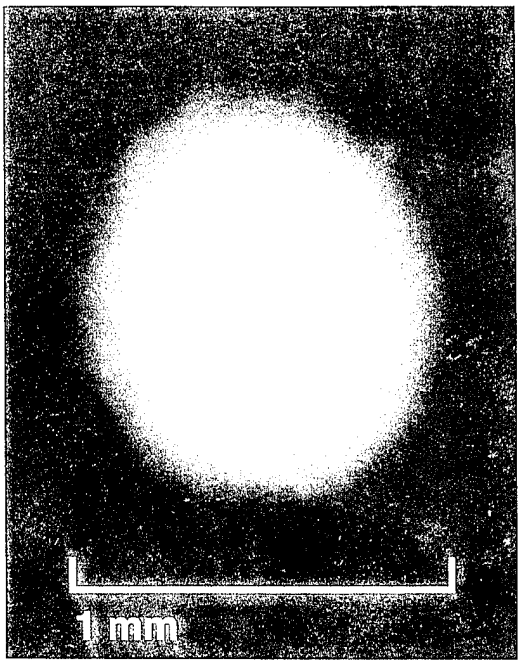

Fig. 6. Photograph of the phase-conjugate return taken from a position corresponding to the detector.

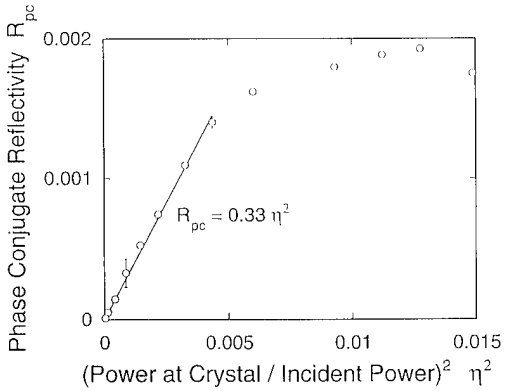

Fig. 7. Phase-conjugate reflectivity as a function of the square of the fraction of the total scattered light that is incident on the conjugator, in the case of the thick scatterer. The circles represent the measurements and the solid line are fits of $R_{pc} = \rho\,\eta^2$, as predicted by the reciprocity theorem. The excellent agreement of the functional form for most of the data indicates the validity of reciprocity theorem for predicting the results of partial phase conjugation of scattered light. The saturation of the phase-conjugate reflectivity is thought to be due to aberrations in our condensers at low f-number that do not permit the focusing of all of the light into the conjugator and/or spatial variations in the phase-conjugate reflectivity when the cone angle of the light incident on the conjugator becomes large.

Light from an argon laser at 515 nm is focused by a lens of 1 m focal length onto the surface of the scatterer. A pair of condenser lenses (32.5 mm diameter, 23.5 mm focal length) is used to gather and focus the scattered light into a crystal of barium titanate that acts as a self-pumped phase conjugator of the "cat" configuartion [4]. The distance between the first condenser and the scatterer is adjusted to collimate the light exiting from first condenser as well as is possible. The laser power is adjusted to have approximately 14 mW incident on the crystal. A polarizer placed between the condensers insures that the light incident on the crystal is extraordinary. The conjugate return is reflected from a beam splitter and measured by a detector. A photograph of the conjugate return at a position corresponding to the detector (approximately 2 m from the scatterer) is shown in the Fig. 6. A variable aperture placed between the condensers allows us to vary the amount of light incident on the phase conjugator. When the measurements of the phase-conjugate return were completed, the conjugator was removed and replaced with a detector to measure the amount of light passing through the aperture, which was previously incident on the conjugator, as a function of the aperture setting. A calibration for 100% reflectivity was made by temporarily placing a mirror at the position of the scatterer and aligning it to retroreflect the light from the laser back to the detector.

The circles in Figs. 7 and 8 show the measurements of the phase-conjugate reflectivity as a function of the square of the fraction of the total scattered light that is

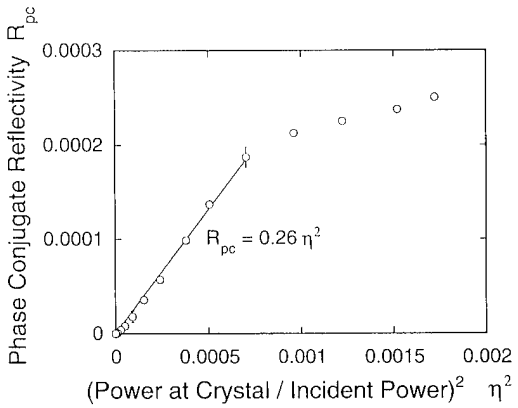

Fig. 8. Phase-conjugate reflectivity as a function of the square of the fraction of the total scattered light that is incident on the conjugator, in the case of the thin scatterer.

incident on the conjugator η^2, and the solid lines are fits of $R_{pc} = \rho\ \eta^2$, as predicted by the reciprocity theorem. Representative error bars are given for two of the points in both Fig. 7 and Fig. 8. The excellent agreement of the functional form for most of the data indicates the validity of reciprocity theorem for predicting the results of partial phase conjugation of scattered light. The constant ρ from the fits is the phase-conjugate reflectivity of the self-pumped crystal of barium titanate. The values of 33% and 26% are in good agreement with an independent measurement of 30% using unscattered light.

We are not sure why the phase-conjugate reflectivity saturates, but it may be due to residual aberrations in our condensers at low f-number that do not permit the focusing of all of the light into the conjugator and/or spatial variations in the phase-conjugate reflectivity when the cone angle of the light incident on the conjugator becomes large. The effective f-number at which the saturation behavior takes place is quite low, and the corresponding cone angle is rather large. Saturation begins at about f/1.3 or 42° in Fig. 7, and f/1.0 or 53° in Fig. 8. The fact that the data agree with reciprocity to such low f-numbers and large cone angles is satisfying in and of itself. It is probably not too surprising that the phase conjugate reflectivity saturates at lower f-numbers and larger cone angles. After all, neither the condensers, nor the conjugator are ideal. For example, the condensers are manufactured for light gathering, not for imaging, and the residual aberrations are severe. The supplier of the condensers believes that they can be modeled by an odd asphere with second order correction for the first surface, and a 120 mm radius for the second surface. This would yield a focal length that varies by about 3 mm (or 13% of the specified focal length) over the zones of the lens aperture. An ideal conjugator will correct for aberrations and this is verified by the fact that most of the data agree with reciprocity. However, in practice conjugators have both finite spatial and angular apertures, and their operation depends on the focusing conditions. The reflectivity as a function of the angles of incidence, in one plane, on a cat conjugator for a single narrow beam [8] and for a pair of narrow beams [9] has been measured, but it is not clear that these apply to our situation of a single extremely wide angle beam in two dimensions with our particular aberrations.

In conclusion, for any reciprocal optical system, if a fraction η of the incident light is incident on a phase-conjugate mirror having reflectivity ρ, then a fraction $\rho\ \eta^2$ returns as a conjugate, with the remaining fraction $\rho\ (\eta - \eta^2)$ distributed over other modes of the system. Our experimental results demonstrate this principle of reciprocity in one of the most complicated cases (the case of scattering).

This research was sponsored by the Office of Naval Research under contract N00014-93-C-0010 and by the U.S. Air Force Office of Scientific Research under contract F49620-92-C-0023.

References

[1] H. Butterweck, J. Opt. Soc. Am. 73 (1977) 60.
[2] G. Agarwal, A Friberg and E. Wolf, J. Opt. Soc. Am. 73 (1983) 529.
[3] M. Nazarathy and J. Shamir, J. Opt. Soc. Am. 73 (1983) 910.
[4] Z. Bouchal, Optik 93 (1993) 170.
[5] C. Gu and P. Yeh, Optics Comm. 107 (1994) 353.
[6] I. McMichael, P. Yeh and P. Beckwith, Optics Lett. 12 (1987) 507.
[7] S. Campbell, P. Yeh, C. Gu and Q. He, Optics Comm. 114 (1995) 50.
[8] J. Feinberg, Optics Lett. 7 (1982) 486.
[9] J. Feinberg, Optics Lett. 8 (1983) 481.

Instructions to Authors (short version)

(A more detailed version of the instructions is published in the preliminary pages of each volume)

Submission of papers

Manuscripts (one original and two copies), should be sent to one of the Editors, whose addresses are given on the inside of the journal cover.

Original material. Submission of a manuscript implies that the paper is not being simultaneously considered for publication elsewhere and that the authors have obtained the necessary authority for publication.

Refereeing. Submitted papers will be refereed and, if necessary, authors may be invited to revise their manuscript. Authors are encouraged to list the names (addresses and telephone numbers) of up to five individuals outside their institution who are qualified to serve as referees for their paper. The referees selected will not necessarily be from the list suggested by the author.

Types of contributions

The journal Optics Communications publishes short communications and full length articles in the field of optics and quantum electronics.

Short communications are brief reports of significant, original and timely research results that warrant rapid publication. The length of short communications is limited to six journal pages. Proofs will not be mailed to authors prior to publication unless specifically requested.

Full length articles are subject to the same criteria of significance and originality but give a more complete and detailed account of the research results. Proofs of all full length articles will be mailed to the corresponding author, who is requested to return the corrected version to the publisher within two days of receipe.

Manuscript preparation

All manuscripts should be written in good English. The paper copies of the text should be prepared with double line spacing and wide margins, on numbered sheets. See notes opposite on electronic version of manuscripts.

Structure. Please adhere to the following order of presentation: Article title, Author(s), Affiliation(s), Abstract, PACS codes and keywords, Main text, Acknowledgements, Appendices, References, Figure captions, Tables.

Corresponding author. The name, complete postal address, telephone and Fax numbers and the E-mail address of the corresponding author should be given on the first page of the manuscript.

PACS codes/keywords. Please supply one or more relevant PACS-1995 classification codes and 1–6 keywords of your own choice for indexing purposes.

References. References to other work should be consecutively numbered in the text using square brackets and listed by number in the Reference list. Please refer to a recent issue of the journal or to the more detailed instructions for examples.

Illustrations

Illustrations should also be submitted in triplicate: one master set and two sets of copies. The *line drawings* in the master set should be original laser printer or plotter output or drawn in black india ink, with careful lettering, large enough (3–5 mm) to remain legible after reduction for printing. The *photographs* should be originals, with somewhat more contrast than is required in the printed version. They should be unmounted unless part of a composite figure. Any scale markers should be inserted on the photograph itself, not drawn below it.

Colour plates. Figures may be published in colour, if this is judged essential by the editor. The publisher and the author will each bear part of the extra costs involved. Further information is available from the publisher.

After acceptance

Important. When page proofs are made and sent out to authors, this is in order to check that no undetected errors have arisen in the typesetting (or file conversion) process. No changes in, or additions to, the edited manuscript will be accepted.

Copyright transfer. You will be asked to transfer copyright of the article to the publisher. This transfer will ensure the widest possible dissemination of information.

Electronic manuscripts

The publisher welcomes the receipt of an electronic version of your accepted manuscript (preferably encoded in LaTex). If you have not already supplied the final, revised version of your article (on diskette) to the Journal Editor, you are requested to send a file with the text of the accepted manuscript directly to the Publisher by e-mail or on diskette (allowed formats 3.5″ or 5.25″ MS-DOS, or 3.5″ Macintosh) to the address given below. Please note that no deviations from the version accepted by the Editor of the journal are permissible without the prior and explicit approval by the Editor. Such changes should be clearly indicated on an accompanying printout of the file.

Author benefits

No page charges. Publishing in Optics Communications is free.

Free offprints. The corresponding author will receive 50 offprints free of charge. An offprint order form will be supplied by the publisher for ordering any additional paid offprints.

Discount. Contributors to Elsevier Science journals are entitled to a 30% discount on all Elsevier Science books.

Further information (after acceptance)

Elsevier Science B.V., Optics Communication
Desk Editorial Department
P.O. Box 103, 1000 AC Amsterdam, The Netherlands
Fax: +30 20 4852319
E-mail: H. OOSTEROM@ELSEVIER.NL

1994 PHYSICS and MATERIALS SCIENCE JOURNALS

Applied Surface Science
Volumes 72-81 in 40 issues. Price: US $ 2114.00 / Dfl. 3910.00

Astroparticle Physics
Volume 2 in 4 issues. Price: US $ 182.00 / Dfl. 336.00

Computational Materials Science
Volume 2 in 4 issues. Price: US $ 211.00 / Dfl. 391.00

Computer Physics Communications
Volumes 79-85 in 21 issues. Price: US $ 2236.00 / Dfl. 4137.00

International Journal of Applied Electromagnetics in Materials
Volume 5 in 4 issues. Price: US $ 203.00 / Dfl. 376.00

Journal of Crystal Growth
Volumes 135-145 in 44 issues. Price: US $ 4822.00 / Dfl. 8921.00

Journal of Geometry and Physics
Volumes 13 and 14 in 8 issues. Price: US $ 358.00 / Dfl. 662.00

Journal of Luminescence
Volumes 59-62 in 24 issues. Price: US $ 1083.00 / Dfl. 2004.00

Journal of Magnetism and Magnetic Materials
Volumes 126-137 in 36 issues. Price: US $ 3347.00 / Dfl. 6192.00

Journal of Non-Crystalline Solids
Volumes 162-176 in 45 issues. Price: US $ 3535.00 / Dfl. 6540.00

Journal of Nuclear Materials
Volumes 206-216 in 33 issues. Price: US $ 3098.00 / Dfl. 5731.00

Materials Letters
Volumes 19-22 in 24 issues. Price: US $ 899.00 / Dfl. 1664.00

Nuclear Instruments and Methods in Physics Research - Section A
Accelerators, Spectrometers, Detectors & Associated Equipment
Volumes 337-351 in 45 issues. Price: US $ 5441.00 / Dfl. 10,065.00

Nuclear Instruments and Methods in Physics Research - Section B
Beam Interactions with Materials and Atoms
Volumes 83-94 in 48 issues. Price: US $ 4352.00 / Dfl. 8052.00
Reduced combined 1994 subscription price to Nuclear Instruments and Methods - A and B: US $ 9063.00 / Dfl. 16,767.00

Nuclear Physics A
Volumes 566-580 in 60 issues. Price: US $ 4792.00 / Dfl. 8865.00

Nuclear Physics B
Volumes 409-432 in 72 issues. Price: US $ 7537.00 / Dfl. 13,944.00

Nuclear Physics B - Proceedings Supplements
Volumes 34-38 in 15 issues. Price: US $ 881.00 / Dfl. 1630.00
Reduced combined 1994 subscription price to Nuclear Physics A + Nuclear Physics B + NPB-Proceedings Supplements: US $ 11,202.00 / Dfl. 20,724.00

Optical Materials
Volume 3 in 4 issues. Price: US $ 206.00 / Dfl. 381.00

Optics Communications
Volumes 103-111 in 54 issues. Price: US $ 2121.00 / Dfl. 3924.00

Physica A - Statistical and Theoretical Physics
Volumes 201-211 in 44 issues. Price: US $ 2503.00 / Dfl. 4631.00*

Physica B - Condensed Matter Physics
Volumes 192-202 in 44 issues. Price: US $ 2503.00 / Dfl. 4631.00*

Physica C - Superconductivity
Volumes 219-236 in 72 issues. Price: US $ 4096.00 / Dfl. 7578.00*

Physica D - Nonlinear Phenomena
Volumes 70-78 in 36 issues. Price: US $ 2048.00 / Dfl. 3789.00*

**Reduced rates are available for combined subscriptions to Physica; please contact the publisher for details.*

Physics Letters A
Volumes 185-197 in 78 issues. Price: US $ 2537.00 / Dfl. 4693.00

Physics Letters B
Volumes 317-340 in 96 issues. Price: US $ 4683.00 / Dfl. 8664.00

Physics Reports
Volumes 240-251 in 72 issues. Price: US $ 2342.00 / Dfl. 4332.00
Reduced combined 1994 subscription price to Physics Letters A, Physics Letters B + Physics Reports: US $ 8502.00 / Dfl. 15,729.00

Solid State Ionics
Volumes 68-76 in 36 issues. Price: US $ 1805.00 / Dfl. 3339.00

Surface Science
(including Surface Science Letters)
Volumes 296-318 in 69 issues. Price: US $ 6104.00 / Dfl. 11,293.00

Surface Science Reports
Volume 18-20 in 24 issues. Price: US $ 618.00 / Dfl. 1143.00
Reduced combined 1994 subscription price to Surface Science (including Surface Science Letters), Applied Surface Science and Surface Science Reports: US $ 8192.00 / Dfl. 15,156.00

Ultramicroscopy
Volumes 52-56 in 20 issues. Price: US $ 1151.00 / Dfl. 2130.00

Dutch Guilder price(s) quoted applies worldwide, except in the Americas (North, Central and South America). US Dollar price(s) quoted applies in the Americas only. Journals are sent by Surface Mail to all countries except to the following where Air Delivery via SAL mail is ensured at no extra cost to the subscriber: Argentina, Australia/New Zealand, Brazil, Hong Kong, India, Israel, Japan, Malaysia, Mexico, Pakistan, P.R. China, Singapore, S. Africa, S. Korea, Taiwan, Thailand, USA & Canada. Customers in the European Community should add the appropriate VAT rate applicable in their country to the price(s).

ELSEVIER SCIENCE

ELSEVIER SCIENCE B.V.

P.O. Box 103, 1000 AC Amsterdam, The Netherlands

Elsevier Science Inc., Journal Information Center, PO Box 882, Madison Square Station, New York, NY 10159, U.S.A.

A.4

High-gain nondegenerate two-wave mixing in $Cr:YAlO_3$

High-gain nondegenerate two-wave mixing in Cr:$YAlO_3$

Ian McMichael, Ragini Saxena, and Tallis Y. Chang

Rockwell International Science Center, 1049 Camino Dos Rios, Thousand Oaks, California 91360

Qize Shu and Stephen Rand

Department of Electrical Engineering and Computer Science, University of Michigan, 1301 Beal Avenue, Ann Arbor, Michigan 48109-2122

Jimmy Chen and Harry Tuller

Department of Materials Science and Engineering, Massachusetts Institute of Technology, 77 Massachusetts Avenue, Cambridge, Massachusetts 02139

Received February 28, 1994

A gain of 22 times was obtained by nondegenerate two-wave mixing in Cr:$YAlO_3$. To our knowledge, this is the largest cw two-wave mixing gain obtained in a bulk solid-state nonphotorefractive material. The measured gain appears to be limited by beam breakup that is due to spatial nonuniformities in the nonlinear refractive-index change that are the result of inhomogeneities in the crystal. Predictions based on our data indicate that gain in excess of 200 times should be possible in Cr:$YAlO_3$ if a homogeneous crystal can be obtained.

Recently we demonstrated a gain of six times by nondegenerate two-wave mixing (NDTWM) in chromium-doped yttrium aluminate (Cr:$YAlO_3$).[1] Here we report new experiments in which we achieved a gain of 22 times by increasing both the interaction length and the doping. To our knowledge, this is the largest cw NDTWM gain obtained in a solid-state nonphotorefractive material. The large gains possible in this material should permit the development of cw oscillators and self-pumped conjugators with properties different from those employing photorefractives.

Experiments demonstrating high-gain NDTWM in new solids by use of low-power cw lasers constitute an essential step in establishing the practicality of alternative materials for applications of nonlinear optics in areas such as signal processing. Availability of high gain can bring about rapid progress in experimental research, as occurred with the discovery of photorefractives such as barium titanate ($BaTiO_3$). To our knowledge, however, no one has demonstrated gain comparable with that of photorefractives by using a solid-state bulk (as opposed to guided-wave) Kerr medium with a cw source. We report properties of a candidate material, Cr:$YAlO_3$, that may significantly advance experimental efforts on nonlinear optics in Kerr-like media, much like the way in which basic studies of $BaTiO_3$ initiated widespread study of nonlinear optics in photorefractives. Motivation for this study was provided by the expectation of new properties that should result from the different nonlinear mechanism (Kerr-like versus photorefractive), such as improved dynamic range in mutually pumped phase conjugation,[2] that is important in wave-front-matched heterodyne receivers.[3]

In some metal-ion-doped insulators, such as ruby, metastable states result in low saturation intensities and correspondingly large optical nonlinearities. The origin of the nonlinearity was previously determined to be the result of light-induced population changes and the difference in the susceptibility between the ground and metastable states.[4] Interest in these materials stems from the fact that they are convenient solid-state materials with large optical nonlinearities that can be utilized with relatively low-power cw lasers. Photorefractives also meet these conditions and have demonstrated two-wave mixing gain of $> 10^3$, but the differences in the nonlinear mechanisms make investigation of the metal-ion-doped insulators of interest because of their potential advantages. As one example, the beam ratio for which mutually pumped phase conjugation will take place in photorefractives is limited, but this is not the case in Kerr materials.[2] Our search of the literature addressing nonlinearities in metal-ion-doped insulators indicated that Cr:$YAlO_3$ stands out as the material having the largest potential index change for a given amount of absorption, i.e., the largest value of $n_2 I_S/\alpha$, where I_S is the saturation intensity, n_2 is the optical Kerr coefficient, and α is the absorption coefficient.[5] We therefore chose this material for experimental attempts to obtain high two-wave mixing gain.

As grown, Cr:$YAlO_3$ has a color-center absorption that competes with the absorption responsible for the optical nonlinearity. To remove the color centers, we heated as-grown material in a forming gas atmosphere.[6] Figure 1 shows absorption spectra for the 12-mm-thick end of a boule of Cr:$YAlO_3$ as grown (dotted curve), after a first anneal (dashed curve) in 95% N_2/5% H_2 at 1050 °C for 8 h with a flow rate of 250 cm^3/min and a ramp rate of 1 °C/min, and after a second anneal (solid curve) at 1300 °C for 24 h with the same atmosphere and the same flow and ramp rates as used in the first anneal. After the

0146-9592/94/191511-03$6.00/0

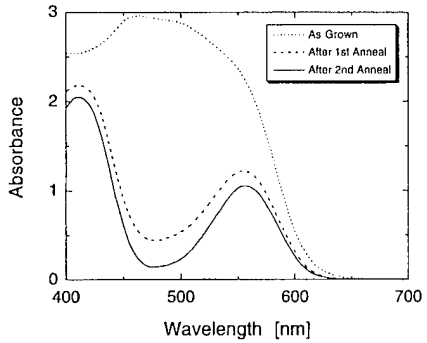

Fig. 1. Cr:$YAlO_3$ absorption spectra showing the bleaching of color centers by heat treatment.

second anneal the boule was fabricated into several crystallographic-cut cubes, one of which was used in these experiments. Microprobe measurements indicated that the Cr concentration was 0.12 wt.%.

Figure 2 is a simplified schematic of the experiment used to measure NDTWM gain.[7] Light from an Ar laser at 514.5 nm is split by a beam splitter into a weak probe beam $I_2(0)$ and a strong pump beam $I_1(0)$. We shift the frequency of the pump with respect to the probe by reflecting it from a mirror mounted to a piezoelectric transducer and driven by a triangle-wave voltage source. This results in a moving interference pattern in the crystal and a population grating that lags in phase because of the finite response time. As in photorefractives, this phase shift is responsible for the energy exchange. The sign of the phase shift depends on the sign of the frequency shift and determines the direction of energy flow. Amplification of the probe results when the mirror moves so that the pump is upshifted, and attenuation results when the mirror moves in the opposite direction so that the pump is downshifted. The triangle-wave frequency and thus the pump frequency was varied to maximize gain. This maximum occurs for a frequency shift of ~5 Hz, consistent with the theoretical behavior described by[7,8] $1/(2\pi\tau) = 4.8$ Hz, where τ is the metastable-state lifetime of 33 ms. Steady state is achieved since the period of our triangle wave (~7 s) greatly exceeds τ.

To obtain the intensities required for high gain, we focus the beams to a $1/e^2$ waist of 210-μm radius at the crystal. We ensure a high degree of overlap in the crystal length $L = 9.1$ mm by having the beams intersect at the small angle of 0.02 rad. The beams were incident nearly parallel to the $\langle 001 \rangle$ direction and s polarized perpendicular to the $\langle \bar{1}10 \rangle$ direction. This polarization and crystal orientation yield the highest peak in the absorption spectrum at 560 nm and the lowest minimum in the residual absorption between peaks at 475 nm. Thus we believe that this configuration yields the greatest interaction with the absorption responsible for the optical nonlinearity and the least interaction with residual color centers. Depletion of the pump is avoided by use of a large input beam ratio, i.e., $I_1(0)/I_2(0) = 1000$.

Figure 3 shows the gain $I_2(L)/I_2(0)$ as a function of the pump intensity. The solid curve is a fit of

$$\frac{I_2(L)}{I_2(0)} = \exp(-\alpha L) \times \exp\left(\left[\frac{1 - \exp(-\alpha L)}{\alpha L}\right]\left\{\frac{2\pi n_2 I_1(0) L/\lambda}{[1 + I_1(0)/I_S]^2}\right\}\right), \quad (1)$$

with $\alpha L = 0.69$, $\lambda = 514.5$ nm, $I_S = \hbar\nu/\sigma\tau = 1.27$ kW/cm^2, where $\hbar$ is Planck's constant, ν is the optical frequency, σ is the absorption cross section, and τ is the metastable-state lifetime. With n_2 as the only adjustable parameter, the fit yields $n_2 = 3.2 \times 10^{-7}$ cm^2/W. The nonlinearity that is due to population effects dominates in both beam coupling and self-focusing because the n_2's for the corresponding thermal effects are at least two orders of magnitude lower. We can derive Eq. (1) from Ref. 8 by including the effect of saturation, which reduces the nonlinear index by a factor $[1 + I_1(0)/I_S]^{-2}$, for $I_1(0) \gg I_2(0)$.

The inset in Fig. 3 shows a plot of the gain for the range from zero to 400 W/cm^2. With the previously stated parameters and n_2 from the fit for the lower-intensity range, the curve in the inset represents a theoretical projection based on Eq. (1). A gain of 22 times was obtained at approximately 400 W/cm^2, but the measured gain does not increase with intensity as much as theory predicts. (Theory predicts a gain of 200 at 400 W/cm^2.) We believe this is due to beam breakup resulting from spatial nonuniformities of the nonlinear refractive-index change in the interaction region. As evidence, Fig. 4 shows the transmitted pump *with the probe off* (a) at low intensity and normal exposure (0.6 W/cm^2, 1/100 s) indicating the transmitted beam size, (b) at low intensity and at a longer exposure (1.4 W/cm^2, 1 s)

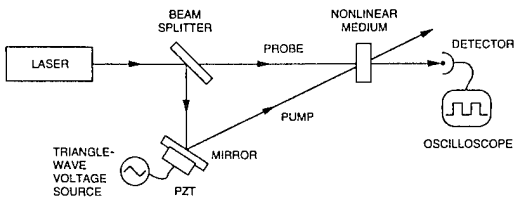

Fig. 2. Simplified schematic of the experiment used to measure NDTWM. PZT, piezoelectric transducer.

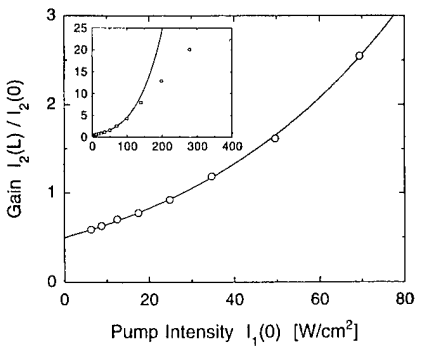

Fig. 3. Gain versus pump intensity. The solid curve is a fit of Eq. (1). The inset shows that, at high intensity, the measured gain does not increase with intensity as much as theory predicts. We believe this is due to beam breakup resulting from spatial nonuniformities of the nonlinear refractive-index change.

(a) (b) (c)

Fig. 4. Transmitted pump with the probe off (a) at low intensity and normal exposure indicating the transmitted beam size, (b) at low intensity and long exposure showing an X-shaped pattern of linear scattering from crystal striae, and (c) at high intensity and an exposure equivalent to that in (b), showing the beam breakup. For all photographs the plane of incidence is the horizontal.

to reveal the X-shaped pattern of weak linear scattering that is believed to be the result of scattering by crystal striae, and (c) at high intensity and an exposure equivalent to that in (b) (140 W/cm^2, 1/100 s) showing the nonlinear scattering that is due to nonuniformities in the nonlinear refractive-index change.

Spatial nonuniformities of the nonlinear refractive-index change in the interaction region can be the result of shadows or distortions from surface or bulk defects or from spatial variations in the Cr-ion concentration. Photographs of the crystal illuminated by a low-intensity collimated beam show radial and concentric patterns thought to be Cr striae. Images of a low-intensity pump beam inside the crystal also indicate that the striae have a significant effect on the beam profile. Beam breakup can result both from variations in Cr concentration, yielding a variation in n_2, and from intensity variations, yielding variations in the induced nonlinear index change.

Qualitative behavior indicated that the scattering at high intensity was nonlinear, but to confirm this we measured the intensity of a small region of the scattering as a function of the pump intensity. An aperture was closed down to a diameter such that, at low intensity, it would pass one half of the pump that transmitted through the crystal, and then it was placed in the speckle of the scatter indicated by the arrow in Fig. 4(c). Measurements indicated that the nonlinear portion of the scatter had a cubic dependence on the pump intensity.

We made the following observations concerning the scattering: (1) the strength of the nonlinear scattering depended on feedback into the crystal and (2) a threshold existed above which the speckle pattern of the scattering was dynamic. An experiment examining the interference between a portion of the transmitted pump and a speckle did not detect any frequency shift. This indicated that the dynamic scattering at high intensities was not due to beating between frequency-shifted stimulated scattering resulting from NDTWM gain and some linear scattering from crystal inhomogeneities. When the crystal was oriented to retroreflect the pump or when an external mirror was used, the strength of the nonlinear scattering increased and the threshold of dynamic scattering decreased. To obtain the highest gains in the NDTWM measurements we rotated the crystal away from normal to reduce the nonlinear scattering. An angle of incidence for the pump of 0.03 rad yielded the largest gains. Further reductions in the feedback resulting from the rear surface reflection might improve the gain.

In conclusion, we demonstrated a gain of 22 times by NDTWM in Cr:$YAlO_3$. The gain appears to be limited by beam breakup resulting from spatial nonuniformities in the nonlinear refractive-index change that are the result of inhomogeneities in the crystal. Theory predicts that gain in excess of 200 times should be possible in a homogeneous crystal. Thus, like photorefractives, Cr:$YAlO_3$ is a convenient solid having the potential for high gain by use of cw lasers. Interest in Cr:$YAlO_3$ stems from the difference in nonlinearity (Kerr-like versus photorefractive) and the resulting potential for new properties rather than from any improvement in sensitivity or speed. Indeed, the sensitivity of Cr:$YAlO_3$ ($\sim 10^{-11}$ m^3/J) is 2 orders of magnitude below that of $BaTiO_3$. Nor is Cr:$YAlO_3$ particularly fast; the grating decay time in Cr:$YAlO_3$ is determined by the metastable lifetime of 33 ms, and this is comparable with the fastest grating decay times obtained in $BaTiO_3$ under moderate illumination. Although speed increases with intensity in photorefractives, it is not clear that they can withstand the intensities used with Cr:$YAlO_3$, making a direct comparison difficult. Gain is determined by the index change, and the maximum possible index change in Cr:$YAlO_3$ ($\Delta n_{max} \sim n_2 I_S = 4 \times 10^{-4}$) is comparable with that of $BaTiO_3$. In addition to its having potential for new properties resulting from the different nonlinear mechanism, we note that Cr:$YAlO_3$ is only one example of a large class of metal-ion-doped insulators. Admittedly, it has the best performance to date, but an effort to develop metal-ion-doped insulators as nonlinear materials that is as extensive as that undertaken for photorefractives may yield new materials with improved figures of merit.

The authors thank R. Hutcheson, R. Belt, M. Kokta, L. DeShazer, M. Weber, S. Payne, D. Steel, R. Powell, and C. Weaver for discussions. This research was sponsored by the U.S. Air Force Office of Scientific Research under contract F49620-92-C-0023, with partial support from grant AFOSR-91-0369.

References

1. I. McMichael, R. Saxena, T. Chang, R. Neurgoankar, and S. Rand, in *Conference on Lasers and Electro-Optics,* Vol. 11 of 1993 OSA Technical Digest Series (Optical Society of America, Washington, D.C., 1993), paper CThS34, pp. 514–515.
2. R. Saxena and P. Yeh, J. Opt. Soc. Am. B **7,** 326 (1990).
3. L. Adams and R. Bondurant, Opt. Lett. **16,** 832 (1991).
4. P. Liao and D. Bloom, Opt. Lett. **3,** 4 (1978).
5. D. Steel, S. Rand, and J. Liu, J. Opt. Soc. Am. B **4,** 1794 (1987).
6. M. J. Weber and T. E. Varitimos, J. Appl. Phys. **45,** 810 (1974).
7. I. McMichael, P. Yeh, and P. Beckwith, Opt. Lett. **13,** 500 (1988).
8. P. Yeh, J. Opt. Soc. Am. B **3,** 747 (1986).

A.5

Brillouin Induced Mutually Pumped Phase Conjugation in Reflection Geometry

Brillouin Induced Mutually Pumped Phase Conjugation in Reflection Geometry

R. Saxena and I. McMichael

Rockwell International Science Center

Thousand Oaks, CA 91360

(805) 373-4157

Abstract

We study the problem of two beams phase conjugating each other via mutually generated reflection gratings in an electrostrictive medium. We present the first solutions to the transcendental equation that illustrate large dynamic range.

Brillouin Induced Mutually Pumped Phase Conjugation in Reflection Geometry

R. Saxena and I. McMichael
Rockwell International Science Center
Thousand Oaks, CA 91360
(805) 373-4157

SUMMARY

A mutually pumped phase conjugator (MPPC) generates the phase-conjugate replicas of *two* incoherent incident beams. Each input beam is converted into the phase-conjugate replica of the other by Bragg diffraction off a shared grating. In photorefractive media, several configurations differing in their number of internal reflections from the crystal surfaces were demonstrated;[1] for efficient operation, the two incoherent beams must have comparable input intensities. However, applications like phase-conjugate heterodyne detection[2] require the device to work for large imbalance of input beam intensities, when a weak optical signal from a remote transmitter is combined with the strong beam from a local oscillator. A modest extension of the dynamic range can be obtained by increasing the photorefractive gain;[1] however, it is desirable to extend the dynamic range of the device to several orders of magnitude.

MPPC has also been studied in electrostrictive Kerr media by utilizing the Brillouin gain in a transmission geometry.[3] An advantage of MPPC in electrostrictive Kerr media over photorefractive media is the large dynamic range of input beam ratio over which the process will occur. This is because if one beam intensity is large enough to satisfy the threshold condition for the total beam intensity, then a small intensity of the second beam will initiate the process of MPPC. However, none of this work has been corroborated experimentally. There has been recent theoretical and experimental work on MPPC in electrostrictive Kerr media using the reflection geometry.[4] That large dynamic range was also possible in reflection geometry was discussed in Ref. 4, but here we present the first solutions to the transcendental equation that illustrate this possibility.

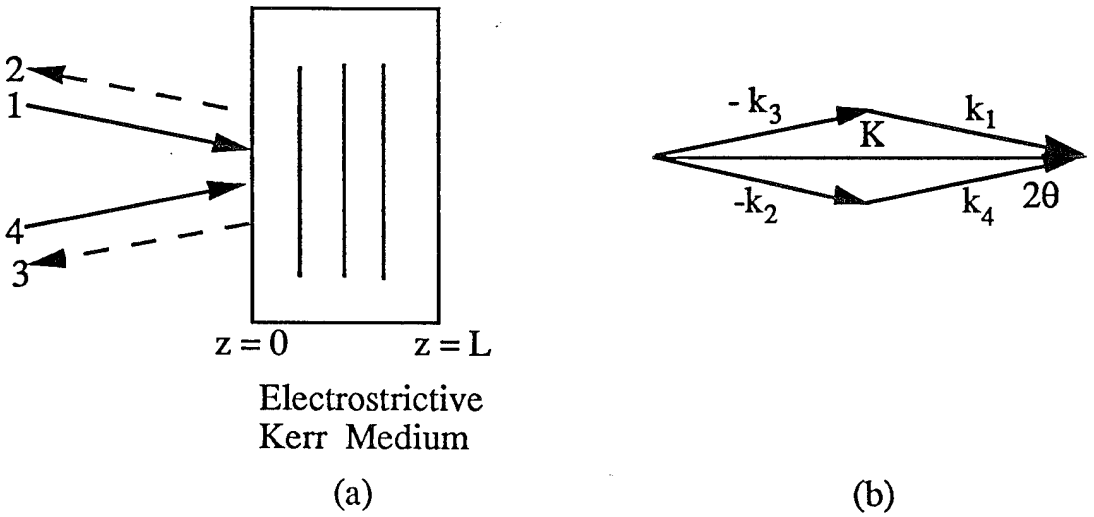

Fig. 1 (a) Schematic diagram showing MPPC using reflection gratings in an electrostrictive Kerr medium. (b) Wave vector diagram for MPPC using reflection gratings.

The geometry for the nonlinear interaction responsible for MPPC is shown in Fig.1(a) and Fig.1(b). Input beams 1 and 4 are a pair of mutually incoherent beams that enter through the front face of the nonlinear medium and intersect at an angle 2θ. Acoustic phonons that are initially present in a transparent Kerr medium like CS_2 due to thermal and quantum noise cause Stokes scattering of the input beams in all directions. Also, a photon from each input beam can be spontaneously converted into a frequency downshifted Stokes photon and an acoustic phonon. The coherently generated Stokes waves will interfere with the input beam to produce interference patterns which travel at the acoustic velocity, and which drive acoustic waves by electrostriction.[5] These acoustic waves induce index gratings in the medium, and the index grating that diffracts each incoherent input beam into the phase-conjugated output of the other input beam beam will be reinforced by both the beams. Hence this mutual index grating has the maximum gain compared to all the other possible gratings, and we label the corresponding Stokes scattered wave of input beam 1 as beam 3, beam 3 being the phase-conjugate of input beam 4. Similarly, the relevant Stokes wave of input beam 4 is beam 2, and this is the phase-conjugate of pump beam 1. Coupled-wave equations for the complex beam amplitudes A_i (i=1to 4) describe the energy exchanged between the various beams at steady-state:

$$\frac{dA_1}{dz} = -\frac{g}{2}\,(A_1A_3^* + A_2^*A_4)\,A_3$$

$$\frac{dA_2}{dz} = -\frac{g}{2}\,(A_1^*A_3 + A_2A_4^*)\,A_4$$

$$\frac{dA_3}{dz} = -\frac{g}{2}\,(A_1^*A_3 + A_2A_4^*)\,A_1$$

$$\frac{dA_4}{dz} = -\frac{g}{2}\,(A_1A_3^* + A_2^*A_4)\,A_2 \quad , \tag{1}$$

where g is the Brillouin gain coefficient. Assuming non-zero Stokes seeds at the z = L backplane that arise from the mutual scattering of each input beam in a direction counterpropagating to the other input beam: $A_{2L} = f\,A_4(L)$, $A_{3L} = f\,A_1(L)$, f being the mutual scattering coefficient that is equal in amplitude and phase for both the pumps, we obtain the following transcendental equation for the phase-conjugate reflectivity $R \equiv |A_3(0)/A_{40}^*|^2$:

$$R = q\,|f|^2 \exp[G(1-R/q)] \quad . \tag{2}$$

Here q is the intensity ratio of the two incoherent beams at the z= 0 input plane: $q \equiv I_{10}/I_{40}$, and $G \equiv g(I_{10}+I_{40})L$ is the total Brillouin gain. The phase-conjugate reflectivity S in the other arm is equal to $|A_2(0)/A_{10}^*|^2$ and is related to R by: $S = R/q^2$. The device transmissivity T measures the fraction of each input beam that is converted into the phase-conjugate output of the other beam, and is equal for both inputs. Note that if $|f|^2 = 0$, i.e., $I_{2L} = I_{3L} = 0$, then the phase-conjugate reflectivities R and S are equal to zero. Hence finite seed values of the Stokes waves are required for MPPC to work in reflection geometry. Fig. 2 is a plot of the solutions of Eq. (2) showing the phase-conjugate reflectivities R, S and transmissivity T as a function of the input intensity ratio q on a log-log scale, for a fixed value of Brillouin gain G_4=18 satisfied by the strong input beam 4. This is below the threshold value required for self-SBS (~ 23) of input beam 4. We take $|f|^2 = 10^{-12}$ for noise induced Stokes scattering. Increasing q is equivalent to

increasing I_{10}, keeping I_{40} and hence G_4 fixed. Note that the weak input beam I_{10} ($q = 10^{-6}$) is phase-conjugated with a reflectivity greater than unity. ($S = 60$). Since S is inversely proportional to I_{10}, S decreases with increasing q for $q \leq 10^{-1}$. As q is further increased, the total Brillouin gain increases, leading to increased conversion of input beam I_{40} into the Stokes beam $I_2(0)$, as seen by the increase in T. This compensates for the decrease of S with increasing I_{10}, so that S actually increases for a limited range of q values. When the total Brillouin gain is enough to convert most of the input beams into their Stokes waves, then any further increase in q results in decreasing S once again. R is a monotonically increasing function of q because its denominator I_{40} is a fixed quantity, and increase in I_{10} results in more conversion of this input beam into its Stokes wave $I_3(0)$.

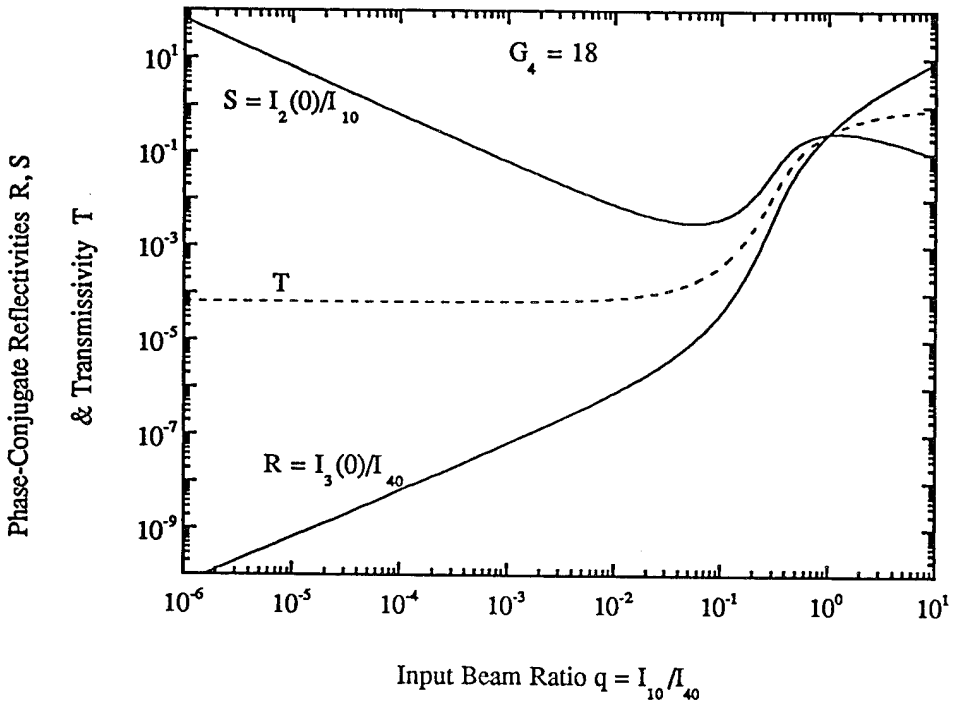

Fig. 2 Phase-conjugate reflectivities R, S and transmissivity T as a function of intensity ratio of the two input beams q, for $|f|^2 = 10^{-12}$ and $G_4 = 18$.

In conclusion, we studied Brillouin induced MPPC in the reflection geometry and obtained solutions illustrating that a weak beam can be phase-conjugated with reflectivities larger than unity. The technique works for a large dynamic range of input beam ratio as the intensity of the weak input beam is increased, while the intensity of the strong incoherent input beam is kept constant below the threshold value for self-SBS.

REFERENCES

1. S. Sternklar, S. Weiss and B. Fischer, Opt. Eng. **26**, 423 (1987)
2. L. E. Adams and R. S. Bondurant, Opt. Lett. **16**, 832 (1991).
3. R. Saxena and P. Yeh, J. Opt. Soc. Am. B **7**, 326 (1990).
4. S. Sternklar, Opt. Lett. **17**, 1403 (1992).
5. A. M. Scott and K. D. Ridley, IEEE J. Quanum Electron. **QE-25**, 438 (1989).

A.6

High Gain Nondegenerate Two-Wave Mixing in $Cr:YAlO_3$

High Gain Nondegenerate Two-Wave Mixing in $Cr:YAlO_3$

Ian McMichael, Ragini Saxena, and Tallis Y. Chang

Rockwell International Science Center

1049 Camino Dos Rios

Thousand Oaks, CA 91360

(805) 373-4508

Qize Shu and Stephen Rand

Department of Electrical Engineering and Computer Science

University of Michigan

1301 Beal Avenue

Ann Arbor, MI 48109-2122

Jimmy Chen and Harry Tuller

Materials Science & Engineering Department

Massachusetts Institute of Technology

77 Massachusetts Avenue

Cambridge, MA 02139

Abstract

A gain of 22 times was obtained by nondegenerate two-wave mixing in $Cr:YAlO_3$. Theoretical predictions based on our experimental data indicate that gain in excess of 200 times should be possible in $Cr:YAlO_3$ if a homogeneous crystal can be obtained.

High Gain Nondegenerate Two-Wave Mixing in $Cr:YAlO_3$

Ian McMichael, Ragini Saxena, and Tallis Y. Chang
Rockwell International Science Center
1049 Camino Dos Rios
Thousand Oaks, CA 91360
Phone: (805) 373-4508
Fax: (805) 373-4775

Qize Shu and Stephen Rand
Department of Electrical Engineering and Computer Science
University of Michigan
1301 Beal Avenue
Ann Arbor, MI 48109-2122

Jimmy Chen and Harry Tuller
Materials Science & Engineering Department
Massachusetts Institute of Technology
77 Massachusetts Avenue
Cambridge, MA 02139

Summary

Recently we demonstrated a gain of 6 times that was obtained by nondegenerate two-wave mixing in $Cr:YAlO_3$.[1] Here we report new experiments in which a gain of 22 times was achieved by increasing both the interaction length and the doping of the material. To our knowledge, this is the largest cw two-wave mixing gain obtained in a bulk, solid state, non-photorefractive material. Experiments demonstrating high gain, nondegenerate two-wave mixing in new solids using low power cw lasers constitute an essential step in establishing the viability of alternative materials for applications of nonlinear optics in areas such as signal processing. Availability of high gain can bring about rapid progress in experimental research, as occurred with the discovery of photorefractive materials such as barium titanate. To our knowledge however, no one has demonstrated gain comparable to that of photorefractive materials by using a solid state bulk (as opposed to guided wave) Kerr medium with a cw source. We report properties of a candidate material, chromium-doped yttrium aluminate ($Cr:YAlO_3$), that may significantly advance experimental efforts on nonlinear optics in Kerr-like media, much the way basic studies of barium titanate initiated widespread study of nonlinear optics in photorefractive materials. Motivation for the present work was provided by the expectation of new properties that should result from the different nonlinear mechanism (Kerr-like vs. photorefractive), such as improved dynamic range in mutually pumped phase conjugation[2] that is important in wavefront matched heterodyne receivers.[3]

Figure 1 is a simplified schematic of the experiment used to measure gain in nondegenerate two-wave mixing.[4] Light from an argon laser is split into a weak probe beam $I_2(0)$ and a strong pump $I_1(0)$, with a fixed ratio $I_2(0)/I_1(0) = 1/1000$. The frequency of the pump is shifted by approximately 5 Hz with respect to the probe by reflecting it from a mirror mounted to a piezoelectric transducer and driven by a triangle-wave voltage source. The grating formed by the interaction of the pump and probe in the crystal of $Cr:YAlO_3$ results in amplification for the probe when the mirror is moving in one direction, and attenuation when the mirror moves in the opposite direction.

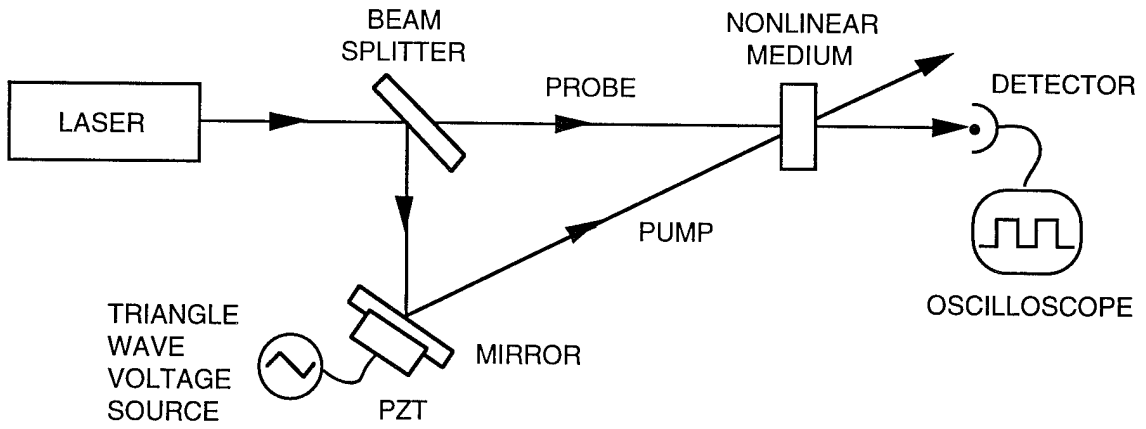

Fig. 1 Schematic of experiment used to measure nondegenerate two-wave mixing gain.

Figure 2 (a) shows a plot of the gain as a function of the intensity of the pump for the range from 0 to 80 W/cm^2. The circles are the experimental measurements, and the line is a fit of the theoretical form,

$$\frac{I_2(L)}{I_2(0)} = e^{-\alpha L} \exp\left\{\left(\frac{1-e^{-\alpha L}}{\alpha L}\right)\left[\frac{2\pi n_2 I_1(0) L/\lambda}{\left(1+I_1(0)/I_S\right)^2}\right]\right\} \tag{1}$$

with $\alpha L = 0.69$, L = 9.1 mm, $\lambda = 514.5$ nm and $I_S = h\nu/\sigma\tau = 1.27$ kW/cm^2, where h is Planck's constant, ν is the optical frequency, σ is the absorption cross-section and τ is the metastable state lifetime. Using n_2 as the only adjustable parameter, the fit yields $n_2 = 3.2 \times 10^{-7}$ cm^2/W.

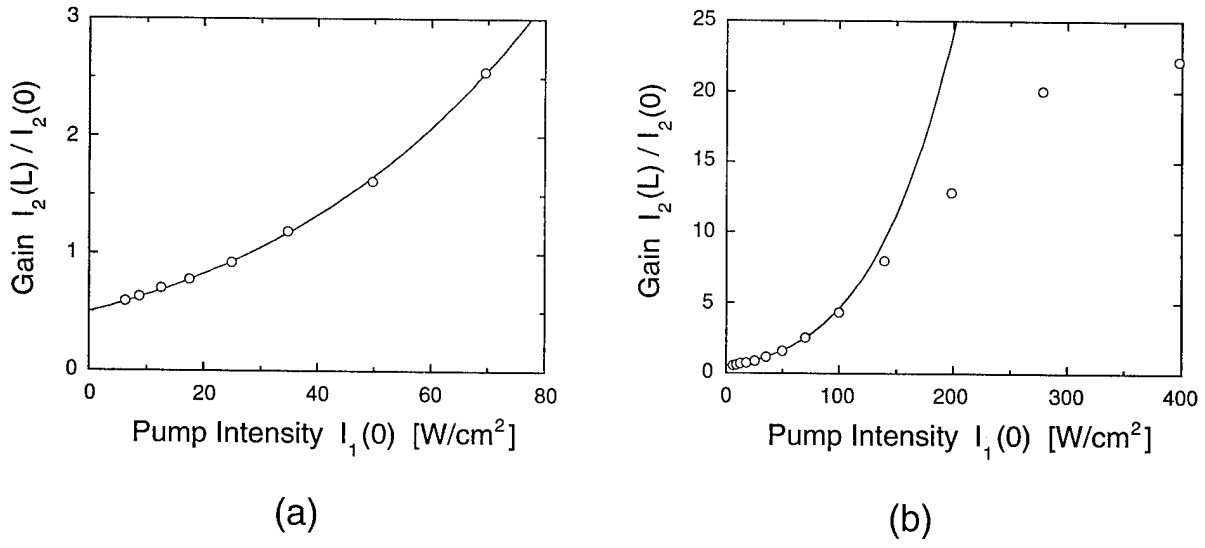

Fig. 2 Gain vs. pump intensity: (a) from 0 to 70 W/cm^2, and (b) from 0 to 400 W/cm^2.

Figure 2 (b) shows the gain for the range from 0 to 400 W/cm^2. Using the previously stated parameters and n_2 as determined from the fit for the lower intensity range of Fig. 2(a), the line in Fig. 2(b) represents projections based on the theoretical form expressed by Eq. (1). A gain of 22 times was obtained at approximately 400 W/cm^2, but the measured gain does not increase with intensity as much as theory predicts. (Theory predicts a gain of 200 at 400 W/cm^2.) We believe this is due to "beam break-up" resulting from spatial nonuniformities of the nonlinear refractive index change in the interaction region. As evidence, Fig. 3 shows photographs of the transmitted pump beam with the probe beam off, (a) at low intensity and normal exposure indicating the transmitted beam size, (b) at low intensity and long exposure showing an "X" shaped pattern of linear scattering that is believed to be the result of scattering from surface and bulk defects, and (c) at high intensity and exposure equivalent to case (b) showing both the nonlinear scattering due to nonuniformities in the nonlinear refractive index change, and the linear scattering due to surface and bulk defects. Spatial nonuniformities of the nonlinear refractive index change in the interaction region can be the result of shadows or distortions from surface or bulk defects, or from spatial variations in the Cr-ion concentration.

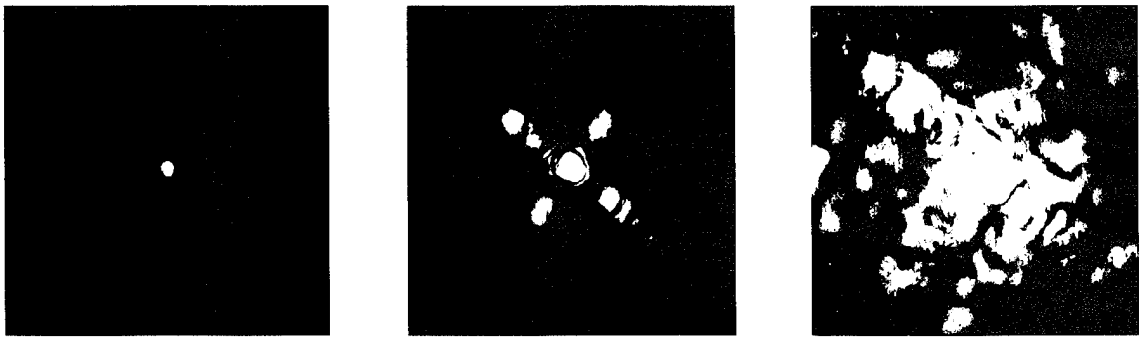

Fig. 3 Photographs of the transmitted pump beam, (a) Gaussian beam size, (b) "X" shaped pattern resulting from linear scattering, and (c) nonlinear scattering.

In conclusion, we have demonstrated a gain of 22 times by nondegenerate two-wave mixing in Cr:$YAlO_3$. The experimentally measured gain appears to be limited by "beam break-up" due to spatial nonuniformities in the nonlinear refractive index change, that are the result of inhomogeneities in the crystal. Theoretical predictions based on our experimental data indicate that gain in excess of 200 times should be possible in Cr:$YAlO_3$ if a homogeneous crystal can be obtained. Due to its potential for such high gain, Cr:$YAlO_3$ is a very promising material for applications of nonlinear optics in areas such as signal processing, making it clear that additional experimental efforts are warranted to explore nonlinear response in solid-state Kerr-like media generally, and to investigate further the potential advantages of materials like Cr:$YAlO_3$ over photorefractive crystals.

References

1. I. McMichael, R. Saxena, T. Chang, R. Neurgoankar, and S. Rand, in *Conference on Lasers and Electro-Optics, 1993* (Optical Society of America, Washington, D.C., 1993), paper CThS34, pp. 514-515.
2. R. Saxena and P. Yeh, J. Opt. Soc. Am. **B 7**, 326 (1990).
3. L. Adams and R. Bondurant, Opt. Lett. **16**, 832 (1991).
4. I. McMichael, P. Yeh, and P. Beckwith, Opt. Lett. **13**, 500 (1988).

A.7

High Gain Nondegenerate Two-Wave Mixing in Cr:$YAlO_3$

High Gain Nondegenerate Two-Wave Mixing in $Cr:YAlO_3$

Ian McMichael, Ragini Saxena, Tallis Y. Chang, and Ratnakar Neurgaonkar

Rockwell International Science Center

1049 Camino Dos Rios

Thousand Oaks, CA 91360

(805) 373-4508

Stephen Rand

Department of Electrical Engineering and Computer Science

University of Michigan

1301 Beal Avenue

Ann Arbor, MI 48109-2122

Abstract

Beam coupling gain of 6 times was obtained by nondegenerate two-wave mixing in $Cr:YAlO_3$. To our knowledge, this is the largest cw gain obtained in a solid state, non-photorefractive material. This material will allow the study of cw oscillators and self-pumped conjugators, with properties different from those using photorefractives.

High Gain Nondegenerate Two-Wave Mixing in Cr:$YAlO_3$

Ian McMichael, Ragini Saxena, Tallis Y. Chang, and Ratnakar Neurgaonkar

Rockwell International Science Center

1049 Camino Dos Rios

Thousand Oaks, CA 91360

Phone: (805) 373-4508

Fax: (805) 373-4775

Stephen Rand

Department of Electrical Engineering and Computer Science

University of Michigan

1301 Beal Avenue

Ann Arbor, MI 48109-2122

Phone: (313) 763-6810

Fax: (313) 763-1503

Summary

Beam coupling gain of 6 times was obtained by nondegenerate two-wave mixing in Cr:$YAlO_3$. To our knowledge, this is the largest cw gain obtained in a solid state, non-photorefractive material. This material will allow the study of cw oscillators and self-pumped conjugators, with properties different from those of photorefractives.

In some metal-ion doped insulators, such as ruby, metastable states result in low saturation intensities and correspondingly large optical nonlinearities. The origin of the nonlinearity in these materials was previously determined to be the result of light induced

population changes and the difference in the susceptibility between the ground and metastable states.[1] Interest in these materials stems from the fact that they are convenient, solid state materials with large optical nonlinearities that can be utilized with relatively low power cw lasers. Photorefractive materials also meet these conditions and have demonstrated very large beam coupling gain, but the difference in the nonlinear mechanisms makes investigation of the metal-ion doped insulators of interest. As one example, the beam ratio for which mutually-pumped phase conjugation will take place in photorefractives is limited, but this is not the case in Kerr materials.[2] Our search of the literature on nonlinearities in metal-ion doped insulators indicated that $Cr:YAlO_3$ stands out as the material having the largest potential index change for a given amount of absorption (i.e., largest value of $n_2 I_S/\alpha$, where I_S is the saturation intensity and n_2 and α are the optical Kerr and absorption coefficients, respectively).[3] We therefore chose this material for our experimental attempts to obtain high gain.

Figure 1 is a simplified schematic of the experiment used to measure gain in nondegenerate two-wave mixing.[4] Light from an argon laser at 515 nm is split by a beam splitter into a weak probe beam and a strong pump beam, with the probe to pump beam ratio of 1:100. The frequency of the pump beam is shifted with respect to the probe beam by reflecting it from a mirror mounted to a piezoelectric transducer and driven by a triangle wave voltage source. The grating formed by the interaction of the pump and probe beams in the nonlinear medium results in amplification for the probe when the mirror is moving in one direction, and attenuation of the probe when the mirror moves in the opposite direction. After transmission through the nonlinear medium, the probe is detected and the signal is recorded on an oscilloscope. Figure 2 shows the signal recorded on the oscilloscope at a pump intensity of 0.6 kW/cm^2. The triangle wave is the voltage applied to the piezoelectric transducer, the solid line at the base corresponds to zero signal, the dashed line corresponds to the signal level with the pump off, and the remaining line is the signal with the pump on. When the triangle wave is ramping down, there is gain for the probe, and at its maximum amplitude the gain is approximately 6 times. Figure 3 shows the gain

as a function of the pump intensity. The crosses are the data and the solid line is a fit to theory yielding $n_2 \sim 1.4 \times 10^{-7}$ cm^2/W.

The 6-times gain is nearly enough to demonstrate a ring conjugator. We are currently attempting to obtain higher gain by using materials with higher Cr doping. This research was sponsored by the U.S. Air Force Office of Scientific Research under contract F49620-92-C-0023.

References

1. P. Liao and D. Bloom, Opt. Lett. **3**, 4 (1978).
2. R. Saxena and P. Yeh, J. Opt. Soc. Am. **B7**, 326 (1990).
3. D. Steel, S. Rand and J. Liu, J. Opt. Soc. Am. **B4**, 1794 (1987).
4. I. McMichael, P. Yeh and P. Beckwith, Opt. Lett. **13**, 500 (1988).

Figure Captions

Fig. 1 Simplified schematic of the experiment used to measure gain in nondegenerate two-wave mixing.

Fig. 2 Signal recorded on the oscilloscope at a pump intensity of 0.6 kW/cm^2. The triangle wave is the voltage applied to the piezoelectric transducer, the solid line at the base corresponds to zero signal, the dashed line corresponds to the signal level with the pump off, and the remaining line is the signal with the pump on.

Fig. 3 Gain as a function of the pump intensity. The crosses are data and the solid line is a fit to theory.

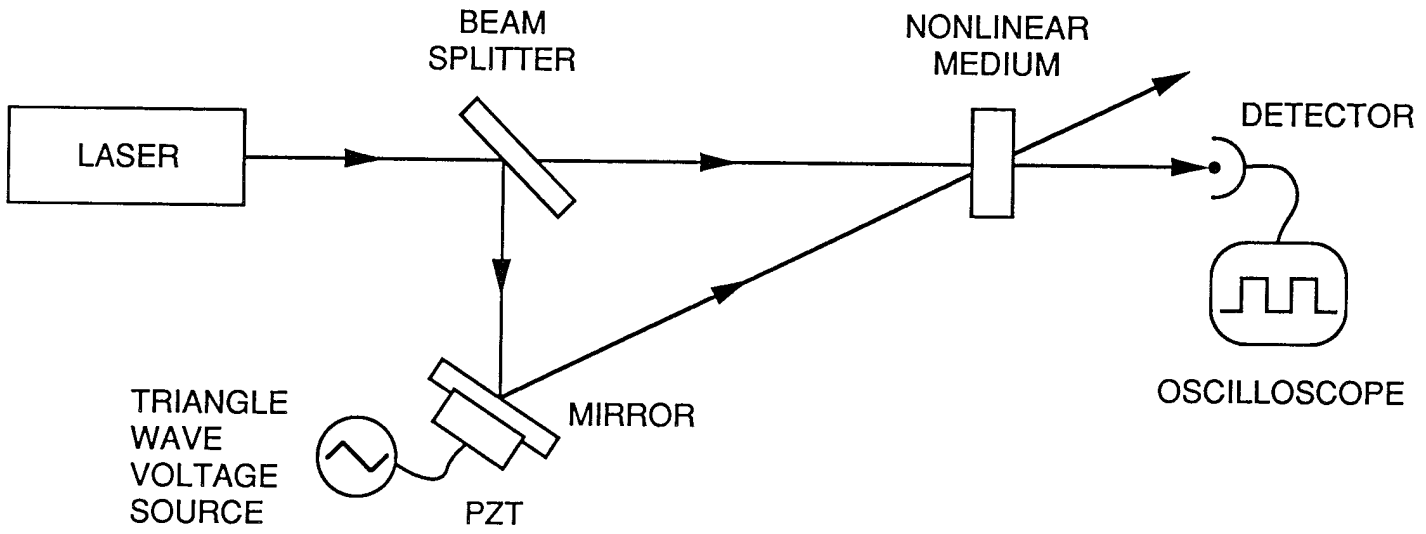

Fig. 1

McMichael, et. al.
CLEO 93

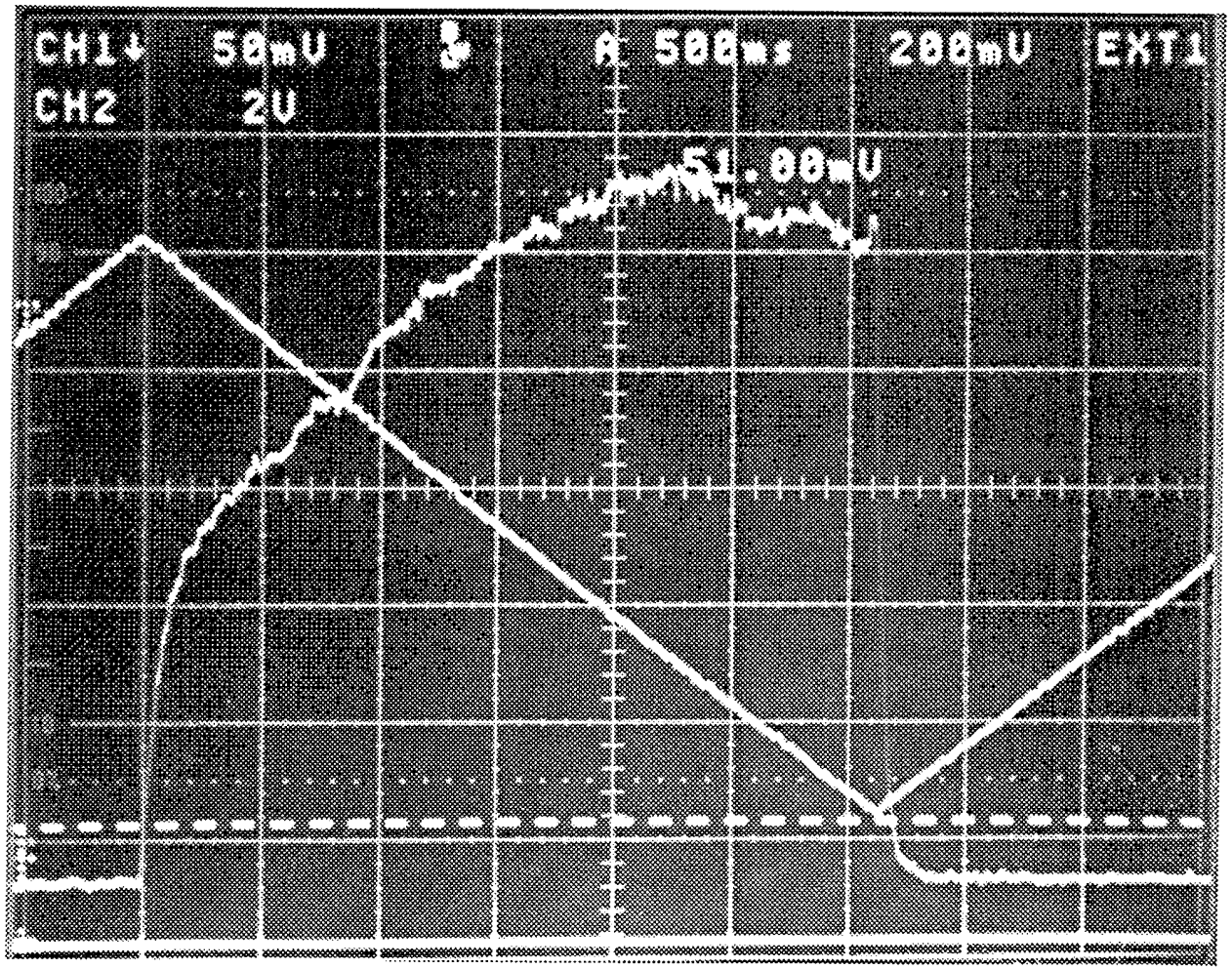

Fig 2
McMichael, et al
CLEO 93

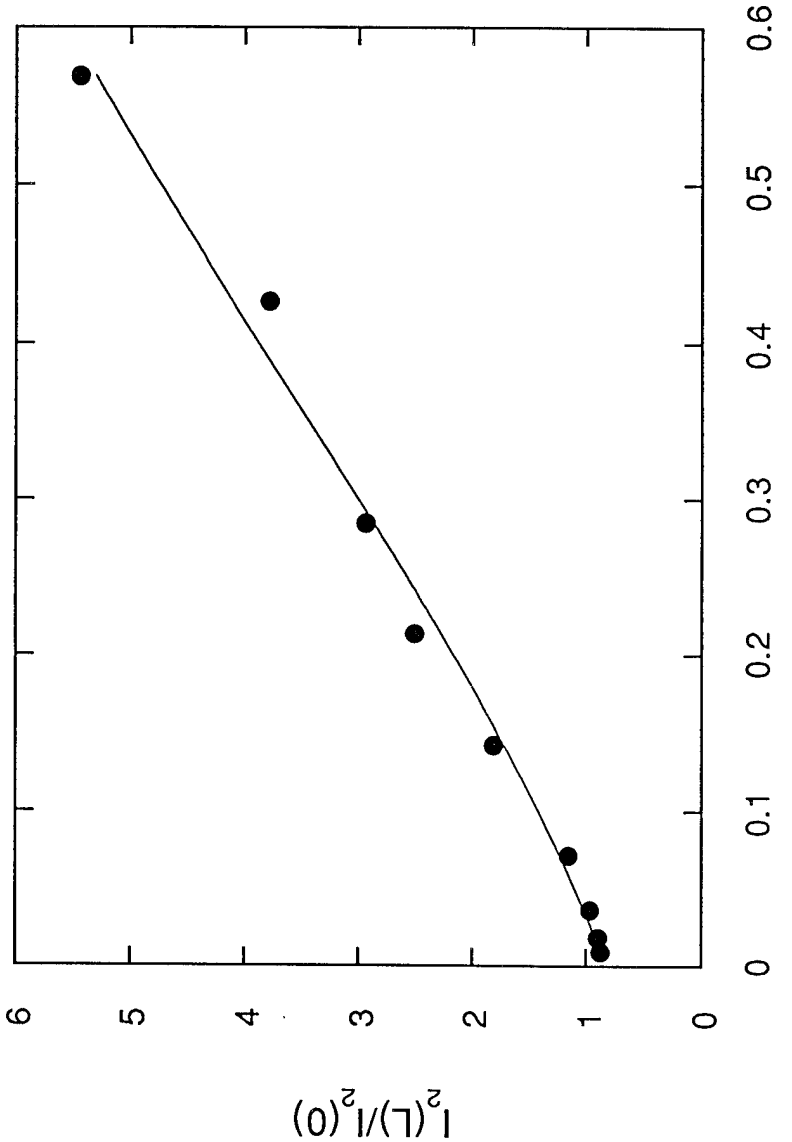

Fig. 3

A.8

Brillouin Induced Mutually Pumped Phase Conjugation in Reflection Geometry

Brillouin Induced Mutually Pumped Phase Conjugation in Reflection Geometry

R. Saxena and I. McMichael

Rockwell International Science Center

Thousand Oaks, CA 91360

Abstract

Two incoherent laser beams mutually pump each other to generate Stokes-shifted phase-conjugate replicas of each other via reflection gratings in an electrostrictive medium. For Stokes scattering initiated by noise, a phase-conjugate reflectivity of 1% in each arm requires a combined Brillouin gain of 23. The technique works for a large dynamic range of input beam ratio as the intensity of a weak input beam is increased, while the intensity of the second input beam is fixed below the threshold value for self-stimulated Brillouin scattering. The weak beam is phase-conjugated with reflectivities larger than unity, and the upper limit to the dynamic range is set by competition from self-stimulated Brillouin scattering.

1. INTRODUCTION

A mutually pumped phase conjugator (MPPC) generates the phase-conjugate replicas of *two* incoherent incident beams. Each input beam is converted into the phase-conjugate replica of the other by Bragg diffraction off a shared grating. In photorefractive media, several configurations differing in their number of internal reflections from the crystal surfaces were demonstrated using transmission gratings.[1-5] MPPC has been used for beam cleanup[6] of a pulsed laser beam,[7] self-aligning injection locking of a laser diode array,[8,9] two-way optical communication,[10] interferometry,[11] dynamically programmable self-aligning optical interconnects,[12] and phase-conjugate heterodyne detection.[13] For an efficient MPPC, the two incoherent beams must have comparable input intensities.[14] However, applications like phase-conjugate heterodyne detection[13] require the device to work for large imbalance of input beam intensities, when a weak optical signal from a remote transmitter is combined with the strong beam from a local oscillator. A modest extension of the dynamic range can be obtained by increasing the photorefractive gain;[14] however, it is desirable to extend the dynamic range of the device to several orders of magnitude. We also note that MPPC using reflection gratings in photorefractive media has been demonstrated for two configurations: a single interaction region with no internal reflection,[15] and the geometry of two interconnected rings.[16]

Saxena and Yeh[17] have shown theoretically that MPPC is also possible in electrostrictive Kerr media by Brillouin gain in a transmission geometry. Their results showed that the Brillouin intensity gain required for this process was 4, much lower than that required for self-stimulated Brillouin scattering (~25) or Brillouin enhanced four-wave mixing (~10).[18] This value is identical to the threshold gain required for the double phase-conjugate mirror in photorefractive media.[1,19] An advantage of MPPC in electrostrictive Kerr media over photorefractive media is the large dynamic range of input beam ratio over which the process will occur.[17] This is because if one beam is strong

enough to satisfy the threshold condition, then a mere presence of the second beam will initiate the process of MPPC. Ridley[20] extended the steady-state analysis of Ref. 17 to a time-dependent one, and arrived at an expression for the growth rate of the forward scattered light by ignoring pump depletion. To the best of our knowledge, none of this work has been corroborated experimentally. There has been recent theoretical and experimental work by Sternklar[21] on MPPC in electrostrictive Kerr media using the reflection geometry. His results showed that the *combined* Brillouin gain required for this process is of the same order as that for self-stimulated Brillouin scattering (SBS); however, the issue of large dynamic range for the input beam ratio was not examined. In this paper, we study Brillouin induced MPPC in the reflection geometry and compare its performance with that in the transmission geometry. We show that the device works for a large dynamic range of input beam ratio by increasing the intensity of a weak input beam, while fixing the intensity of the second input beam below the threshold value for self-SBS. The upper limit to the dynamic range is set by competition from self-SBS of the first beam. We also note that Brillouin induced self-pumped phase conjugation of a single beam using reflection gratings and external mirrors in linear and loop cavities has been studied in the context of lowering threshold pump intensity for SBS.[22]

The paper is organized as follows. In Section 2, we present the general theoretical formulation of the problem and derive the coupled wave equations. In Section 3A, we obtain the threshold condition ignoring pump depletion. Analytic solutions that take into account depletion of the pump beams are obtained in section 3B, with numerical plots of the results shown in section 3C. Comparisons with MPPC in transmission geometry are made in section 4, while competing effects due to self-SBS of each pump are discussed in section 5. Finally, the results obtained in this paper are summarized in Section 6.

2. THEORETICAL FORMULATION

The geometry for the nonlinear interaction responsible for MPPC is shown in Fig. 1a. Input beams 1 and 4 are a pair of mutually incoherent beams (called the "pump" beams) that enter through the front face of the nonlinear medium and intersect at an angle 2θ. Acoustic phonons that are initially present in a transparent Kerr medium like CS_2 due to thermal and quantum noise cause Stokes scattering of the pump beams in all directions. Also, a photon from each pump beam can be spontaneously converted into a frequency downshifted Stokes photon and an acoustic phonon. The coherently generated Stokes waves will interfere with the pump beam to produce interference patterns which travel at the acoustic velocity, and which drive acoustic waves by electrostriction.[23] These acoustic waves induce index gratings in the medium, and the index grating that diffracts each incoherent input beam into the phase-conjugated output of the other input beam beam will be reinforced by both the beams. Hence this mutual index grating has the maximum gain compared to all the other possible gratings, and we label the corresponding Stokes scattered wave of input beam 1 as beam 3, beam 3 also being the phase-conjugate of pump beam 4. Similarly, the relevant Stokes wave of pump beam 4 is beam 2, and this is the phase-conjugate of pump beam 1. Steady-state beam coupling is described by nondegenerate four-wave mixing equations in the nonlinear medium with appropriate boundary conditions.

We assume that the various optical fields are plane waves, so that the total electric field **E** in the nonlinear medium can be represented as

$$\mathbf{E}(\mathbf{r},t) = \frac{\mathbf{e}_m}{2} \sum_{m=1}^{4} A_m(z) \exp[i(\mathbf{k}_m \cdot \mathbf{r} - \omega_m t)] + \text{c.c.} \quad , \tag{1}$$

where $\mathbf{e}_m$, A_m, $\mathbf{k}_m$, and ω_m are the unit polarization vector, complex steady-state amplitude, wave vector and frequency of the m-th wave. The z axis is taken normal to the surface of the medium, and the complex amplitudes are assumed to be functions of z

due to energy transfer by beam coupling. The intensity pattern generated by the interference of the coherent beams 1 and 3, and the coherent beams 2 and 4, is given by

$$\langle E^2(\mathbf{r},t)\rangle = \frac{1}{2}\left\{\sum_{m=1}^{4}|A_m|^2 + \left[(\mathbf{e}_1\cdot\mathbf{e}_3^*)\,A_1A_3^*\exp[i(\mathbf{K}_{13}\cdot\mathbf{r}-\omega_{13}t)]\right.\right.$$

$$\left.\left. + (\mathbf{e}_4\cdot\mathbf{e}_2^*)\,A_4\,A_2^*\exp[i(\mathbf{K}_{42}\cdot\mathbf{r}-\omega_{42}t)] + \text{c.c.}\right]\right\}, \qquad (2)$$

where the angular brackets indicate averaging over times long compared to the optical periods, $\mathbf{K}_{ij} \equiv \mathbf{k}_i - \mathbf{k}_j$, and $\omega_{ij} \equiv \omega_i - \omega_j$. Each interference term induces a volume index grating in the medium via the electrostrictive Kerr effect, given by[23,24]

$$\Delta n_{ij} = \frac{(\mathbf{e}_i\cdot\mathbf{e}_j^*)\,K_{ij}^2\gamma^2}{8n_0\rho\varepsilon_0\,(v^2K_{ij}^2 - \omega_{ij}^2 - i\,\omega_{ij}\,\Gamma_{ij})}\,A_iA_j^*\exp[i(\mathbf{K}_{ij}\cdot\mathbf{r}-\omega_{ij}t)] + \text{c.c.} \qquad , \qquad (3)$$

where γ is the electrostrictive coefficient, n_0 is the linear refractive index of medium in absence of light, ρ is the mass density, ε_0 is the dielectric constant of vacuum, v is the acoustic speed and Γ_{ij} is the Brillouin linewidth that depends on experimental geometry. We wish to consider the case of equal frequencies and wavevectors for the two index gratings induced by the intensity pattern to yield a common or shared grating: $\omega_{13} = \omega_{42} \equiv \Delta\omega$, $K_{13} = K_{42} \equiv K$, and $\Gamma_{13} = \Gamma_{42} \equiv \Gamma$. Then the total light induced change in the refractive index of the medium is given by

$$\Delta n = \Delta n_{13} + \Delta n_{42} = \frac{K^2\gamma^2\,[(\mathbf{e}_1\cdot\mathbf{e}_3^*)\,A_1A_3^* + (\mathbf{e}_4\cdot\mathbf{e}_2^*)\,A_4A_2^*]}{8n_0\rho\varepsilon_0\,(v^2K^2 - \Delta\omega^2 - i\,\Delta\omega\,\Gamma)}\,\exp[i(\mathbf{K}\cdot\mathbf{r}-\Delta\omega t)]$$

$$+ \text{c.c.} \quad . \qquad (4)$$

To describe the propagation and coupling of the waves in the nonlinear medium at steady-state, we start with the scalar wave equation

$$\nabla^2 E + \frac{n^2\omega^2}{c^2} E = 0 \quad , \tag{5}$$

where $n = (n_0 + \Delta n)$ is the total refractive index of the medium. Since $\Delta\omega << \omega$, we have ignored the small frequency differences between the waves and taken $\omega_m \approx \omega$ for all the waves. We have also neglected the small absorption of the waves in the transparent Kerr medium. Substituting for n and E in the wave equation, using the slowly varying envelope approximation and ignoring terms that are quadratic in the index change, we arrive at the following coupled wave equations

$$\frac{dA_1}{dz} = \frac{g}{2} [(\mathbf{e}_1 \cdot \mathbf{e}_3^*) A_1 A_3^* + (\mathbf{e}_4 \cdot \mathbf{e}_2^*) A_2^* A_4] A_3$$

$$\frac{dA_2}{dz} = \frac{g^*}{2} [(\mathbf{e}_1^* \cdot \mathbf{e}_3) A_1^* A_3 + (\mathbf{e}_4^* \cdot \mathbf{e}_2) A_2 A_4^*] A_4$$

$$\frac{dA_3}{dz} = \frac{g^*}{2} [(\mathbf{e}_1^* \cdot \mathbf{e}_3) A_1^* A_3 + (\mathbf{e}_4^* \cdot \mathbf{e}_2) A_2 A_4^*] A_1$$

$$\frac{dA_4}{dz} = \frac{g}{2} [(\mathbf{e}_1 \cdot \mathbf{e}_3^*) A_1 A_3^* + (\mathbf{e}_4 \cdot \mathbf{e}_2^*) A_2^* A_4] A_2 \quad . \tag{6}$$

Here g is the complex Brillouin gain coefficient that is given by

$$g = \frac{i\omega}{c \cos\theta} \frac{K^2 \gamma^2}{4 n_0 \rho \varepsilon_0 (v^2 K^2 - \Delta\omega^2 - i\Delta\omega\Gamma)} \quad . \tag{7}$$

Note that g has units of inverse of the product of intensity-length. The complex gain coefficient is a negative real number when the frequency difference between two coherent

waves is equal to the acoustic frequency: $\omega_1 - \omega_3 = \omega_4 - \omega_2 = \Delta\omega = vK$, indicating a 90° phase shift between the index grating and the intensity pattern.[23,24] In Sternklar's experiment,[21] the two input beams were orthogonally polarized with respect to one another to enable tagging of the Stokes photons of each pump by virtue of their polarization. Let input beam 1 be linearly polarized in the plane of incidence (p-polarization), and let input beam 4 be linearly polarized perpendicular to the plane of incidence (s-polarization). Since each coherently generated Stokes wave has the same polarization as its pump wave, $\mathbf{e}_1 \cdot \mathbf{e}_3 = \cos 2\theta$, $\mathbf{e}_4 \cdot \mathbf{e}_2 = 1$. The angle 2θ between the incoherent beams is typically small (~1°),[21] so that the dot product between the unit p-vectors may also be taken equal to unity. At resonance ($\Delta\omega = vK$), the coupled wave equations (6) reduce to

$$\frac{dA_1}{dz} = -\frac{g_R}{2}\left(A_1 A_3^* + A_2^* A_4\right) A_3$$

$$\frac{dA_2}{dz} = -\frac{g_R}{2}\left(A_1^* A_3 + A_2 A_4^*\right) A_4$$

$$\frac{dA_3}{dz} = -\frac{g_R}{2}\left(A_1^* A_3 + A_2 A_4^*\right) A_1$$

$$\frac{dA_4}{dz} = -\frac{g_R}{2}\left(A_1 A_3^* + A_2^* A_4\right) A_2 \quad , \tag{8}$$

where

$$g_R \equiv \frac{\omega K_R \gamma^2}{4 c n_0 \varepsilon_0 v \rho \Gamma_R \cos\theta} \quad , \tag{9}$$

and the subscript R indicates the shared reflection grating under consideration, and $K_R = 2k\cos\theta$. The electrostrictive response of the medium has been stated in general terms, and can be easily changed from reflection to transmission geometry[17] by changing the interference terms. From the coupled wave eqs. (8), we note that that there is no phase

mismatch associated with the four-wave mixing term along the z-direction for equal frequencies of the two incoherent pump beams. We now solve the coupled wave equations (8) with and without pump depletion.

3A. Threshold Condition using Undepleted Pump Approximation

If the two input pump beams are much stronger than the self-generated Stokes beams (A_1, $A_4 >> A_2, A_3$), then we can take $dA_1/dz = dA_4/dz = 0$, so that A_1, A_4 are constant for all z, i.e., $A_1(z) = A_1(0) \equiv A_{10}$, and $A_4(z) = A_4(0) \equiv A_{40}$. Hence the coupled-wave equations (8) reduce to

$$\frac{dA_2}{dz} = -\frac{g_R}{2}\,(A_{10}^{*}\,A_{40}\,A_3 + I_{40}\,A_2)$$

$$\frac{dA_3}{dz} = -\frac{g_R}{2}\,(I_{10}\,A_3 + A_{10}\,A_{40}^{*}\,A_2) \quad , \tag{10}$$

where $I_i \equiv |A_i|^2$. The two equations can be easily decoupled and solved to give

$$A_2(z) = \frac{I_{10} + I_{40}\exp(-g_R I_0 z/2)}{I_0}\,A_2(0) - \frac{A_{10}^{*}\,A_{40}\,[1-\exp(-g_R I_0 z/2)]}{I_0}\,A_3(0)$$

$$A_3(z) = \frac{I_{40} + I_{10}\exp(-g_R I_0 z/2)}{I_0}\,A_3(0) - \frac{A_{10}A_{40}^{*}[1-\exp(-g_R I_0 z/2)]}{I_0}\,A_2(0) \quad , \tag{11}$$

where $I_0 \equiv I_{10}+I_{40}$ is the sum of the input pump intensities. If $A_2(L) \equiv A_{2L}$ and $A_3(L) \equiv A_{3L}$ represent the small, nonzero seed values of the Stokes waves at the z = L plane, where L is the interaction length, then the expressions for the Stokes waves at the z = 0 plane simplify to

$$A_2(0) = \frac{I_{10} + I_{40}\,e^{0.5G}}{I_0}\,A_{2L} + \frac{A_{10}^{*}\,A_{40}\,(e^{0.5G}-1)}{I_0}\,A_{3L}$$

$$A_3(0) = \frac{I_{40} + I_{10}\, e^{0.5G}}{I_0}\ A_{3L} + \frac{A_{10}A_{40}^{*}(e^{0.5G} - 1)}{I_0}\ A_{2L} \quad , \tag{12}$$

where $G \equiv g_R I_0 L$ is the total intensity Brillouin gain for the two incoherent pumps. These simple solutions contain interesting information about MPPC using reflection gratings. There will not be any Stokes waves at the z = 0 plane if both the seeds are zero at the back plane: $A_{2L} = A_{3L} = 0$. However, only one nonzero seed is sufficient to generate both the Stokes waves at the output. As discussed by Tikhonchuk and Zozulya[25] for similar configurations, the MPPC process under consideration in this paper is not an oscillator but an amplifier of small input seed values of the scattered radiation. The reflection geometry MPPC has a hard excitation threshold in that nonzero seeds are required for operation. Notice also that each Stokes wave has contributions from two terms. The first term is due to the exponential buildup of the seed in the presence of two pumps, one coherent and the other incoherent with respect to the Stokes wave. The incoherent pump also contributes to the Brillouin gain due to cross readout of the mutual reflection grating. The second term is the 4WM term that leads to phase conjugation. If one of the pump beams is zero along with its coherently generated Stokes wave, then the MPPC solutions of Eqs. (12) reduce to the familiar exponential buildup of the remaining Stokes wave. The finite Stokes seeds at the z = L backplane arise from the mutual scattering of each pump in a direction counterpropagating to the other pump:

$$A_{2L} = f\ A_4(L) \quad , \qquad A_{3L} = f\ A_1(L) \quad , \tag{13}$$

where f is the mutual scattering coefficient, assumed equal in amplitude and phase for both the pumps. A realistic picture should describe seeding by distributed noise terms, yet we use the simplified approach of self-SBS in assuming deterministic seed levels at a point boundary. Since the pumps are assumed to be constant throughout the interaction

region, we have $A_{2L} = f A_{40}$, $A_{3L} = f A_{10}$. Substituting boundary conditions (13) into the solutions (12) and simplifying, we obtain

$$I_2(0) = |f|^2 I_{40} e^G , \quad I_3(0) = |f|^2 I_{10} e^G . \tag{14}$$

In SBS, a Stokes wave originates from spontaneous scattering of the pump beam by index gratings induced by the acoustic noise that is always present in a medium at thermal equilibrium. Since the spontaneous scattering coefficient is very small, and the Brillouin gain is large only in a narrow solid angle for a focused pump beam, the intensity of the Stokes seed is taken to be 10^{-11} to 10^{-13} of the pump intensity.[26] In our calculations, we take $|f|^2 = 10^{-12}$. If we define threshold as the condition when 1% of each pump is converted to its Stokes wave at the output, i.e., $I_2(0)/I_{40} = I_3(0)/I_{10} = 0.01$, then the Brillouin gain at threshold is given by

$$G_{th} = g_R(I_{10}+I_{40}) L = 10 \ln_e 10 = 23.2 , \tag{15}$$

so that the sum of the input intensities of both the pumps have to yield a Brillouin gain of 23 at threshold. This number is comparable to Brillouin gain required for SBS initiated by noise. Hence the intensity of each pump can be below the threshold value required for self-SBS, and yet MPPC will build up from noise to 1% phase-conjugate reflectivities if the sum of the Brillouin gain for the two pumps satisfies Eq. (15).

3B. Analytic solutions with Pump Depletion

The boundary conditions appropriate for this problem are the field strengths A_{10}, A_{40} of the two pumps at the $z = 0$ input plane, and the finite seed values of the Stokes waves

A_{2L}, A_{3L} at the z = L plane. As the beams propagate in the nonlinear medium, the following quantities are conserved:[27,28]

$$\begin{aligned} I_1(z) - I_3(z) &= c_1 \\ I_4(z) - I_2(z) &= c_2 \\ A_1(z)A_2(z) - A_3(z)A_4(z) &= d_1 \\ A_2(z)A_3^*(z) - A_1^*(z)A_4(z) &= d_2 \end{aligned} \quad , \tag{16}$$

where c_1, c_2, d_1, and d_2 are integration constants that are yet to be determined. With the help of these conservation laws, the four coupled equations of Eqs. (8) can be decoupled to yield the following two first-order differential equations for the new variables $A_{21} \equiv A_2/A_1^*$ and $A_{34} \equiv A_3/A_4^*$:

$$\begin{aligned} \frac{dA_{21}}{dz} &= -\frac{g_R}{2}\,[d_1^* A_{21}^2 + N\,A_{21} - d_1\,] \\ \frac{dA_{34}}{dz} &= -\frac{g_R}{2}\,[-d_1^* A_{34}^2 + N\,A_{34} + d_1\,] \end{aligned} \quad , \tag{17}$$

where $N \equiv c_1+c_2$. Equations (17) can be readily solved to yield the following solutions

$$A_{21}(z) = \frac{QA_{21}(0) + \tanh\left(\frac{g_R Q z}{4}\right)[2d_1 - N\,A_{21}(0)]}{Q + \tanh\left(\frac{g_R Q z}{4}\right)[N + 2\,d_1^* A_{21}(0)]} \quad ,$$

$$A_{34}(z) = \frac{QA_{34}(0) - \tanh\left(\frac{g_R Q z}{4}\right)[2d_1 + N\,A_{34}(0)]}{Q - \tanh\left(\frac{g_R Q z}{4}\right)[2\,d_1^* A_{34}(0) - N]} \quad , \tag{18}$$

where the parameter Q is defined as

$$Q \equiv (N^2 + 4\,|d_1|^2)^{1/2} \tag{19}$$

In obtaining the solutions for $A_{21}(z)$ and $A_{34}(z)$ given by Eqs. (18), no approximations have been made regarding d_1 and N. If we define the phase-conjugate reflection

coefficients as: $\rho \equiv A_3(0)/A_{40}^* = A_{34}(0)$ and $\sigma \equiv A_2(0)/A_{10}^* = A_{21}(0)$, then from the above equations, we obtain

$$\rho = \frac{QA_{34}(L) + T_L [N A_{34}(L) + 2d_1]}{Q + T_L [2 d_1^* A_{34}(L) - N]} \quad ,$$

$$\sigma = \frac{QA_{21}(L) + T_L [N A_{21}(L) - 2d_1]}{Q - T_L [N + 2 d_1^* A_{21}(L)]} \quad , \tag{20}$$

where $T_L \equiv \tanh (g_R QL/4)$. We now assume the same form of boundary conditions as given by Eqs. (13) of the previous section: $A_{2L} = f A_4(L)$, $A_{3L} = f A_1(L)$, i.e., the mutual scattering is equal in amplitude and phase for both the pumps at the end face of the nonlinear medium. Then the first and second conservation laws yield the pump intensities at the end face

$$I_1(L) = \frac{I_{10} - R I_{40}}{1 - |f|^2}$$

$$I_4(L) = \frac{I_{40} - S I_{10}}{1 - |f|^2} \quad , \tag{21}$$

where R and S are the power phase-conjugate reflectivities: $R \equiv |\rho|^2$, $S \equiv |\sigma|^2$. With the boundary conditions given by Eqs. (13), the third conservation law shows that the integration constant $d_1 = 0$. Consequently

$$\frac{R}{S} = q^2 \quad , \tag{22}$$

where q is defined as the intensity ratio of the pump beams at the input: $q \equiv I_{10} / I_{40}$. This relationship is also true for MPPCs in photorefractive media.[1-5,28] From the definition of

phase-conjugate reflectivities R and S, it is obvious that their maximum values occur when all of the pump beams are converted into the Stokes beams. Hence $R_m = I_{10}/I_{40} = q$, and $S_m = I_{40}/I_{10} = 1/q$, where the subscript m denotes maximum value. Another relevant unknown for MPPC is the device transmissivity in each direction: $T_{ij} \equiv I_i(0)/I_{j0}$, and it reveals the fraction of each input beam that is converted into the phase-conjugate output of the other beam. Using Eq. (22), it can be shown that $T_{31} = T_{24} \equiv T$, so that both input beams have equal transmissivity.[21] This relationship is also true for MPPCs in photorefractive media.[1-5] The maximum value of the device transmissivity is unity, when all the energy of an input beam is converted into the phase-conjugate of the other beam. Since $d_1 = 0$, $Q = N$ and $T_L \equiv \tanh(g_R NL/4)$. Hence Eqs. (20) simplify to

$$R = \exp(g_R NL)\,|A_{34}(L)|^2 \quad , \qquad S = \exp(g_R NL)\,|A_{21}(L)|^2 \quad . \tag{23}$$

Now $N = I_{10} + I_{40} - I_2(0) - I_3(0)$ is still an unknown quantity and may be expressed as $N = I_0(1-R/q)$. Using Eqs. (21), we may also show that $|A_{34}(L)|^2 = q\,|f|^2$. Substituting N and $|A_{34}(L)|^2$ in the above equation for R, we obtain the following transcendental equation for R:

$$R = q\,|f|^2 \exp[G(1-R/q)] \quad . \tag{24}$$

Note that if $|f|^2 = 0$, i.e., $I_{2L} = I_{3L} = 0$ in eqs. (13), then the phase-conjugate reflectivities R and S are equal to zero. Hence finite seed values of the Stokes waves are required at the back surface of the nonlinear medium for MPPC to work in reflection geometry. This is in contrast to MPPC using transmission gratings,[17] where steady-state phase-conjugate reflectivities can be obtained with zero Stokes seeds at either edge of the nonlinear medium. Equation (24) can be solved numerically for R using known values for the combined Brillouin intensity gain G, intensity ratio q for input beams, and the mutual

scattering coefficients of the pumps equal to $|f|^2$. Knowing R, we can calculate S using Eq. (22): $S = R/q^2$.

3C. Numerical Results

Figs. 2a,b are plots of the phase-conjugate reflectivities R, S and transmissivity T as a function of Brillouin gain $G_4 \equiv g_R I_{40} L$ for $|f|^2 = 10^{-12}$, and different values of beam ratio q: (a) q = 1, (b) q = 0.5. Note that the input beam ratio $q \equiv I_{10} / I_{40}$ affects the total Brillouin gain: $G = g_R(I_{10}+I_{40}) L = G_4(1+q)$ as we keep I_{40} and hence G_4 constant. For equal input intensities of beam 1 and 4, the two phase-conjugate reflectivities and transmissivity are all equal and approach the limiting value of unity for large coupling gain. The threshold Brillouin gain for beam 4 is around 11.5, and since q = 1, this corresponds to a total Brillouin gain of 23 at threshold, as shown in section 3A. If pump beam 4 is twice as intense as pump beam 1 at the input (i.e. q = 0.5, as in Fig. 2b), then the weaker pump has a larger phase-conjugate reflectivity (= S) that approaches the limiting value of 2 (= 1/q) for large Brillouin gain. The stronger pump has a smaller phase-conjugate reflectivity (= R) that approaches the value 0.5 (= q) for large Brillouin gain. Transmissivity T (shown as a dashed curve) approaches the maximum value of unity for large gain. Since pump beam 1 is now weak, G_4 at threshold has to be larger in Fig. 2b than the threshold value in Fig. 2a so that condition given by Eq. (15) is still satisfied for the total gain.

Figs. 3a,b are a plot of the phase-conjugate reflectivities R, S and transmissivity T as a function of the input intensity ratio q of the two pumps on a log-log scale, for different values of Brillouin gain G_4 satisfied by pump beam 4. The values of G_4 are chosen below the threshold value required for self-SBS (~ 23) of pump beam 4. The upper limit for q value is set by self-SBS of beam 1; since the coupled wave eqs. (8) do not include self-SBS terms for each pump, our formulation is not valid when competing effects such as self-SBS set in when each pump has a Brillouin gain > 23. However, in

section 5, we show that the gain for phase-conjugation by MPPC is twice as large as phase-conjugation by self-SBS, so that the Brillouin gain would have to be very large before self-SBS begins to compete with MPPC. Increasing q is equivalent to increasing I_{10}, keeping I_{40} and hence G_4 fixed. For $G_4 = 12$ (Fig. 3a) and small q values, (10^{-8} to 10^{-2}) the total Brillouin gain is roughly half that required for threshold. Consequently, very little energy of the pump beams is converted into the Stokes waves, and since S is inversely proportional to I_{10}, S decreases with increasing q. As q is further increased, the combined Brillouin gain approaches threshold, leading to increased conversion of pump beam I_{40} into the Stokes beam $I_2(0)$, as seen by the increase in T. This compensates for the decrease of S with increasing I_{10}, so that S actually increases for a limited range of q values. When the total Brillouin gain is enough to convert most of the pumps into their Stokes waves, then any further increase in q results in decreasing S once again. R is a monotonically increasing function of q because its denominator I_{40} is a fixed quantity, and increase in I_{10} results in more conversion of this pump beam into its Stokes wave $I_3(0)$. Fig. 3b is a similar plot for $G_4 = 18$. Notice that the variation between the maximum and minimum values of S is nearly 3 orders of magnitude smaller in Fig. 3b than in Fig. 3a due to the larger Brillouin gain G_4 to begin with in Fig. 3b. Even when the Brillouin gain of each beam is smaller than the threshold gain for self-SBS, figures 3 reveal that the weak beam can be phase-conjugated with a reflectivity greater than 1, opening the possibilities for a variety of applications in phase-conjugate resonators, phase-conjugate interferometers and phase-conjugate gyros. When $G_4 = 12$, $S \geq 1$ for $q \leq 10^{-7}$ (fig. 3a), and when $G_4 = 18$, $S \geq 1$ for $q \leq 10^{-4}$.

4. Comparison with MPPC in transmission geometry

To facilitate this comparison, figures 4a and 4b show MPPC in electrostrictive media using transmission geometry. The corresponding coupled-wave equations from Ref. 17 are:

$$\frac{dA_1}{dz} = \frac{g_T}{2}\left(A_1 A_4^* + A_2^* A_3\, e^{i\Delta kz}\right) A_4$$

$$\frac{dA_2}{dz} = \frac{g_T}{2}\left(A_1^* A_4\, e^{i\Delta kz} + A_2 A_3^*\right) A_3$$

$$\frac{dA_3}{dz} = -\frac{g_T}{2}\left(A_1 A_4^*\, e^{-i\Delta kz} + A_2^* A_3 \right) A_2$$

$$\frac{dA_4}{dz} = -\frac{g_T}{2}\left(A_1^* A_4 + A_2 A_3^* e^{-i\Delta kz}\right) A_1 \quad , \tag{25}$$

where

$$g_T = \frac{\omega K_T \gamma^2}{4cn_0\varepsilon_0 v\rho\Gamma_T \cos\theta} \quad . \tag{26}$$

For transmission geometry denoted by subscript T, 2θ is the angle between coherent beam pairs 1, 4, and 2, 3, so that $K_T = 2k\sin\theta$. To compare the Brillouin gain coefficients g_i and phonon lifetimes τ_i for the various geometries, we must express the geometrical dependence contained in the acoustic wavevector magnitude K_i and Brillouin linewidth Γ_i explicitly. We use the relationship[24,29]: $\Gamma_i = \tau_i^{-1} = \eta K_i^2/\rho$, η being the viscosity of the medium. This equation is true only for acoustic frequencies larger than the vibrational relaxation frequency of the electrostrictive medium, when acoustic absorption can be described by classical mechanisms only.[30] Contradirectional SBS corresponds to $\theta = 0$ in reflection geometry (the angle between a pair of coherent beams is π-2θ), and $g_{SBS} = \gamma^2/8\varepsilon\eta v$, $\tau_{SBS} = \rho/4\eta k^2$, ε being the uniform dielectric constant of the medium. Hence $g_R/g_{SBS} = 1/\cos^2\theta = \tau_R/\tau_{SBS}$, so that a 2k SBS grating has a smaller gain than the reflection grating, and acoustic phonons corresponding to contradirectional SBS have the shortest lifetime. Similarly, $g_T = 2g_{SBS}/\sin 2\theta$, and $\tau_T/\tau_{SBS} = 1/\sin^2\theta$.[24,29] Hence the Brillouin gain is minimum for contradirectional SBS, and increases with smaller beam angles in the forward direction. Yet the acoustic phonons are difficult to build up

in forward MPPC as they tend to walk off the interaction region. Also, the lifetime of the acoustic phonons is much longer in the forward direction, so that MPPC in transmission geometry requires not only intense pump beams but also large pulsewidths to achieve steady-state. This may explain why MPPC in electrostrictive media has not been observed in the transmission geometry. Notice the phase mismatch $\Delta k = (2\ n\ \Delta\omega\ /\ c)$ associated with the transmission geometry that is absent in the reflection geometry (compare with Eqs. (8) of section 3A). Also note that the phase-conjugate reflectivities in Ref. 16 were obtained with the boundary conditions of zero seeds at their startup planes: $I_{10} = I_{3L} = 0$. In reflection geometry, non-zero seeds: $I_{2L} \neq 0$, $I_{3L} \neq 0$ have to be assumed at the end face of the nonlinear medium to obtain finite phase-conjugate reflectivities. Hence MPPC in reflection geometry has a hard excitation threshold. Another related difference in the two formulations is the manner in which the threshold condition is derived, along with the value of the Brillouin gain required for threshold. For equal intensity incoherent beams, the threshold condition in Ref. 16 is derived from the transcendental equation: $g_T(I_{40}+I_{2L})L = 4$. No physical solutions will be obtained below this threshold value of intensity Brilloiun gain, and the phase-conjugate reflectivities are 92% at threshold gain. In this paper, the threshold condition is defined as the Brillouin gain required to give 1% phase-conjugate reflectivities. For Stokes waves initiated by noise ($|f|^2 = 10^{-12}$), this requires a combined Brillouin gain of $g_R(I_{10}+I_{40})L = 23$.

5. Competition due to self-SBS

The coupled wave Eqs. (8) are no longer valid if one or both the pump beams is intense enough to satisfy the threshold for self-SBS. Two additional waves must be included in the formalism to describe the Stokes scattering of each pump beam due to backward SBS. Let E_5 (E_6) be the coherently generated Stokes wave of pump beam 1 (pump beam 4) due to 2k gratings (see Fig. 5). Wave E_5 (E_6) is collinear with beam 2 (beam 3), but it has a

frequency equal to $\omega - \Delta\omega_{SBS}$, where $\Delta\omega_{SBS}$ is the SBS acoustic frequency equal to 2kv. Hence the modified coupled wave Eqs. (8) with terms due to self-SBS are

$$\frac{dA_1}{dz} = -\frac{g_R}{2}\left(A_1A_3^* + A_2^*A_4\right)A_3 - \frac{g_{SBS}}{2}A_1|A_5|^2$$

$$\frac{dA_2}{dz} = -\frac{g_R}{2}\left(A_1^*A_3 + A_2A_4^*\right)A_4$$

$$\frac{dA_3}{dz} = -\frac{g_R}{2}\left(A_1^*A_3 + A_2A_4^*\right)A_1$$

$$\frac{dA_4}{dz} = -\frac{g_R}{2}\left(A_1A_3^* + A_2^*A_4\right)A_2 - \frac{g_{SBS}}{2}A_4|A_6|^2$$

$$\frac{dA_5}{dz} = -\frac{g_{SBS}}{2}A_5|A_1|^2$$

$$\frac{dA_6}{dz} = -\frac{g_{SBS}}{2}A_6|A_4|^2 \quad , \tag{27}$$

where g_{SBS} has been defined in Section 3.1. Note that since both Stokes waves 3 and 5 are coherently generated from pump beam 1, they could, in principle, write a transmission grating between themselves. Such secondary gratings written among the various noise terms would be very weak compared to the primary gratings written by the pumps and noise, except near the input face of the nonlinear medium where the Stokes waves undergo considerable amplification. In what follows, we will ignore such gratings. Similar remarks apply for the Stokes waves 2 and 6 that are coherently generated from pump beam 4.

If we assume that both the pumps are much stronger than their Stokes waves, we can ignore pump depletion and consider the input pump amplitudes as constant quantities throughout the interaction region. In that case, the above equations reduce to

$$\frac{dA_2}{dz} = -\frac{g_R}{2}\left(A_{10}^*A_{40}A_3 + I_{40}A_2\right)$$

$$\frac{dA_3}{dz} = -\frac{g_R}{2}\,(I_{10}\,A_3 + A_{10}\,A_{40}^*\,A_2)$$

$$\frac{dA_5}{dz} = -\frac{g_{SBS}}{2}\,A_5\,I_{10}$$

$$\frac{dA_6}{dz} = -\frac{g_{SBS}}{2}\,A_6\,I_{40} \qquad (28)$$

In this limit, the coupled wave equations for beams 2 and 3 are still independent of beams 5 and 6. With A_{10} and A_{40} as constant quantities, the solutions given by Eqs. (12) for $A_2(0)$ and $A_3(0)$ are still valid, despite the presence of additional Stokes wave 5 and 6. Hence self-SBS does not modify the solutions for MPPC for negligible pump depletion.

The solutions for waves 2 and 3 will be affected by self-SBS of the pumps only if we take into account pump depletion. To do this, one must solve the six nonlinear coupled wave equations (26) numerically, with two-point boundary values. However, we will now show qualitatively that the Brillouin gain coefficient for the mutual reflection grating can be twice as large as the 2k SBS gratings, so that the latter may be discriminated against owing to a lower gain. We use the formulation developed by Yeh[31] for MPPC in photorefractive media to arrive at this qualitative result. We have seen in sections 3.2 and 3.3 that the two phase-conjugate reflectivities are comparable for similar intensity of the two input beams. Let the amplitudes of the various Stokes waves be expressed as the phase-conjugates of the relevant pumps:

$$A_2 = \rho_{MPPC}\,A_1^* \quad , \quad A_3 = \rho_{MPPC}A_4^* \quad , \quad A_5 = \rho_{SBS}A_1^* \quad , \quad A_6 = \rho_{SBS}A_4^* \qquad (29)$$

where ρ_R and ρ_{SBS} are arbitrary constants. Substitution of Eqs. (29) into (27) results in the following set of coupled-wave equations:

$$\frac{dA_1}{dz} = -\,(g_R\,|\rho_{MPPC}|^2\,|A_4|^2 + \frac{g_{SBS}}{2}\,|\rho_{SBS}|^2\,|A_1|^2)\,A_1$$

$$\frac{dA_2}{dz} = -\,g_R\,\rho_{MPPC}\,A_1^*\,|A_4|^2$$

$$\frac{dA_3}{dz} = -g_R \rho_{MPPC} A_4^* |A_1|^2$$

$$\frac{dA_4}{dz} = -\left(g_R |\rho_{MPPC}|^2 |A_1|^2 + \frac{g_{SBS}}{2} |\rho_{SBS}|^2 |A_4|^2 \right) A_4$$

$$\frac{dA_5}{dz} = -\frac{g_{SBS}}{2} \rho_{SBS} A_1^* |A_1|^2$$

$$\frac{dA_6}{dz} = -\frac{g_{SBS}}{2} \rho_{SBS} A_4^* |A_4|^2 \qquad (30)$$

Hence if the ρ's and g's have comparable magnitudes, then the above equations show that phase conjugation due to MPPC builds at twice the gain as SBS of each pump beam because of the reinforcement of the mutual reflection grating in MPPC from both pairs of coherent beams. This factor of 2 in the exponential gain is similar to the gain for the phase-conjugate wave due to SBS being twice as large as the gain for any other scattered wave, so that the scattered waves are discriminated against owing to their lower gain.[26]

6. Conclusions

We studied Brillouin induced MPPC in the reflection geometry, and showed that a phase-conjugate reflectivity of 1% in each arm requires a *combined* Brillouin gain of 23 for Stokes scattering initiated by noise. MPPC works for a large dynamic range of input beam ratio by increasing the intensity of a weak input beam, and fixing the intensity of the second input beam below the threshold value for self-SBS. Our numerical plots show that the weak beam is phase-conjugated with reflectivities larger than unity, and the upper limit to the dynamic range is set by competition from self-SBS of the first beam. We have also compared the performance of MPPC with reflection gratings to that using transmission gratings, and commented on why the latter may be difficult to observe experimentally. We have shown that the performance of MPPC is not affected by self-SBS for negligible pump depletion near threshold. Even under conditions where pump depletion takes place, we have presented an argument indicating that the gain for phase

conjugation by MPPC is twice that for self-SBS due to the mutual reflection grating formed in MPPC.

Acknowledgement

This research is supported, in part, by the U. S. Air Force Office of Scientific Research under contract F49620-92-C-0023.

FIGURE CAPTIONS

Fig. 1a Schematic diagram showing MPPC using reflection gratings in an electrostrictive Kerr medium.

Fig. 1b Wave vector diagram for MPPC using reflection gratings.

Figs. 2 Phase-conjugate reflectivities R, S and transmissivity T as a function of Brillouin gain G_4 for $|f|^2 = 10^{-12}$ and (a) q = 1 (b) q = 0.5.

Figs. 3 Phase-conjugate reflectivities R, S and transmissivity T as a function of intensity ratio of the two input beams q for $|f|^2 = 10^{-12}$ and (a) $G_4 = 12$ (b) $G_4 = 18$.

Fig. 4a Schematic diagram showing MPPC using transmission gratings in an electrostrictive Kerr medium.

Fig. 4b Wave vector diagram for MPPC using transmission gratings.

Fig. 5 Schematic diagram showing MPPC reflection gratings and 2k SBS gratings.

REFERENCES

1. S. Weiss, S. Sternklar and B. Fischer, Opt. Lett. **12**, 114 (1987).
2. R. W. Eason and A. M. C. Smout, Opt. Lett.**12**, 51 (1987); A. M. C. Smout and R. W. Eason, Opt. Lett. **12**, 498 (1987).
3. M. D. Ewbank, Opt. Lett. **13**, 47 (1988).
4. D. Wang, Z. Zhang, Y. Zhu, S. Zhang, and P. Ye, Opt. Commun. **73**, 495 (1989).
5. M. D. Ewbank, R. A. Vazquez, R. R. Neurgaonkar, and J. Feinberg, J. Opt. Soc. Am. B **7**, 2306 (1990).
6. S. Sternklar, S. Weiss, M. Segev, and B. Fischer, Opt. Lett. **11**, 528 (1986).
7. T. Y. Chang, Opt. Lett. **15**, 1342 (1990).
8. M. Segev, S. Weiss, and B. Fischer, Appl. Phys. Lett. **50**, 1397 (1987).
9. S. MacCormack, J. Feinberg, and M. H. Garrett, in *Conference on Lasers and Electro-optics*, Technical Digest **11**, (Optical Society of America, Washington, D.C., 1993), paper CThS55.
10. Q.-C. He, J. Shamir, and J. G. Duthie, Appl. Opt. **28**, 306 (1989); J. Shamir, H. J. Caulfield, and B. M. Hendrickson, Appl. Opt. **27**, 2912 (1988).
11. S. Sternklar, S. Weiss, M. Segev, and B. Fischer, Appl. Opt. **25**, 4518 (1986).
12. M. Cronin-Golomb, Appl. Phys. Lett. **54**, 2189 (1989).
13. L. E. Adams and R. S. Bondurant, Opt. Lett. **16**, 832 (1991).
14. S. Sternklar, S. Weiss and B. Fischer, Opt. Eng. **26**, 423 (1987); Q. C. He, IEEE J. Quantum Electron. **QE-24**, 2507 (1988).
15. A. V. Mamaev and V. V. Shkunov, Sov. J. Quantum Electron. **20**, 323 (1990).
16. A. V. Mamaev and A. A. Zozulya, J. Opt. Soc. Am. B **8**, 1447 (1991).
17. R. Saxena and P. Yeh, J. Opt. Soc. Am. B **7**, 326 (1990).
18. N. Basov and I. G. Zubarev, Appl. Phys. **20**, 261 (1979); N. F. Andreev, V. I. Bespalov, A. M. Kiselev, A. Z. Matveev, G. A. Pasmanik and A. A. Shilov, Sov.

Phys. JETP Lett. **32**, 625 (1980); A. M. Scott, Opt. Commun. **45**, 127 (1983); A. Z. Matveev, Sov. J. Quantum Electron. **15**, 783 (1985); P. Narum and R. W. Boyd, IEEE J. Quantum Electron. **QE-23**, 1211 (1987); A. M. Scott and K.D. Ridley, IEEE J. Quantum Electron. **QE-25**, 438 (1989).

19. M. Cronin-Golomb, B. Fischer, J.O. White and A. Yariv, IEEE J. Quantum Electron. **QE-20**, 12 (1984).

20. K. D. Ridley, Opt. Commun. **82**, 351 (1991).

21. S. Sternklar, Opt. Lett. **17**, 1403 (1992).

22. V. I. Odintsov and L. F. Rogacheva, JETP Lett. **36**, 344 (1982); M. G. Zhanuzakov, A. A. Zozulya, and V. T. Tikhonchuk, Sov. J. Quantum Electron. **19**, 254 (1989); G. K. N. Wong and M. J. Damzen, IEEE J. Quantum Electron. **QE-26**, 139 (1990); S. Pfeifer, R. Johnson, and W. Carrion, in *Conference on Lasers and Electro-optics*, Technical Digest **10**, (Optical Society of America, Washington, D.C., 1991), paper CMG3; C. Gu, R. Saxena. L. C. Huang, Q. B. He, and P. Yeh, Proceed. SPIE **1626**, 243 (1992); A. M. Scott, W. T. Whitney, M. T. Duignan, in *Conference on Lasers and Electro-optics*, Technical Digest **11**, (Optical Society of America, Washington, D.C., 1993), paper CThJ3.

23. W. Kaiser and M. Maier, "Stimulated Rayleigh, Brillouin and Raman Spectroscopy," Chap. E2 in *Laser Handbook*, eds. F.T. Arecchi and E.O. Schulz-Dubois (North-Holland Publ. Co., 1972); A. Yariv and P. Yeh, "Optical Waves in Crystals," Chap. 9 (Wiley, 1984); Y. R. Shen, "Principles of Nonlinear Optics," Chap. 11, (Wiley, 1985).

24. P. Yeh, IEEE J. Quantum Electron. **QE-25**, 484 (1989).

25. V. T. Tikhonchuk and A. A. Zozulya, Prog. Quant. Electr. **15**, 231 (1991).

26. B. Ya. Zel'dovich, N. F. Pilipetsky and V. V. Shkunov in *Principles of Phase Conjugation*, Springer-Verlag, Berlin, 1985; R. W. Boyd, A. L. Gaeta, R.

Petrozzo and K. Rzazewski, Technical Digest of Optical Society of America Annual Meeting **18**, TuA1, 1989.

27. N. V. Kukhtarev, T. I. Semenets, K. H. Ringhofer, and G. Tomberger, Appl. Phys. B **41**, 259 (1986).

28. C. Gu and P. Yeh, Opt. Lett. **16**, 455 (1991).

29. A. Corvo and A. Gavrielides, J. Appl. Phys. **63**, 5220 (1988).

30. A. Laubereau, W. Englisch, and W. Kaiser, IEEE J. Quantum Electron. **QE-5**, 410 (1969).

31. P. Yeh, Appl. Opt. **28**, 1961 (1989).

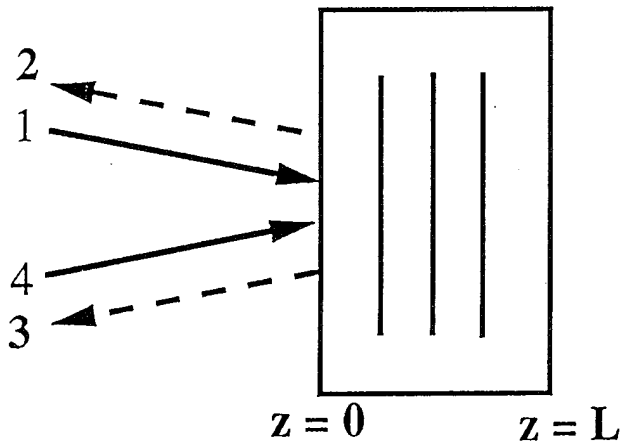

(a)

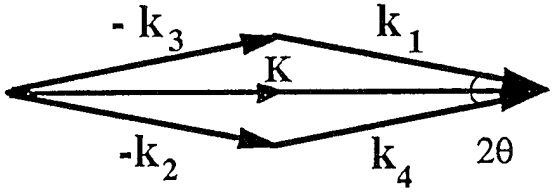

(b)

Saxena & McMichael
Figs. 1

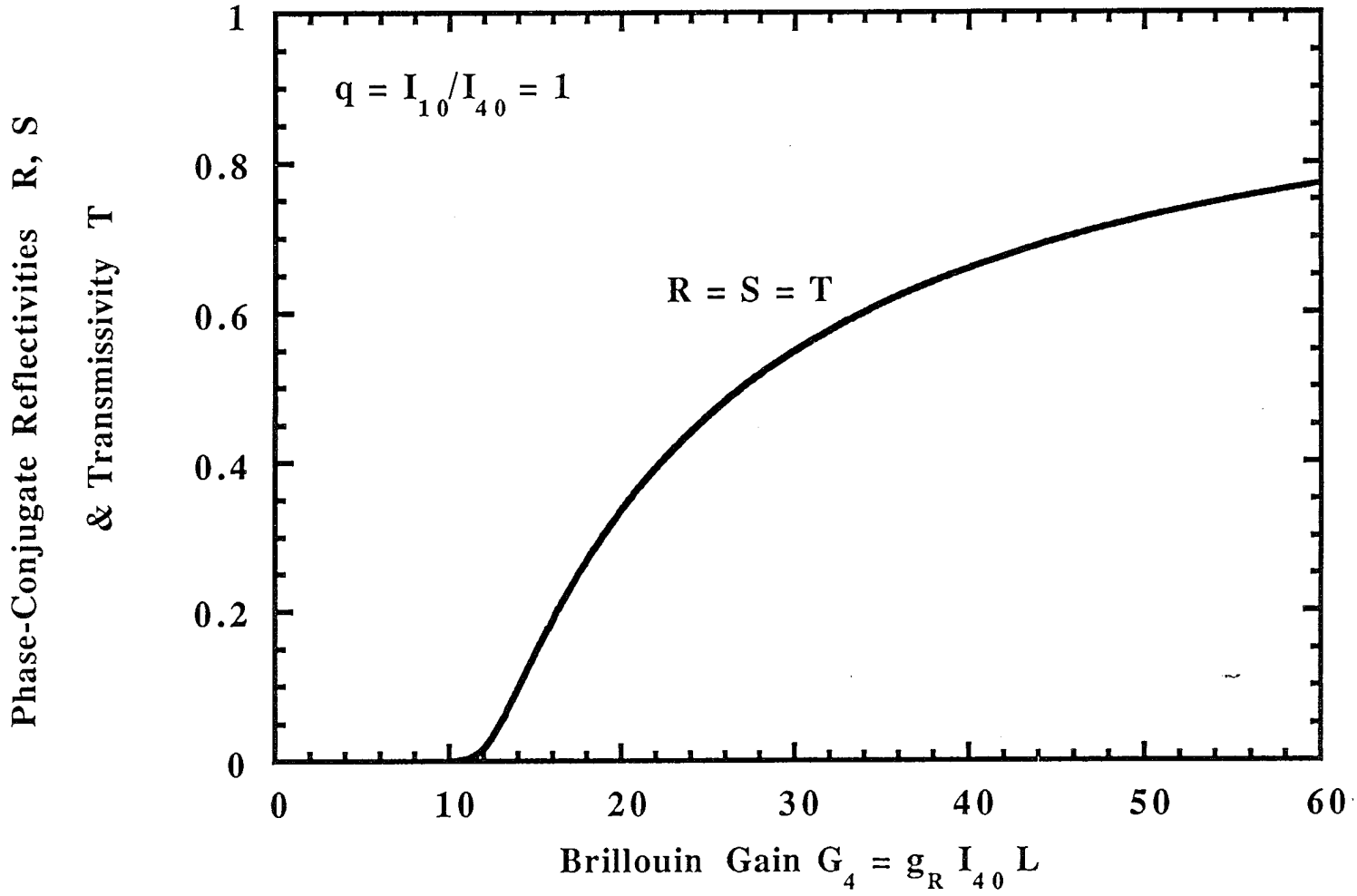

Saxena & McMichael
Fig. 2a

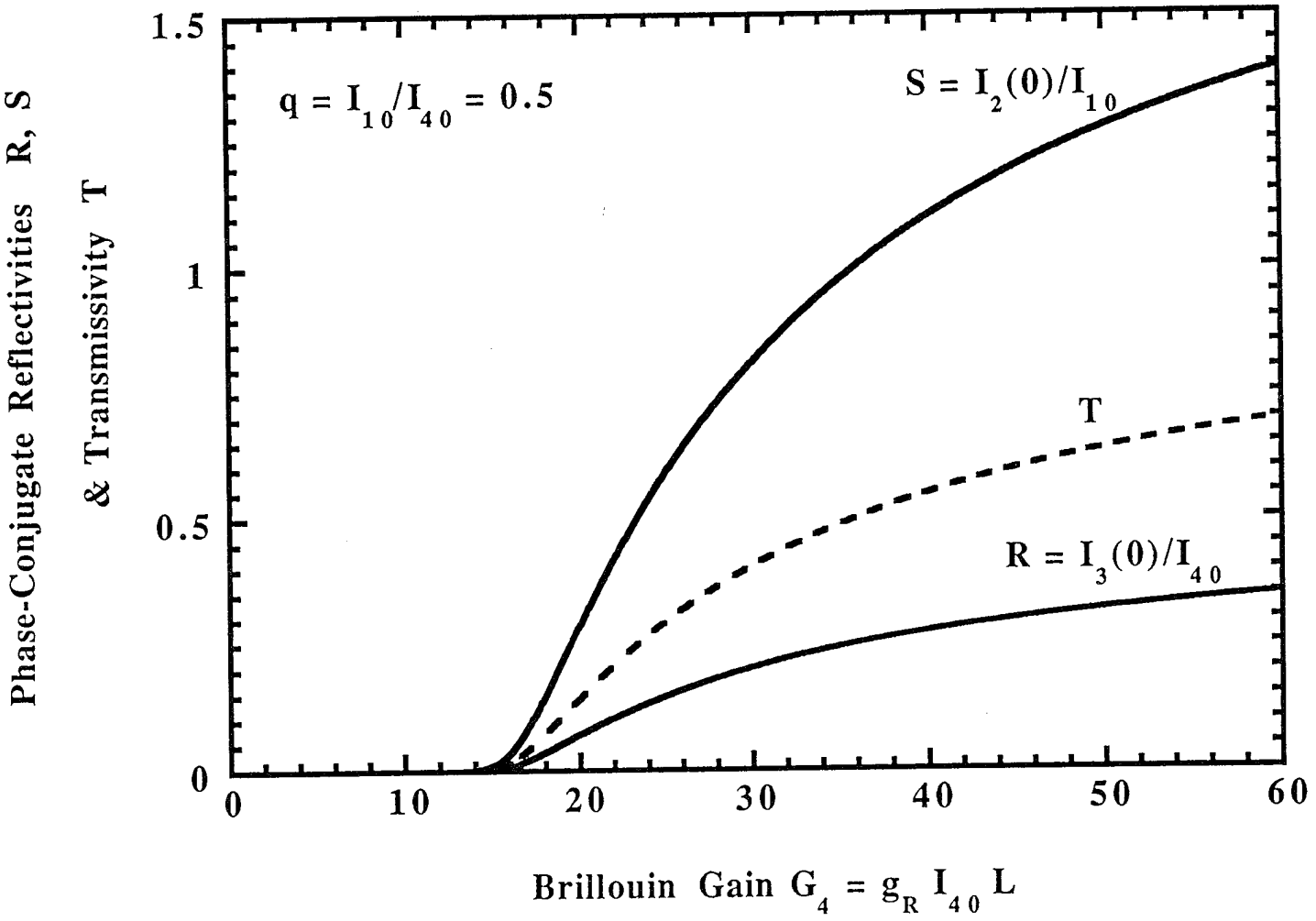

Saxena & McMichael
Fig. 2b

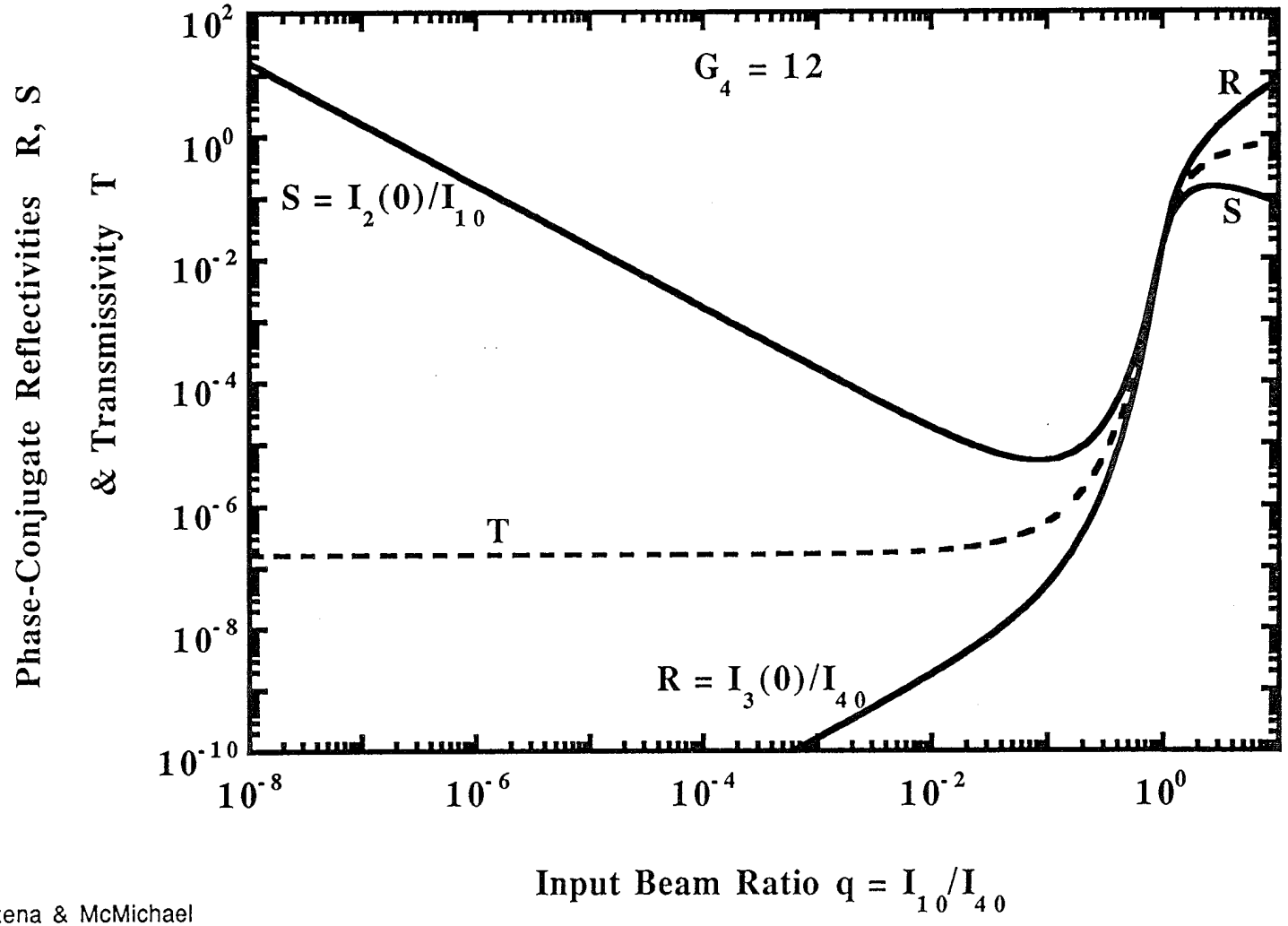

Saxena & McMichael
Fig. 3a

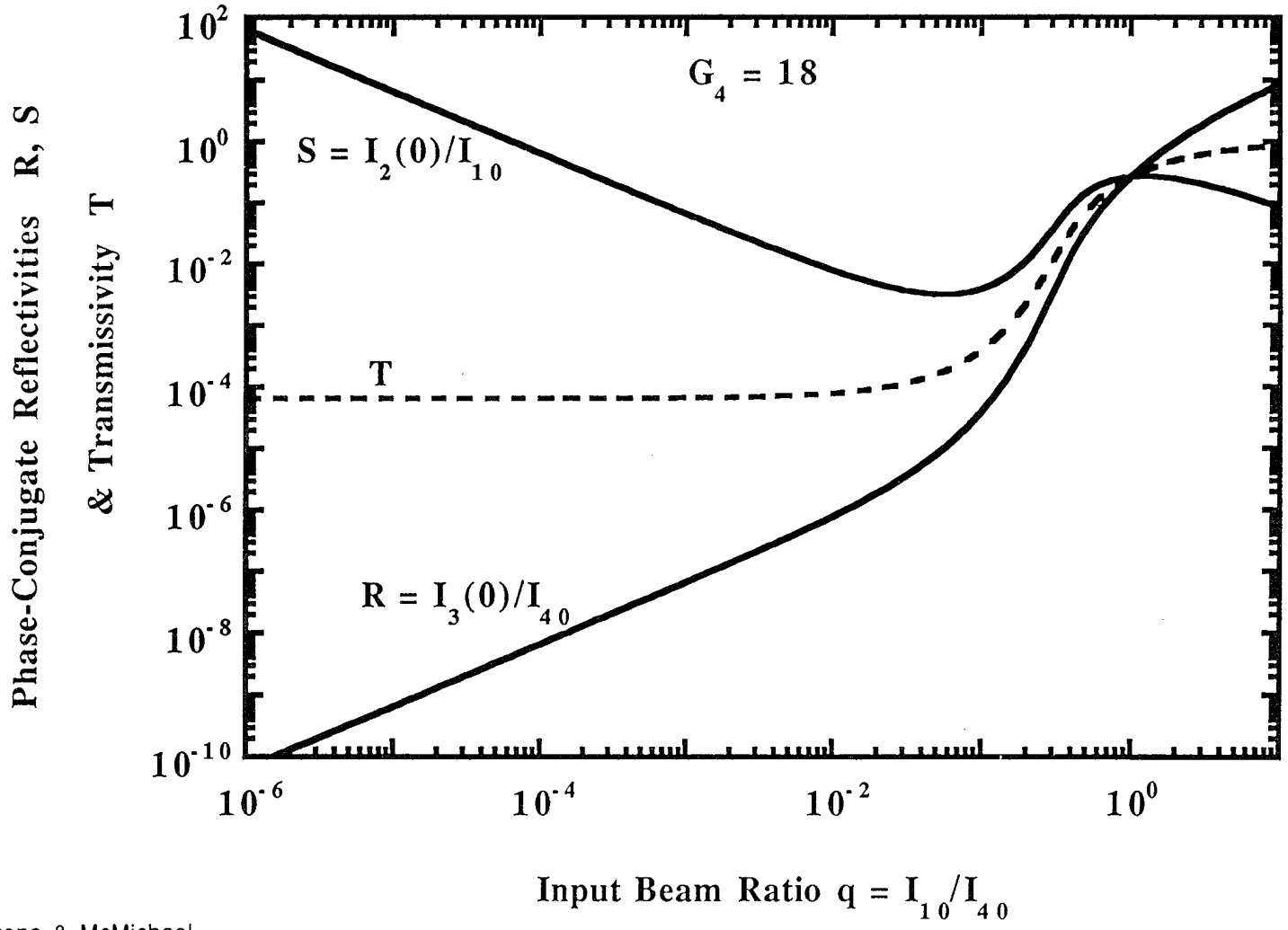

Saxena & McMichael
Fig. 3b

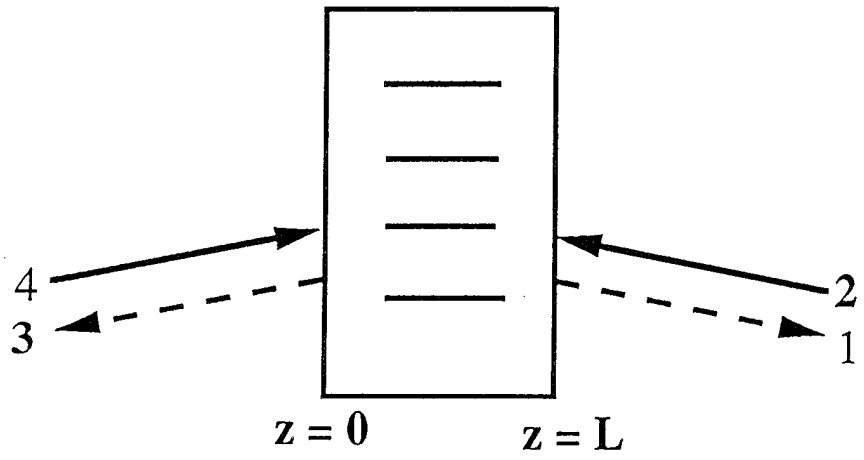

(a)

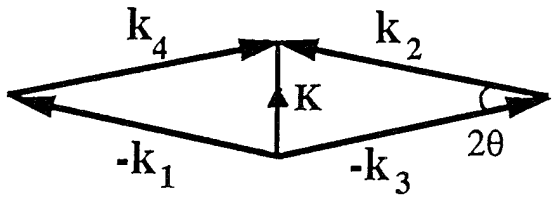

(b)

Saxena & McMichael
Figs. 4

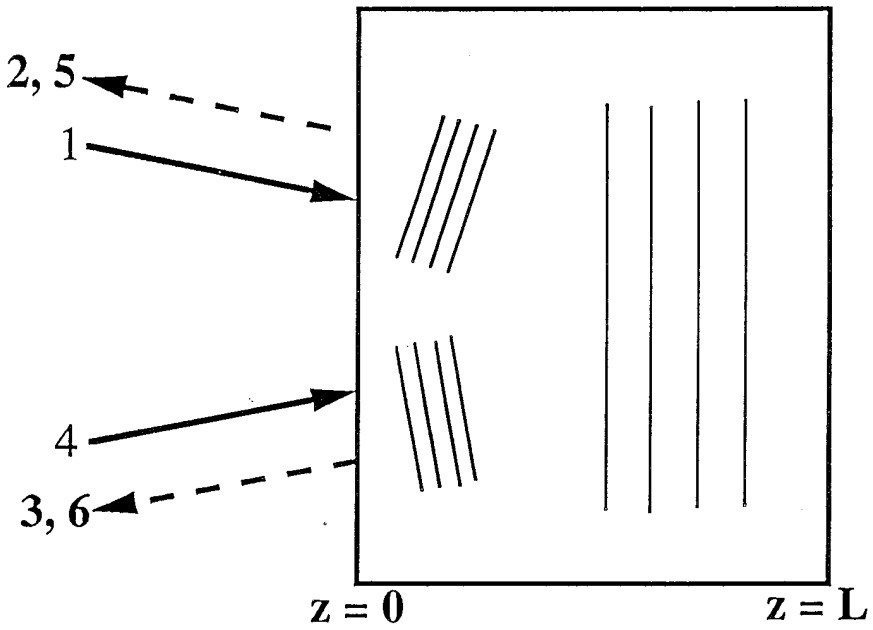

Saxena & McMichael
Fig. 5

A.9

Nonlinear Optical Phase Conjugation by Four-Wave Mixing in Kerr Media

2 Nonlinear Optical Phase Conjugation by Four-Wave Mixing in Kerr Media

R. Saxena and P. Yeh[1]

2.1 Introduction

Optical phase conjugation is a technique for reversing both the direction of propagation and the overall phase factor of an incoming light wave [2.1–5]. This retroreflecting property of phase-conjugate waves is useful in applications requiring automatic pointing and tracking [2.1–5], phase aberration corrections [2.1–5], phase-conjugate resonators [2.6–8], interferometers [2.9–15], gyros [2.16–20], and many other devices.

Various nonlinear optical effects can be utilized to conjugate the phase of an optical beam in real time. Nonlinear optical phase conjugation was first observed in the backward scattered light produced by stimulated Brillouin scattering (SBS) [2.21, 22]. No pump beams are required for phase conjugation by SBS, but the intensity of the incident wave must exceed a threshold value (~ 1 MV/cm^2) for the process to occur. Nonlinear photon echoes [2.23] in an atomic medium provide another technique for generating phase-conjugate waves; however, atomic motion has a serious adverse effect on phase conjugation. Three-wave mixing [2.24] in asymmetric crystals can also yield wave-front reversed replicas, but the phase matching condition restricts the angular field of view of the input wave to very small values. This restriction is eliminated in phase conjugation by four-wave mixing (FWM) [2.25–27], a process that will be studied in detail in this chapter. FWM uses the optically induced polarization of a nonlinear medium that is cubic in the electric field strength, and can occur in all isotropic materials like gases, liquids, and glasses, as well as crystals. In this chapter we will restrict our attention to nonsaturable, transparent Kerr media. We will consider the frequency of all the interacting optical waves to be equal and far removed from any material resonance, and will refer to this as degenerate four-wave mixing (DFWM).

We start by defining phase-conjugate waves and give a simple proof of how aberrations due to propagation in a distorting medium can be corrected by phase conjugation. We then describe the nonlinear optical polarization induced in the medium in the presence of electromagnetic waves, and discuss FWM via a third-order, nonlinear susceptibility. The discussion is then directed to the

---

[1] Pochi Yeh is also a Professor at the Department of Electrical and Computer Engineering, University of California at Santa Barbara.

derivation of the coupled wave equations describing the spatial evolution of the interacting waves. Analytic solutions for the phase-conjugate reflectivity are obtained with negligible pump depletion for both equal and different pump intensities. The case of pump depletion is solved exactly for transmission and reflection geometries. We also consider mutually pumped phase conjugation (MPPC) in Kerr media with electrostrictive nonlinearity. We conclude the chapter with a summary of our results.

2.2 Phase-Conjugate Electromagnetic Waves

Consider the propagation of an electromagnetic wave along the forward z-direction. Its electric field can be written as

$$E = A\cos(\omega t - kz - \phi), \tag{2.1}$$

where ω is the frequency and k is the wave number of the monochromatic optical wave. The amplitude A and the phase ϕ are real functions of position (x, y, z). If the amplitude is a slowly varying function of z compared with $\cos(\omega t - kz - \phi)$, then the propagation of the wave can be easily understood in terms of the motion of the wave fronts: three-dimensional surfaces defined by $kz + \phi(r) =$ constant. The phase-conjugate of an electromagnetic wave defined by (2.1) is given by

$$E_C = A\cos(\omega t + kz + \phi). \tag{2.2}$$

By examining (2.1) and (2.2) we find that these two waves have exactly the same wave fronts at any point in space. However, the motion of these two sets of wave fronts is in opposite directions. In fact, if we reverse the sign of the time variable t in E we obtain E_C, and thus the phase-conjugate wave is often referred to as the time-reversed wave.

Using analytic representation we may write (2.1) as

$$\tilde{E} = A(r)\,e^{i[\omega t - kz - \phi(r)]}, \tag{2.3}$$

where only the real part of the right-hand side is the physical value of the electric field. If we further define a complex amplitude

$$A_1(r) = A(r)e^{-i\phi(r)}, \tag{2.4}$$

then the electric field of (2.3) may be written in analytic representation as

$$\tilde{E} = A_1(r)\,e^{i(\omega t - kz)}. \tag{2.5}$$

Using these definitions the phase-conjugate wave given by (2.2) can be written as

$$\tilde{E}_C = A_1^*(r)\,e^{i(\omega t + kz)}. \tag{2.6}$$

We note that the phase-conjugate wave propagates along the backward z-direction with a complex amplitude A_1^*. To get $\tilde{E}_C$ from $\tilde{E}$ we take the complex conjugate of the *spatial part only*, leaving intact the factor $\exp(i\omega t)$.

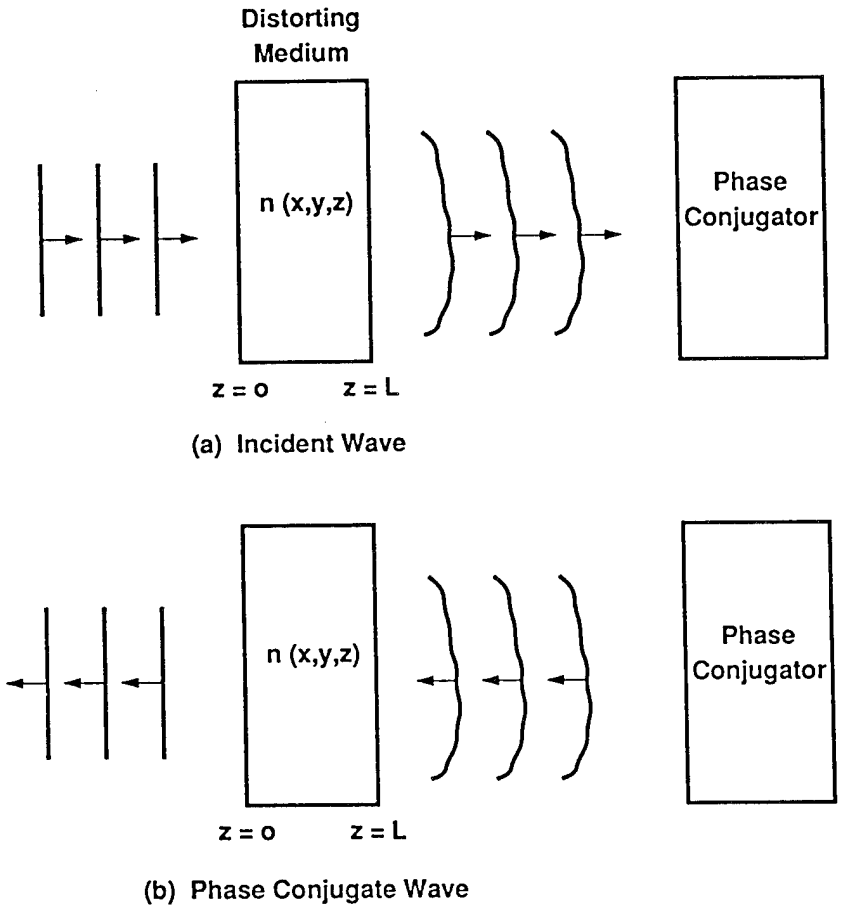

Fig. 2.1. Propagation of phase-conjugate waves

To appreciate the property of phase conjugation we consider the propagation of a plane wave through a distorting medium such as the atmosphere (Fig. 2.1a). Let the distorting medium be confined to the region between $z = 0$ and $z = L$. As a result of the nonuniformity of the refractive index $n(x, y, z)$ of the distorting medium, the wave fronts of the transmitted wave are no longer planar. Let the electric field of the beam propagating in the forward z-direction be represented by (2.5). The wave equation in MKS units is given [2.1] by

$$\nabla^2 \boldsymbol{E} - \mu_0 \varepsilon \frac{\partial^2 \boldsymbol{E}}{\partial t^2} - \mu_0 \sigma \frac{\partial \boldsymbol{E}}{\partial t} = \mu_0 \frac{\partial^2 \boldsymbol{P}_{\mathrm{NL}}}{\partial t^2}, \tag{2.7}$$

where μ_0 is the permeability of the nonmagnetic medium and σ is its conductivity, which is included to account for possible absorption losses. $\varepsilon(x, y, z)$ is the dielectric constant of the distorting medium and $\boldsymbol{P}_{\mathrm{NL}}$ is the nonlinear polarization induced in the medium. In deriving the wave equation (2.7), we have assumed that the fractional change of ε in one optical wavelength is small. If we consider the propagation of the wave given by (2.5) in a medium with negligible absorption ($\sigma = 0$) and negligible nonlinear effects ($\boldsymbol{P}_{\mathrm{NL}} = 0$), then its complex amplitude A_1 must satisfy the following equation:

$$\nabla_\perp^2 A_1 + \left[\frac{\omega^2}{c^2} n^2(x,y,z) - k^2\right] A_1 - 2ik\frac{\partial}{\partial z} A_1 = 0, \tag{2.8}$$

where the subscript $\perp$ denotes spatial derivatives transverse to the z-axis. In deriving (2.8) we have used the slowly varying envelope approximation ($|k_j \partial A_j/\partial z| \gg |\partial^2 A_j/\partial z^2|$), and the relation $\varepsilon = \varepsilon_0 n^2$. This is a first-order differential equation in z; thus, if A_1 is known at $z = z_0$ for all x and y, then A_1 is determined for all points in space, provided that $n(x, y, z)$ is known.

We now consider the complex conjugation of (2.8) as a purely mathematical operation, and assume that the refractive index of the distorting medium is real (i.e., the medium is lossless):

$$\nabla_\perp^2 A_1^* + \left[\frac{\omega^2}{c^2} n^2(x,y,z) - k^2\right] A_1^* + 2ik\frac{\partial}{\partial z} A_1^* = 0. \tag{2.9}$$

This is a scalar wave equation and is obeyed by a wave propagating in the backward z-direction with the form

$$\tilde{E}_C = A_2 \, e^{i(\omega t + kz)}, \tag{2.10}$$

provided that we put

$$A_2 = \rho A_1^* \quad \text{for all } x, y, z, \tag{2.11}$$

where ρ is an arbitrary constant. We have thus shown that a wave $A_2 \exp[i(\omega t + kz)]$, whose spatial portion is everywhere the complex conjugate of $A_1 \exp[i(\omega t - kz)]$, satisfies the same scalar wave equation. Since the scalar wave equation is first order in z, $A_2(x, y, z)$ can be determined for all x, y and z provided that A_2 is known at some $z = z_0$ for all x and y. In addition, if

$$A_2(x, y, z_0) = \rho A_1^*(x, y, z_0) \quad \text{for all } x, y, \tag{2.12}$$

then

$$A_2(x, y, z) = \rho A_1^*(x, y, z) \quad \text{for all } x, y, z. \tag{2.13}$$

Physically, this means that if in some plane $z = z_0$ (say $z_0 > L$ in Fig. 2.1) we generate a wave $\tilde{E}_C$ whose amplitude is the complex conjugate of that of $\tilde{E}$, then $\tilde{E}_C$ will propagate backward and remain the phase conjugate of $\tilde{E}$ everywhere. Its wave fronts will thus coincide with those of $\tilde{E}$ at all points in space. Figure 2.1b illustrates that the propagation of $\tilde{E}_C$ is free of aberrations after traversing the distorting medium.

2.3 Phase Conjugation by Externally Pumped DFWM

2.3.1 Coupled Wave Equations

We consider transparent Kerr media that are nonsaturable and nondispersive. In phase conjugation by FWM [2.25–27] (Fig. 2.2), three optical waves are

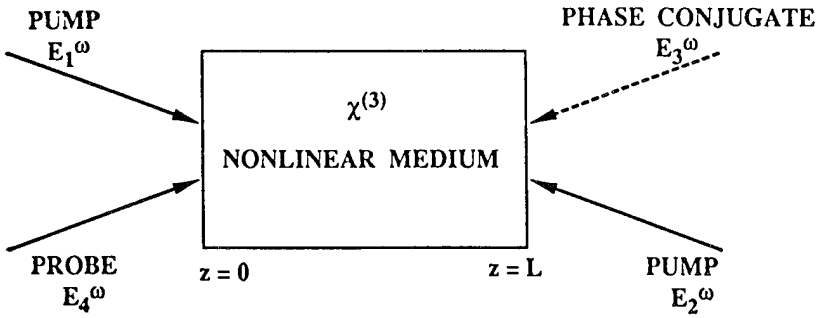

Fig. 2.2. The basic geometry of phase conjugation via FWM

incident simultaneously on the nonlinear medium: two intense, counterpropagating pump beams E_1 and E_2; and a third, weak probe beam E_4 at a small angle ($=2\theta$) to the pump beams. Owing to nonlinear interactions in the medium, a fourth beam E_3 is generated which is the phase conjugate of the probe beam. The frequency of each interacting optical wave is equal to ω, and is far removed from any material resonance. If we assume that all the fields are linearly polarized in the same direction, then the total electric field E is given by

$$E(r,t) = \sum_{j=1}^{4} E_j(r,t) = \frac{1}{2}\sum_{j=1}^{4} A_j(z)\exp[\mathrm{i}(\omega t - \boldsymbol{k}_j\cdot\boldsymbol{r})] + \text{c.c.}, \tag{2.14}$$

where A_j is the complex amplitude of the jth wave in the steady state, and c.c. denotes the complex conjugate. The z-axis is defined to be normal to the surface of the medium, with the complex amplitudes assumed to be functions only of z owing to energy transfer by beam coupling. The polarization induced in the lossless, isotropic Kerr medium is in the same direction as the electric fields, and is given by

$$P = \chi^{(1)}E + \chi^{(2)}E^2 + \chi^{(3)}E^3 + \cdots, \tag{2.15}$$

where $\chi^{(n)}$ is the nth-order electric susceptibility of the medium.

In the following discussion we will consider the polarization term proportional to $\chi^{(3)}$ only, since it can generate the phase-conjugate wave by DFWM. Of all the possible third-order terms that arise from E^3 we are interested only in terms which satisfy the frequency and momentum relation for phase conjugation by FWM: $\omega_1 + \omega_2 = \omega_3 + \omega_4 = 2\omega$, and $\boldsymbol{k}_1 + \boldsymbol{k}_2 = \boldsymbol{k}_3 + \boldsymbol{k}_4$. The quantum-mechanical picture of the process involves annihilation of a photon from each pump wave with the simultaneous creation of a photon for both the probe and the phase-conjugate wave. The wave equation (2.7) is satisfied separately by each frequency component of the total electric field. Using the slowly varying envelope approximation we obtain the following coupled wave equations [2.28–31]

$$\frac{dA_1}{dz} = -\alpha A_1 - i\kappa[A_1(3|A_1|^2 + 6|A_2|^2 + 6|A_3|^2 + 6|A_4|^2) + 6A_2^* A_3 A_4],$$

$$\frac{dA_2}{dz} = \alpha A_2 + i\kappa[A_2(6|A_1|^2 + 3|A_2|^2 + 6|A_3|^2 + 6|A_4|^2) + 6A_1^* A_3 A_4],$$

$$\frac{dA_3}{dz} = \alpha A_3 + i\kappa[A_3(6|A_1|^2 + 6|A_2|^2 + 3|A_3|^2 + 6|A_4|^2) + 6A_1 A_2 A_4^*], \tag{2.16}$$

$$\frac{dA_4}{dz} = -\alpha A_4 - i\kappa[A_4(6|A_1|^2 + 6|A_2|^2 + 6|A_3|^2 + 3|A_4|^2) + 6A_1 A_2 A_3^*],$$

where

$$\alpha \equiv \frac{\sigma}{2\cos\theta}\sqrt{\frac{\mu_0}{\varepsilon}}, \qquad \kappa \equiv \frac{\omega\chi^{(3)}}{8\cos\theta}\sqrt{\frac{\mu_0}{\varepsilon}}. \tag{2.17}$$

In arriving at (2.16) and (2.17) we have assumed that the z-axis coincides with the bisectrix of the beams. The first term on the right-hand side of each equation of (2.16) represents linear absorption in the Kerr medium. In isotropic media the phase-matched, third-order polarization terms in the above equations have different origins: phase modulation, both self and crossed (denoted by PM), transmission gratings (T), reflection gratings (R), and two-photon excitation (2P). The relative magnitude of each process depends strongly on the nonlinear medium, and on the polarization and the relative angles of the interacting waves. Writing the contribution due to each process separately, we obtain the following coupled wave equations:

$$\begin{aligned}
\frac{dA_1}{dz} = {} & -\alpha A_1 - 2i\kappa_{PM} A_1(|A_1|^2 + |A_2|^2 + |A_3|^2 + |A_4|^2) \\
& - 2i\kappa_T A_4(A_1 A_4^* + A_2^* A_3) - 2i\kappa_R A_3(A_1 A_3^* + A_2^* A_4) \\
& - 2i\kappa_R' A_2(A_1 A_2^*) - i\kappa_{2P}[A_1^*(A_1 A_1) + 2A_2^*(A_1 A_2 + A_3 A_4) \\
& + 2A_3^*(A_1 A_3) + 2A_4^*(A_1 A_4)], \\
\frac{dA_2}{dz} = {} & \alpha A_2 + 2i\kappa_{PM} A_2(|A_1|^2 + |A_2|^2 + |A_3|^2 + |A_4|^2) \\
& + 2i\kappa_T A_3(A_1^* A_4 + A_2 A_3^*) + 2i\kappa_R A_4(A_1^* A_3 + A_2 A_4^*) \\
& + 2i\kappa_R' A_1(A_1^* A_2) + i\kappa_{2P}[2A_1^*(A_1 A_2 + A_3 A_4) + A_2^*(A_2 A_2) \\
& + 2A_3^*(A_2 A_3) + 2A_4^*(A_2 A_4)], \\
\frac{dA_3}{dz} = {} & \alpha A_3 + 2i\kappa_{PM} A_3(|A_1|^2 + |A_2|^2 + |A_3|^2 + |A_4|^2) \\
& + 2i\kappa_T A_2(A_1 A_4^* + A_2^* A_3) + 2i\kappa_R A_1(A_1^* A_3 + A_2 A_4^*) \\
& + 2i\kappa_R' A_4(A_3 A_4^*) + i\kappa_{2P}[2A_1^*(A_1 A_3) + 2A_2^*(A_2 A_3) + A_3^*(A_3 A_3) \\
& + 2A_4^*(A_1 A_2 + A_3 A_4)],
\end{aligned} \tag{2.18}$$

$$\begin{aligned}\frac{dA_4}{dz} = &-\alpha A_4 - 2i\kappa_{PM}A_4(|A_1|^2 + |A_2|^2 + |A_3|^2 + |A_4|^2)\\ &- 2i\kappa_T A_1(A_1^* A_4 + A_2 A_3^*) - 2i\kappa_R A_2(A_1 A_3^* + A_2^* A_4)\\ &- 2i\kappa_R' A_3(A_3^* A_4) - i\kappa_{2P}[2A_1^*(A_1 A_4) + 2A_2^*(A_2 A_4)\\ &+ 2A_3^*(A_1 A_2 + A_3 A_4) + A_4^*(A_4 A_4)],\end{aligned} \tag{2.18}$$

where

$$\begin{aligned}&\kappa_{PM} = \frac{\omega\chi_{PM}^{(3)}}{8\cos\theta}\sqrt{\frac{\mu_0}{\varepsilon}}, \quad \kappa_T = \frac{\omega\chi_T^{(3)}}{8\cos\theta}\sqrt{\frac{\mu_0}{\varepsilon}}, \quad \kappa_R = \frac{\omega\chi_R^{(3)}}{8\cos\theta}\sqrt{\frac{\mu_0}{\varepsilon}},\\ &\kappa_R' = \frac{\omega\chi_R'^{(3)}}{8\cos\theta}\sqrt{\frac{\mu_0}{\varepsilon}}, \quad \kappa_{2P} = \frac{\omega\chi_{2P}^{(3)}}{8\cos\theta}\sqrt{\frac{\mu_0}{\varepsilon}}.\end{aligned} \tag{2.19}$$

Note that if all the third-order electric susceptibilities are equal ($\chi_{PM}^{(3)} = \chi_T^{(3)} = \chi_R^{(3)} = \chi_R'^{(3)} = \chi_{2P}^{(3)} \equiv \chi^{(3)}$) then we recover the coupled wave equations of (2.16).

The first nonlinear term on the right-hand side of each equation in (2.18) represents self and crossed phase modulation terms, so called because these terms modify the phase of each wave without contributing to the energy exchange. The next two mechanisms, with coupling constants κ_T and κ_R, κ_R', can be viewed as a holographic process as shown in Fig. 2.3. Transmission gratings are formed by the interference of the forward pump with the probe beam, and the backward pump with the phase-conjugate beam, both gratings having large spacing and the same wavevector. Reflection gratings are formed by the interference of the forward pump with the phase-conjugate beam, and the backward

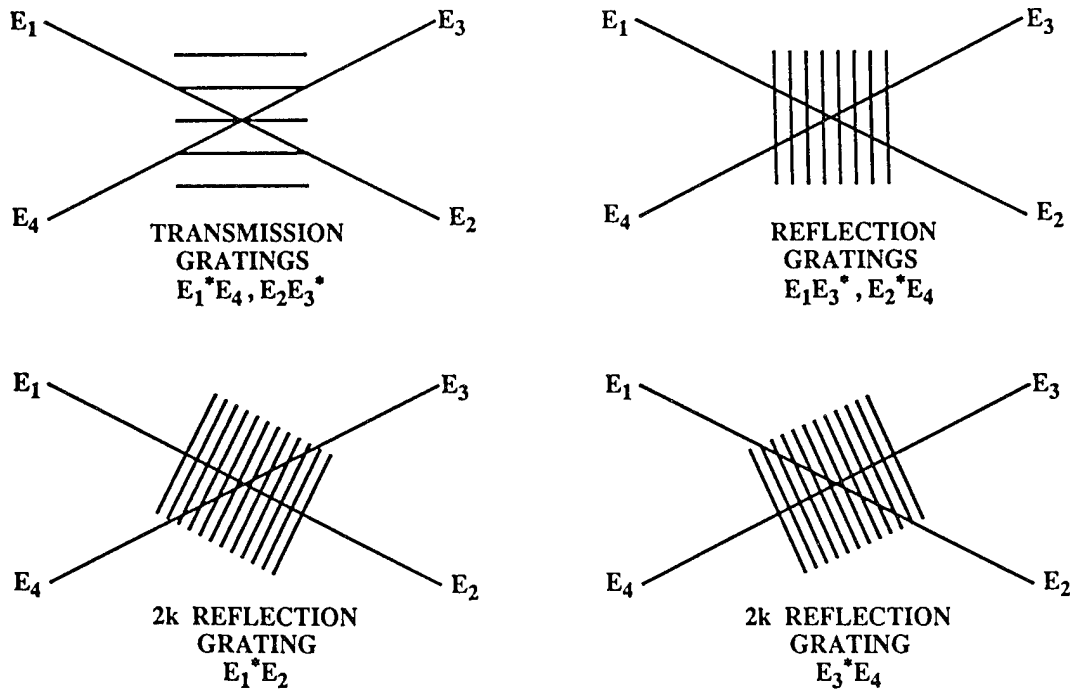

Fig. 2.3. Gratings formed in FWM

pump with the probe beam, both gratings having the same wavevector and smaller spacing than the transmission gratings. Two additional reflection gratings (known as the '$2k$' gratings because of the magnitudes of their grating wavevectors) are formed by both pairs of counterpropagating beams in the FWM geometry: one pair is formed by the oppositely travelling pump waves, and the other is formed by the probe and phase-conjugate waves. The '$2k$' gratings have a very fine grating spacing and the response of the medium at such high spatial frequencies is usually small. The last mechanism has no holographic analog, and corresponds to a nonlinear index that has no spatial modulation but temporal oscillations at frequency 2ω. It arises because of self- or induced two-photon absorption. Readout (or interaction) of the nonlinear index with a third wave generates the desired polarization.

The formidable task of solving the complete nonlinear coupled equations (2.16) in the presence of linear absorption and pump depletion in the medium, with the effects of nonlinear refraction included, was undertaken numerically by *Guha* and *Conner* [2.31]. Their method does not require the determination of the first integrals of the coupled nonlinear differential equations, and the effects of linear absorption can be incorporated in the theory in a straightforward manner. *Marburger* and *Lam* [2.28] also examined this problem for collinear geometry of all the interacting waves, with the pumps polarized orthogonally to the probe and phase-conjugate beams. This results in the elimination of terms with coupling constants κ_T and κ_R, as well as two terms with coupling constant κ_{2P}, on the right-hand side of the coupled wave equations (2.18) because the scalar product of the two fields is zero for this choice of polarization. For negligible absorption, the equations have also been solved by *Maruani* [2.29], *Ujihara* [2.30], and *Lytel* [2.33]. *Kaplan* and *Law* [2.32] showed the existence of multistable roots and isolas in the input–output response of FWM in Kerr media.

2.3.2 Analytic Solutions with Negligible Absorption and Undepleted Pumps

We now limit our attention to the case of negligible absorption in the medium ($\alpha = 0$), and equal third-order electric susceptibilities for all the processes. We also assume that the pump fields are much stronger than the probe and conjugate fields, so that $|A_1|, |A_2| \gg |A_3|, |A_4|$. The coupled wave equations (2.16) then simplify to

$$\frac{dA_1}{dz} = -3i\kappa A_1(|A_1|^2 + 2|A_2|^2),$$

$$\frac{dA_2}{dz} = 3i\kappa A_2(2|A_1|^2 + |A_2|^2),$$

$$\frac{dA_3}{dz} = 6i\kappa[A_3(|A_1|^2 + |A_2|^2) + A_1 A_2 A_4^*],$$

$$\frac{dA_4}{dz} = -6i\kappa[A_4(|A_1|^2 + |A_2|^2) + A_1 A_2 A_3^*]. \tag{2.20}$$

The terms involving the square of the modulus of the complex amplitudes on the right-hand side modify the phases of the waves without affecting the energy exchange between the waves. In the limit of strong pumps the pump equations are not coupled to the weak probe and its phase conjugate, and can be solved separately. One can show from the pump equations that $d|A_1|^2/dz = d|A_2|^2/dz = 0$, so that as the pumps propagate through the medium their intensities remain constant at $|A_{10}|^2$ and $|A_{2L}|^2$ respectively, using the notation $A_1(0) \equiv A_{10}$, and $A_2(L) = A_{2L}$. When the electric fields of the optical waves are described by equations (2.14), then the intensity of the j-th wave is equal to $\varepsilon_0 nc|A_j|^2/2$ in MKS units [2.5]. Ignoring the numerical factor, we use $|A_j|^2$ to represent the intensity of the j-th wave. The pump phases, however, vary linearly with distance owing to the change in their propagation vectors:

$$\begin{aligned} A_1(z) &= A_{10}\exp[-3i\kappa z(|A_{10}|^2 + 2|A_{2L}|^2)], \\ A_2(z) &= A_{2L}\exp[3i\kappa(z - L)(2|A_{10}|^2 + |A_{2L}|^2)]. \end{aligned} \tag{2.21}$$

The product of the two pump amplitudes is now given by

$$\begin{aligned} &A_1(z)A_2(z) \\ &\quad = A_{10}A_{2L}\exp[3i\kappa z(|A_{10}|^2 - |A_{2L}|^2)]\exp[-3i\kappa L(2|A_{10}|^2 + |A_{2L}|^2)]. \end{aligned} \tag{2.22}$$

Note that the z dependence of the product vanishes for equal pump intensities ($|A_{10}|^2 = |A_{2L}|^2$). For unequal pump intensities this product will introduce a phase mismatch in the coupling terms $A_1 A_2 A_4^*$ and $A_1 A_2 A_3^*$ that occur in (2.20) for waves 3 and 4 respectively [2.26].

2.3.2.1 Equal Pump Intensities

We now solve for the probe and the phase-conjugate waves assuming equal pump intensities ($|A_{10}|^2 = |A_{2L}|^2 \equiv I_{10}$). Defining new variables

$$\begin{aligned} B_3 &= A_3\exp[-6i\kappa z(|A_{10}|^2 + |A_{2L}|^2)], \\ B_4 &\equiv A_4\exp[6i\kappa z(|A_{10}|^2 + |A_{2L}|^2)], \end{aligned} \tag{2.23}$$

the equations for A_3 and A_4 in (2.20) become

$$\begin{aligned} \frac{dB_3}{dz} &= i\tilde{\kappa}B_4^*, \\ \frac{dB_4}{dz} &= -i\tilde{\kappa}B_3^*, \end{aligned} \tag{2.24}$$

where

$$\tilde{\kappa} \equiv 6\kappa A_{10} A_{2L} \exp[-3i\kappa L(2|A_{10}|^2 + |A_{2L}|^2)]. \tag{2.25}$$

Boundary conditions specify the complex amplitudes $A_3(L) = A_{3L}$ and $A_4(0) = A_{40}$ of the two waves at their input planes $z = L$ and $z = 0$, respectively. The solutions of (2.24) have the form

$$\begin{aligned} B_3(z) &= \frac{\cos(|\tilde{\kappa}|z)}{\cos(|\tilde{\kappa}|L)} B_{3L} + i\frac{\tilde{\kappa}}{|\tilde{\kappa}|} \frac{\sin[|\tilde{\kappa}|(z-L)]}{\cos(|\tilde{\kappa}|L)} B_{40}^*, \\ B_4(z) &= -i\frac{\tilde{\kappa}}{|\tilde{\kappa}|} \frac{\sin(|\tilde{\kappa}|z)}{\cos(|\tilde{\kappa}|L)} B_{3L}^* + \frac{\cos[|\tilde{\kappa}|(z-L)]}{\cos(|\tilde{\kappa}|L)} B_{40}. \end{aligned} \tag{2.26}$$

For phase conjugation by DFWM the probe wave B_{40} is nonzero at its input plane $z = 0$, while there is no conjugate wave at the $z = L$ plane, i.e., $A_{3L} = 0 = B_{3L}$. In this case the solutions in (2.26) simplify to

$$\begin{aligned} B_3(z) &= -i\frac{\tilde{\kappa}}{|\tilde{\kappa}|} \frac{\sin[|\tilde{\kappa}|(L-z)]}{\cos(|\tilde{\kappa}|L)} B_{40}^*, \\ B_4(z) &= \frac{\cos[|\tilde{\kappa}|(L-z)]}{\cos(|\tilde{\kappa}|L)} B_{40}. \end{aligned} \tag{2.27}$$

Note that wave B_3, generated by nonlinear interactions in the medium, is linearly proportional to the complex conjugate of the input probe wave B_{40}^*. Consider an input probe beam that is not a plane wave but possesses a complex wave front; it can be considered as a continuous superposition of plane waves all having the same frequency but different wave vectors. Owing to the linearity of (2.27), each of the plane wave components of the complex input wave front is phase-conjugated independently, resulting in a phase-conjugate wave front travelling in the backward direction [2.5, 26]. Hence faithful distortion correction is possible for an input probe beam with large angular field of view if we use a phase conjugator that relies on FWM in a Kerr medium. For small coupling strength ($|\tilde{\kappa}|L \ll 1$), the phase-conjugate wave at the output plane simplifies to $A_3(0) \approx -6i\kappa L A_{10} A_{2L} A_{40}^* \exp[-3i\kappa L(2|A_{10}|^2 + |A_{2L}|^2)]$, which shows how the nonlinear mixing of the three input waves in the medium led to the generation of the fourth wave. The phase-conjugate reflectivity R and the coherent transmissivity T are given by [2.1, 5, 26]

$$\begin{aligned} R &= \frac{|A_3(0)|^2}{|A_{40}|^2} = \frac{|B_3(0)|^2}{|B_{40}|^2} = \tan^2(|\tilde{\kappa}|L), \\ T &= \frac{|A_4(L)|^2}{|A_{40}|^2} = \frac{|B_4(L)|^2}{|B_{40}|^2} = \frac{1}{\cos^2(|\tilde{\kappa}|L)}. \end{aligned} \tag{2.28}$$

The expression for T shows that the transmitted probe beam is amplified for all values of pump intensities and coupling strength, while $R \geq 1$ only if $|\tilde{\kappa}|L \geq \pi/4$. When $|\tilde{\kappa}|L = \pi/2$ then $R = T = \infty$, which corresponds to oscillation – nonzero outputs of the phase-conjugate wave and the transmitted probe wave exist at the output planes even in the absence of an input probe wave A_{40}. This depen-

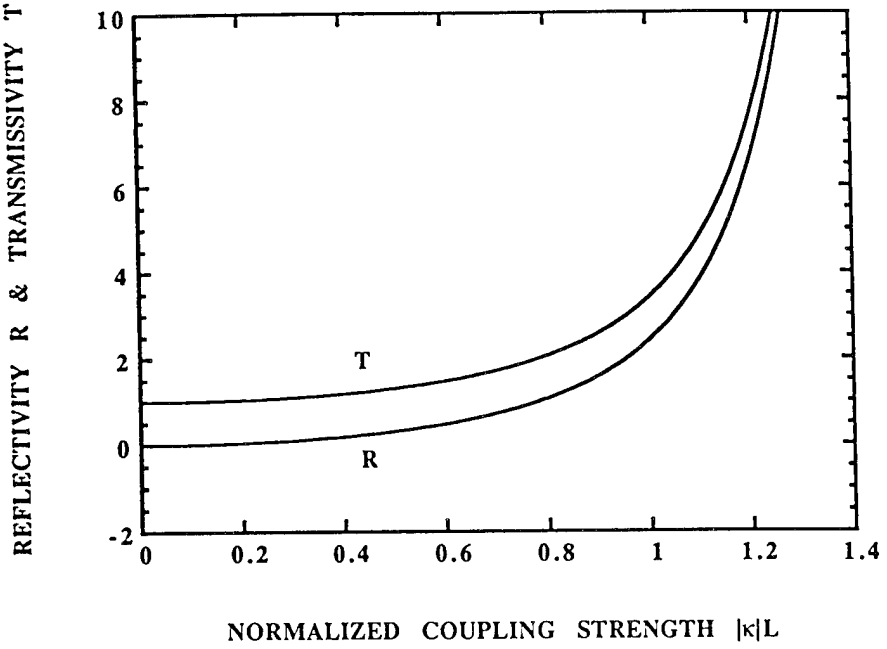

Fig. 2.4. Phase-conjugate reflectivity R and transmissivity T as a function of normalized coupling strength $|\tilde{\kappa}|L$.

dence of R and T on $|\tilde{\kappa}|L$ is shown in Fig. 2.4. In an experiment on phase conjugation by FWM in a $\chi^{(3)}$ nonlinear medium with interaction length L, such a behavior would be obtained by measuring R and T as a function of the equal pump intensity I_{10}. For small nonlinearity (i.e. $|\tilde{\kappa}|L \ll 1$), $R \approx |\tilde{\kappa}|^2L^2 = 36\kappa^2L^2I_{10}^2$ and $T \approx 1 + |\tilde{\kappa}|^2L^2 = 1 + 36\kappa^2L^2I_{10}^2$. Hence a plot of phase-conjugate reflectivity as a function of pump intensity on a log–log scale would have a slope of 2 and an intercept equal to $2\log(6\kappa L)$. An experimental measurement of the phase-conjugate reflectivity R for known values of the equal pump intensity I_{10} and the interaction length L would yield the value of the coupling constant κ, which in turn is a known function [see (2.17)] of the nonlinear susceptibility $\chi^{(3)}$ of the FWM medium.

Figure 2.5 is a plot of the beam intensities $I_3(z)$ and $I_4(z)$, normalized to the input probe intensity I_{40}, as a function of distance inside the interaction region for $|\tilde{\kappa}|L = \pi/3$. The conjugate wave is zero at the input plane $z = L$, and exceeds the probe input intensity at the output plane $z = 0$, leading to a reflectivity greater than unity ($R = 3$). At the same time the transmitted probe beam intensity exceeds its input intensity, leading to a coherent transmission amplification ($T = 4$). The amplifications of the probe and phase-conjugate beams are at the expense of the pump beams.

The case of nearly degenerate FWM (NDFWM), in which the weak incident probe field is at a slightly different frequency to the frequency of the two pump beams, has been considered by Pepper and Abrams [2.34, 26]. For weak nonlinear coupling their results show that the phase-conjugate reflectivity has a

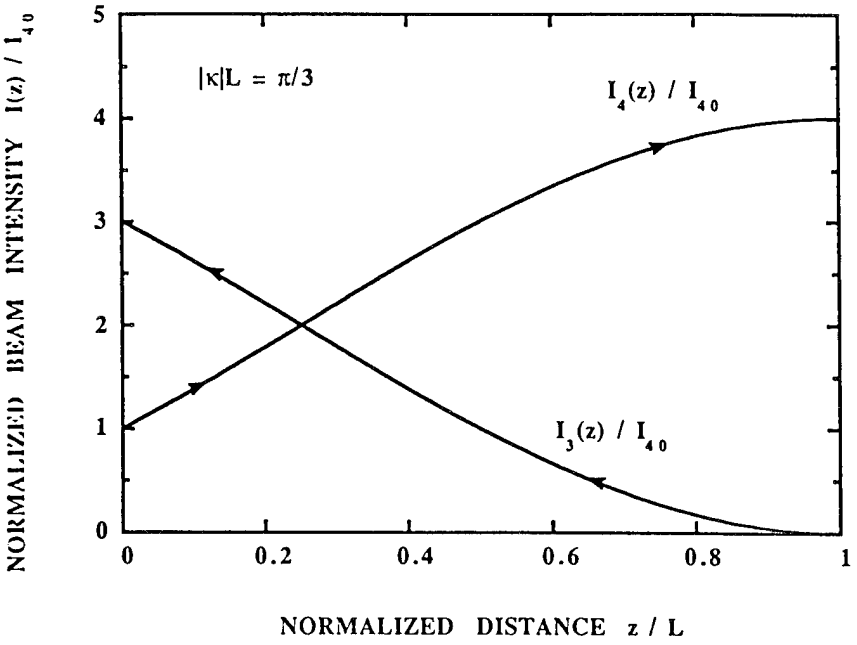

Fig. 2.5. Normalized beam intensities inside the interaction region for $|\tilde{\kappa}|L = \pi/3$

$\mathrm{sinc}^2(x)$ dependence on the phase mismatch, which is a typical result for coherent, phase-mismatched, nondepleted interactions [2.5].

2.3.2.2 Unequal Pump Intensities

The coupled wave equations (2.24) for the probe and the phase-conjugate waves will now have a phase mismatch factor due to the unequal intensities of the pump beams:

$$\frac{dB_3}{dz} = i\tilde{\kappa}e^{i\beta z}B_4^*,$$
$$\frac{dB_4}{dz} = -i\tilde{\kappa}e^{i\beta z}B_3^*, \tag{2.29}$$

where the phase mismatch wavevector β is given from (2.22) by the following quantity:

$$\beta = 3\kappa(|A_{10}|^2 - |A_{2L}|^2)]. \tag{2.30}$$

Note that $\beta = 0$ for equal pump intensities. Assuming the boundary conditions appropriate for phase conjugation by DFWM ($B_{3L} = 0$, $B_{40} \neq 0$), the solutions of (2.29) have the following form:

$$B_3(z) = -i\tilde{\kappa}B_{40}^* e^{i\beta z/2} \frac{\sin[\gamma(L-z)]}{\gamma\cos(\gamma L) - i\frac{\beta}{2}\sin(\gamma L)},$$

$$B_4(z) = B_{40} e^{i\beta z/2} \frac{\gamma \cos[\gamma(L-z)] + i\frac{\beta}{2}\sin[\gamma(L-z)]}{\gamma \cos(\gamma L) + i\frac{\beta}{2}\sin(\gamma L)}, \tag{2.31}$$

where $\gamma \equiv \sqrt{|\tilde{\kappa}|^2 + \beta^2/4}$. If $\beta = 0$, then $\gamma = |\tilde{\kappa}|$ and the solutions given by (2.31) reduce to those in (2.27) for equal pump intensity. The phase-conjugate reflectivity R is given by the simple expression [2.31]

$$R = \frac{\sin^2(\gamma L)}{\frac{\gamma^2}{|\tilde{\kappa}|^2} - \sin^2(\gamma L)}, \tag{2.32}$$

which reduces to (2.28) when $\beta = 0$. For R to be equal to infinity (self-oscillation), $\gamma^2/|\tilde{\kappa}|^2 = \sin^2(\gamma L)$ which can only be true if $\beta = 0$, i.e., only for equal pump intensities [2.28, 31]. If the coupling constant is much smaller than the phase mismatch (i.e., $|\tilde{\kappa}| \ll \beta/2$), then the phase-conjugate reflectivity has a $\mathrm{sinc}^2(x)$ dependence [2.26, 34]: $R \approx [|\tilde{\kappa}| L \sin(\beta L/2)/(\beta L/2)]^2$.

Figure 2.6 is a plot of the phase-conjugate reflectivity R as a function of the normalized phase mismatch βL introduced by the unequal pump intensities, for several values of the coupling strength $|\tilde{\kappa}|L$. For $|\tilde{\kappa}|L = \pi/2$, self-oscillation occurs only at $\beta = 0$; finite values of imbalance in the pump intensities serve to reduce the phase-conjugate reflectivity from this optimum value. The qualitative features of this figure are similar to the frequency bandpass-filter characteristics of the phase-conjugator when the probe frequency has a small detuning from the pump frequency (NDFWM) [2.26, 34].

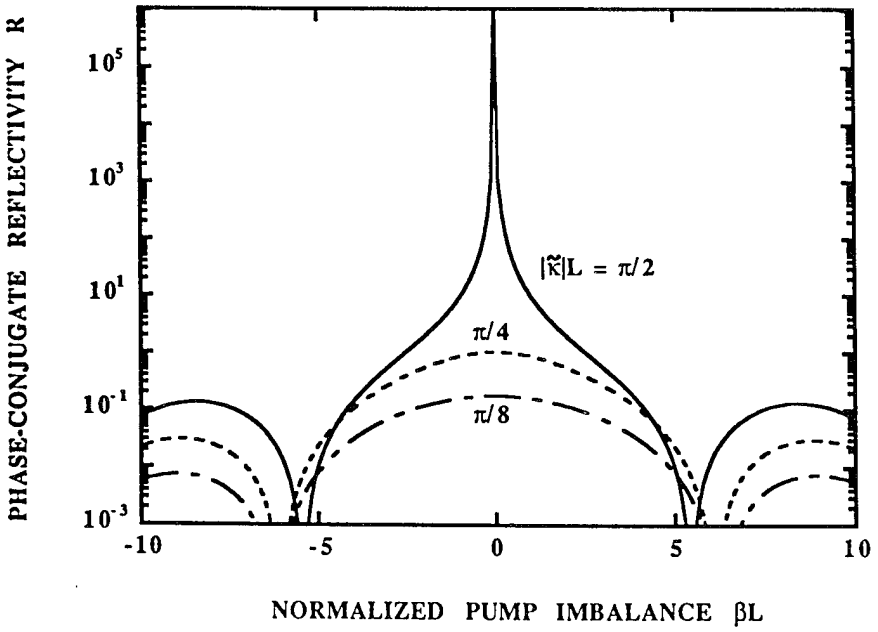

Fig. 2.6. Phase-conjugate reflectivity R as a function of normalized pump imbalance βL for various coupling strengths.

2.3.3 Analytic Solutions with Pump Depletion but Negligible Absorption

2.3.3.1 The Transmission Grating

We now consider a lossless ($\alpha = 0$) Kerr medium with negligible response at high spatial frequencies, so that $\kappa_R = \kappa_R' = 0$. In addition, we neglect two-photon interactions in the medium, so that the coupled wave equations (2.18) simplify to

$$\begin{aligned}
\frac{dA_1}{dz} &= -2i\kappa_{PM}A_1 I_0 - 2i\kappa_T A_4(A_1 A_4^* + A_2^* A_3),\\
\frac{dA_2}{dz} &= 2i\kappa_{PM}A_2 I_0 + 2i\kappa_T A_3(A_1^* A_4 + A_2 A_3^*),\\
\frac{dA_3}{dz} &= 2i\kappa_{PM}A_3 I_0 + 2i\kappa_T A_2(A_1 A_4^* + A_2^* A_3),\\
\frac{dA_4}{dz} &= -2i\kappa_{PM}A_4 I_0 - 2i\kappa_T A_1(A_1^* A_4 + A_2 A_3^*),
\end{aligned} \tag{2.33}$$

where I_0 is proportional to the total intensity of all the beams:

$$I_0 = \sum_{j=1}^{4} |A_j|^2. \tag{2.34}$$

The differential equations (2.33) verify that $dI_0/dz = 0$, so that the total intensity is conserved. As in the previous section the phase modulation terms in each equation modify the phase of the wave, and can be eliminated by introducing new variables B_j in the following manner:

$$\begin{aligned}
B_1 &\equiv A_1 e^{2i\kappa_{PM}I_0 z}, \qquad B_2 \equiv A_2 e^{-2i\kappa_{PM}I_0 z},\\
B_3 &\equiv A_3 e^{-2i\kappa_{PM}I_0 z}, \qquad B_4 \equiv A_4 e^{2i\kappa_{PM}I_0 z}.
\end{aligned} \tag{2.35}$$

In terms of the new variables the coupled wave equations are:

$$\begin{aligned}
\frac{dB_1}{dz} &= -2i\kappa_T B_4(B_1 B_4^* + B_2^* B_3),\\
\frac{dB_2}{dz} &= 2i\kappa_T B_3(B_1^* B_4 + B_2 B_3^*),\\
\frac{dB_3}{dz} &= 2i\kappa_T B_2(B_1 B_4^* + B_2^* B_3),\\
\frac{dB_4}{dz} &= -2i\kappa_T B_1(B_1^* B_4 + B_2 B_3^*).
\end{aligned} \tag{2.36}$$

These equations are similar in form to the coupled wave equations for DFWM in photorefractive media in transmission geometry [2.35, 36], but with a cou-

pling constant κ_T that is purely real. As the beams propagate in the nonlinear medium we find that the following quantities are conserved:

$$\begin{aligned} &I_1(z) + I_4(z) = d_1, \\ &I_2(z) + I_3(z) = d_2, \\ &B_1(z)B_2(z) + B_3(z)B_4(z) = c, \end{aligned} \tag{2.37}$$

where the constants d_1 and d_2 are determined by the boundary values of the problem, and the integration constant c is yet to be determined. The first two equations show that the total forward and backward energies are conserved separately at each plane, while the last conservation law is an outcome of the reciprocity theorem [2.37]. With the help of these conservation laws, the four coupled equations of (2.36) can be decoupled to yield the following two first-order differential equations for the new variables $B_{12} \equiv B_1/B_2^*$ and $B_{34} \equiv B_3/B_4^*$:

$$\begin{aligned} \frac{dB_{12}}{dz} &= -2i\kappa_T[c + (d_1 - d_2)B_{12} - c^*B_{12}^2], \\ \frac{dB_{34}}{dz} &= 2i\kappa_T[c + (d_2 - d_1)B_{34} - c^*B_{34}^2]. \end{aligned} \tag{2.38}$$

These equations can be readily solved to yield the following solutions:

$$\begin{aligned} B_{12}(z) &= \frac{QB_{12}(0) + i\tan(\kappa_T Qz)[\Delta B_{12}(0) - 2c]}{Q - i\tan(\kappa_T Qz)[\Delta + 2c^*B_{12}(0)]}, \\ B_{34}(z) &= \frac{QB_{34}(0) + i\tan(\kappa_T Qz)[\Delta B_{34}(0) + 2c]}{Q - i\tan(\kappa_T Qz)[\Delta - 2c^*B_{34}(0)]}, \end{aligned} \tag{2.39}$$

where the parameters Δ and Q are defined as

$$\begin{aligned} &\Delta = d_2 - d_1, \\ &Q = (\Delta^2 + 4|c|^2)^{1/2}. \end{aligned} \tag{2.40}$$

For phase conjugation by DFWM the boundary conditions are the nonzero values of the two pump fields at $z = 0$ and $z = L$ (A_{10} and A_{2L}, respectively) and the probe field at $z = 0$ (A_{40}), while the phase-conjugate field is zero and its input plane $z = L$ ($A_{3L} = 0$). With $B_{34}(L) = 0$, we obtain the phase-conjugate reflection coefficient ρ ($= B_{34}(0)$):

$$\rho = -\frac{2ic\tan(\kappa_T QL)}{Q + i\Delta\tan(\kappa_T QL)}. \tag{2.41}$$

If we assume that the probe and phase-conjugate waves are much weaker than the two strong, equal intensity pump waves ($I_3, I_4 \ll I_1 = I_2$), then $\Delta = 0$ and $Q^2 = 4|c|^2$. From the third conservation law in (2.37) we find that $c = B_1B_2$, so that $Q = 2|B_1B_2|$. Hence the expression for ρ simplifies to:

$$\rho \approx -\mathrm{i}\frac{B_1 B_2}{|B_1 B_2|}\tan(2\kappa_T |B_1 B_2| L), \tag{2.42}$$

which is identical to the complex phase-conjugate reflection coefficient that can be obtained from (2.27), for negligible pump depletion, but with $2\kappa_T$ in the above equation replaced by 6κ for equal contributions from all the different mechanisms besides the transmission grating. The phase-conjugate intensity reflectivity is defined as $R \equiv |\rho|^2$, and an examination of (2.41) reveals that R is a function of $|c|^2$ only, and not of any linear combinations of c and c^*. We may solve for $|c|^2$ by recalling that $B_{12}(L) = c/I_{2L}$. Also, $B_{12}(0) = I_{10}/(c^* - \rho^* I_{40})$, where we have used the third conservation law of (2.37). Substituting these values of B_{12} and ρ into the first equation of (2.39) evaluated at $z = L$, we obtain the following transcendental equation for $|c|^2$:

$$(|c|^2 - I_{10}I_{2L})[Q^2 + \Delta^2 \tan^2(\kappa_T QL)] + 4|c|^2 I_{2L} I_{40} \tan^2(\kappa_T QL) = 0. \tag{2.43}$$

To study the phase-conjugate reflectivity R numerically, we define beam ratios at input as follows: probe ratio, $q = I_{40}/(I_{10} + I_{2L})$; pump ratio, $r = I_{2L}/I_{10}$; and $I_0 = 1$. In terms of these parameters the input beam intensities, normalized to the total input intensity, are given by: $I_{10}/I_0 = 1/[(1 + q)(1 + r)]$, $I_{2L}/I_0 = r/[(1 + q)(1 + r)]$, and $I_{40}/I_0 = q/(1 + q)$. The argument of the tangent function $(= \kappa_T QL)$ in (2.43) can be expressed as GQ_n, where $G = \kappa_T I_0 L$ is the net coupling strength in the Kerr medium and $Q_n = Q/I_0$.

Figure 2.7 is a plot of the phase-conjugate reflectivity R in transmission geometry versus the net coupling strength G for equal intensity pump beams ($r = 1$), and with a probe as strong as the sum of the two pumps ($q = 1$). The

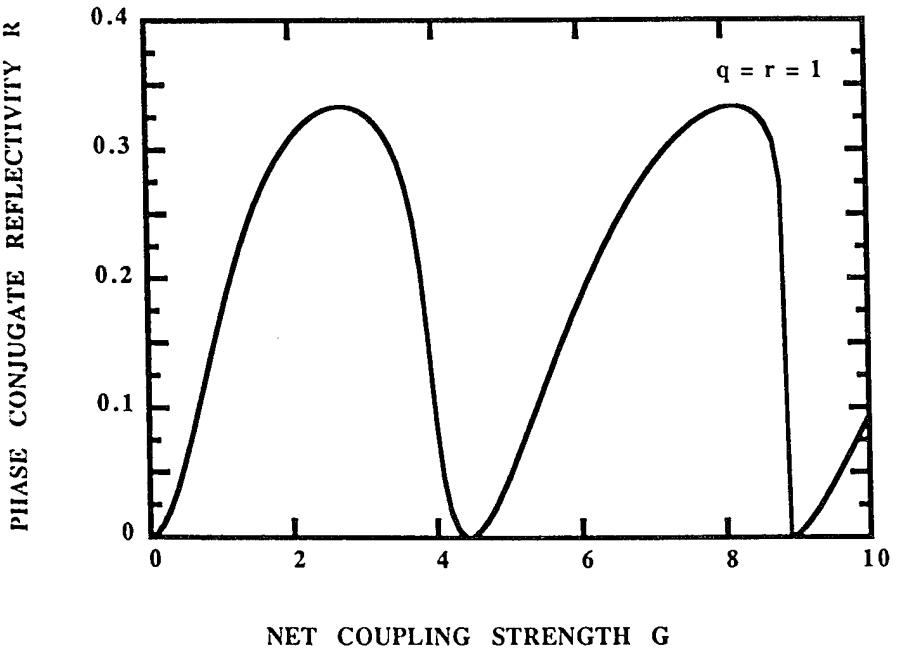

Fig. 2.7. Phase-conjugate reflectivity R as a function of net coupling strength G for $q = r = 1$

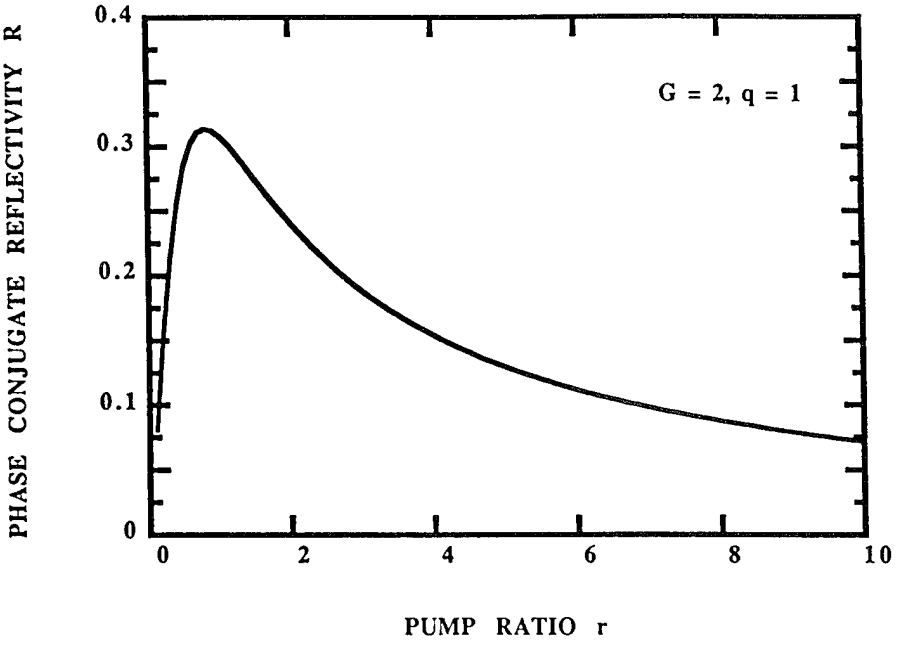

Fig. 2.8. Phase-conjugate reflectivity R as a function of pump ratio r for $G = 2$ and $q = 1$

reflectivity R exhibits oscillations as a function of G, and can even be multivalued for a suitable choice of the parameters q and r, leading to bistability [2.28, 32]. Smaller probe intensity compared to equal intensity of the strong pumps tends to lead to instabilities in the behavior of R versus G. Figure 2.8 is a plot of R versus the pump ratio r for $G = 2$ and $q = 1$. Note that the reflectivity is maximized when the pump beams are of equal intensity

2.3.3.2. The Reflection Grating

We now assume that the response of the medium to two-photon interactions, transmission gratings, and '$2k$' gratings is negligible, so that $\kappa_{2P} = \kappa_T = \kappa'_R = 0$. The coupled equations (2.18) then simplify to

$$\begin{aligned}
\frac{dA_1}{dz} &= -2i\kappa_{PM}A_1 I_0 - 2i\kappa_R A_3(A_1 A_3^* + A_2^* A_4),\\
\frac{dA_2}{dz} &= 2i\kappa_{PM}A_2 I_0 + 2i\kappa_R A_4(A_1^* A_3 + A_2 A_4^*),\\
\frac{dA_3}{dz} &= 2i\kappa_{PM}A_3 I_0 + 2i\kappa_R A_1(A_1^* A_3 + A_2 A_4^*),\\
\frac{dA_4}{dz} &= -2i\kappa_{PM}A_4 I_0 - 2i\kappa_R A_2(A_1 A_3^* + A_2^* A_4).
\end{aligned} \tag{2.44}$$

Once again, these differential equations verify that the total intensity I_0 is a conserved quantity. Defining variables B_j in the same manner as before, we

have:

$$\begin{aligned}
\frac{dB_1}{dz} &= -2i\kappa_R B_3(B_1 B_3^* + B_2^* B_4),\\
\frac{dB_2}{dz} &= 2i\kappa_R B_4(B_1^* B_3 + B_2 B_4^*),\\
\frac{dB_3}{dz} &= 2i\kappa_R B_1(B_1^* B_3 + B_2 B_4^*),\\
\frac{dB_4}{dz} &= -2i\kappa_R B_2(B_1 B_3^* + B_2^* B_4),
\end{aligned} \tag{2.45}$$

which are similar in form to the coupled wave equations for DFWM in photorefractive media for reflection geometry [2.35, 38, 39] but with a coupling constant κ_R that is purely real. As the beams propagate in the nonlinear medium we find that the following quantities are conserved:

$$\begin{aligned}
&I_1(z) + I_4(z) = d_1, \qquad I_2(z) + I_3(z) = d_2, \qquad I_1(z) - I_3(z) = d_3,\\
&I_2(z) - I_4(z) = d_4, \qquad B_1(z)B_2(z) - B_3(z)B_4(z) = c,
\end{aligned} \tag{2.46}$$

where the constants d_1, d_2, d_3 and d_4 are determined by the boundary values of the problem, and the integration constant c is yet to be determined. With the help of these conservation laws the four coupled equations (2.45) can be decoupled to yield the following two first-order differential equations for the new variables $B_{12} \equiv B_1/B_2^*$ and $B_{34} \equiv B_3/B_4^*$:

$$\begin{aligned}
\frac{dB_{12}}{dz} &= 2i\kappa_R[c + (d_1 - d_2)B_{12} - c^* B_{12}^2],\\
\frac{dB_{34}}{dz} &= 2i\kappa_R[c + (d_1 - d_2)B_{34} - c^* B_{34}^2]].
\end{aligned} \tag{2.47}$$

Comparing the equation for B_{34} in reflection geometry with the corresponding equation in transmission geometry (see (2.38)) reveals that besides κ_R replacing κ_T, the sign of Δ is reversed in reflection geometry. Now the phase-conjugate reflectivity $R\,(=|\rho|^2)$ is an even function of Δ (see (2.41)). One can also show that the transcendental equation in reflection geometry for determining $|c|^2$ is identical to (2.43). Hence the reflection and transmission geometries yield the same phase-conjugate reflectivities for identical coupling strengths.

2.4 Mutually Pumped Phase Conjugation (MPPC) in Electrostrictive Kerr Media

Recently, several papers [2.40–44] have reported a new type of phase conjugation process in photorefractive crystals, in which two mutually incoherent laser beams pump each other to generate the respective phase-conjugate reflections.

The nonlinear medium acts like a phase-conjugate mirror to both of the incident beams and generates their phase-conjugate outputs via NDFWM. Several configurations, differing in the number of internal reflections from the sides of the photorefractive crystals, were used to demonstrate this process. As in [2.45] we refer collectively to these phase conjugators as mutually pumped phase conjugators (MPPCs) because of their common property of mutual pumping. Although photorefractive crystals are very efficient at low operating powers, the process is inherently slow due to the need to generate a large number of photoinduced charge carriers [2.46]. In [2.47] the authors have examined the possibility of the same process occurring in a transparent Kerr medium with an electrostrictive nonlinearity, since it offers the advantage of faster response times.

2.4.1 Theoretical Formulation

The geometry for the nonlinear interaction responsible for MPPC is shown in Fig. 2.9. Input beams 2 and 4 are a pair of mutually incoherent beams that enter the medium from opposite sides. Both beams may be obtained from a laser with a short coherence length, such that the difference between the propagation distances from the laser to the Kerr medium for the two incident beams exceeds the coherence length of the laser. In a transparent Kerr medium like CS_2, acoustic phonons that are initially present in the medium owing to thermal and quantum noise will help in Stokes scattering the incident photons via acousto-optic Bragg scattering [2.22]. Also, a photon from each input beam can be spontaneously converted into a frequency-downshifted Stokes photon and an acoustic phonon. The interference between each incident beam and its coherently generated scattered beam will produce a set of fringes which travel at the acoustic velocity, and which drive an acoustic wave by electrostriction. This additional sound wave reinforces the initial acoustic phonons, thereby increasing the coupling between each input beam and its scattered beam. The same acoustic wave may also

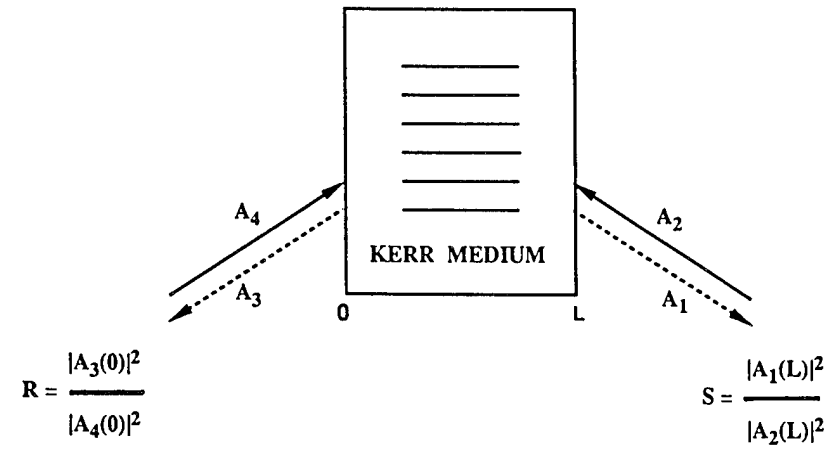

Fig. 2.9. Schematic diagram showing the geometry of NDFWM in electrostrictive Kerr media

diffract the other incoherent input beam to generate the cross-readout phase-conjugated beam at each port, labelled in Fig. 2.9 as beams 1 and 3. Thus, when we inject two input beams, we will observe the buildup of a pair of Stokes downshifted phase-conjugate beams. Interestingly, one beam by itself will not generate a phase-conjugate reflection, and both the incident beams are required for the nonlinear medium to phase conjugate them in MPPC. Since the read–write processes occur simultaneously, the dynamics of the beam coupling are described by NDFWM equations in the nonlinear medium with appropriate boundary conditions.

In Fig. 2.9 beams 2 and 4 are the two input beams of frequency ω, so that $\omega_2 = \omega_4 = \omega$. Beams 1 and 3 are the Stokes-scattered fields from the input fields 4 and 2 respectively, hence their frequency is downshifted and given by $\omega_1 = \omega_3 = \omega - \Omega$, where Ω is the acoustic frequency. This acoustic frequency is equal to $(2n_0\omega v \sin\theta)/c$, where v is the speed of sound in the medium, and 2θ is the angle between the beams 1 and 4, and between beams 2 and 3, respectively, in the medium. The wave equation (2.7) is satisfied separately by each frequency component of the total electric field. Using the slowly varying envelope approximation, and neglecting linear absorption in the medium, we obtain the following coupled wave equations:

$$\begin{aligned}
\frac{dA_1}{dz} &= -2i\kappa_{PM}A_1I_0 - 2i\kappa_T A_4(A_1A_4^* + A_2^*A_3 e^{-i\Delta kz}),\\
\frac{dA_2}{dz} &= 2i\kappa_{PM}A_2I_0 + 2i\kappa_T^* A_3(A_1^*A_4 e^{-i\Delta kz} + A_2A_3^*),\\
\frac{dA_3}{dz} &= 2i\kappa_{PM}A_3I_0 + 2i\kappa_T A_2(A_1A_4^* e^{i\Delta kz} + A_2^*A_3),\\
\frac{dA_4}{dz} &= -2i\kappa_{PM}A_4I_0 - 2i\kappa_T^* A_1(A_1^*A_4 + A_2A_3^* e^{i\Delta kz}),
\end{aligned} \tag{2.48}$$

where we have assumed that the angle between the coherent beam pairs is small ($\cos\theta \approx 1$) in calculating the phase mismatch. Since $\Omega \ll \omega$ we have ignored the small frequency differences between the waves and taken $\omega_j \approx \omega$ for all the waves in the definition of the coupling constants (see (2.19)). The wavevector mismatch, $\Delta k = (2n\Omega/c)$, is the phase mismatch associated with the geometry shown in Fig. 2.9. For media whose Kerr effect is dominated by electrostriction the complex third-order susceptibility can be expressed as [2.22, 47, 48]

$$\chi_T^{(2)} = \frac{-K^2\gamma_e^2}{4\rho_0(\Omega^2 - v^2K^2 + i\Omega\Gamma)}, \tag{2.49}$$

where K is the acoustic wave number, γ_e is the electrostrictive coefficient, ρ_0 is the mass density, and Γ is the inverse of the phonon lifetime. The coupling constant κ_T is now complex, and is a function of the frequency difference between each incident wave and its Stokes scattered wave. At resonance, $\Omega =$

$\pm vK$, and κ_T is purely imaginary ($=ig$), indicating a $\pm 90°$ phase shift between the index grating and the intensity pattern [2.48]. If the Bragg condition is satisfied for the incident wave, the sound wave, and the scattered wave, then a phase shift of 90° is automatically realized for a wave scattered with a frequency downshift (Stokes scattering).

The coupled wave equations in (2.48) describe MPPC in a transparent Kerr medium where depletion of the incident beams has been taken into account. The equation for each beam has contributions from two terms: one due to diffraction from the grating written by the beam itself (the usual two-beam coupling term that arises due to acousto-optic Bragg scattering for MPPC in Kerr media), and the second due to cross-readout of the grating written by the other pair of coherent beams (the FWM term). Both of the self-generated beams 1 and 3 are amplified as they propagate through the interaction region, since both are at the Stokes frequency of their respective forward-going pumps (recall that beam 3 is propagating in the negative z-direction).

We assume that the phase mismatch is small for the geometry and the Kerr medium under consideration, so that $\Delta kL \ll 1$. The coupled wave equations in (2.48) then reduce to equations (2.33) for transmission geometry, with the difference that $\kappa_T = (ig)$ now, owing to electrostrictive resonance. Hence we may use the solutions obtained in Sect. 2.3.3.1 with this replacement for κ_T. We now define the phase-conjugate reflection coefficients in the two arms as the following amplitude ratios: $\rho = B_3(0)/B_4^*(0) = B_{34}(0)$ and $\sigma = B_1(L)/B_2^*(L) = B_{12}(L)$. For MPPC the boundary conditions are the nonzero intensities of the two input beams at the opposite faces of the nonlinear medium (i.e., I_{2L}, $I_{40} \neq 0$), while the two self-generated phase-conjugate beams are zero at their inputs ($I_{10} = I_{3L} = 0$). It follows that $B_{12}(0) = B_{34}(L) = 0$, so that the solutions given in (2.39) simplify to

$$\rho = \frac{2c \tanh \mu L}{Q - \Delta \tanh \mu L}, \qquad \sigma = \frac{2c \tanh \mu L}{Q + \Delta \tanh \mu L}, \tag{2.50}$$

where $\mu = gQ$, $\Delta = I_{2L} - I_{40}$, and $I_0 = I_{2L} + I_{40}$ for MPPC. The phase-conjugate intensity reflectivities in the two arms are defined as $R = |\rho|^2$ and $S = |\sigma|^2$. We still have to determine the integration constant c. An examination of (2.50) reveals that R and S are functions of $|c|^2$ only, and not of any linear combinations of c and c^*. We may solve for $|c|^2$ by recalling that $A_3(0)A_4(0) = c$ from the boundary conditions and from the third conservation law in (2.37). This result can also be written as $\rho = c/I_{40}$. Equating this expression for ρ with that given in (2.50) we finally arrive at the following transcendental equation for $|c|^2$:

$$\tanh(gQL) = \frac{Q}{I_0}. \tag{2.51}$$

Once the root of the nonlinear transcendental equation is determined, the intensity reflectivities can be easily calculated from the relationships $R = |c|^2/I_{40}^2$ and $S = |c|^2/I_{2L}^2$. It is interesting to note that $R/S = I_{2L}^2/I_{40}^2$, so that the ratio of the two phase-conjugate reflection coefficients is equal to the ratio of the two input

beam intensities. For equal intensity input beams ($I_{2L} = I_{40}$), $\Delta = 0$, and $Q^2 = 4|c|^2$ from (2.40). Since the phase-conjugate reflectivity of either beam is proportional to $|c|^2$, and hence also to Q, the value of Q must be small for weak phase-conjugate signals. The threshold for the coupling strength is then obtained by using $\tanh(x) \approx x$ in (2.51):

$$(gI_0L)_{th} \equiv G_{th} = 1, \tag{2.52}$$

where $2g$ is the Kerr amplitude coupling coefficient in equations (2.48). This is lower than the typical threshold values of 25 quoted for phase conjugation by SBS [2.22] and of 10 quoted for Brillouin-enhanced FWM (BEFWM) [2.49–52]. Equation (2.52) is valid for equal intensity input beams. For unequal beam intensities the threshold coupling strength may be obtained in the following manner. Since $4|c|^2 = Q^2 - \Delta^2$ from (2.40), $Q^2 > \Delta^2$ for real values of $|c|^2$ and phase-conjugate reflectivities. The threshold condition corresponds to $Q = \Delta$, in which case the phase-conjugate reflectivity is zero. Substituting this in (2.51) and simplifying, we obtain

$$G_{th} = \frac{I_0}{2\Delta} \ln \frac{I_{2L}}{I_{40}}. \tag{2.53}$$

Figure 2.10 shows the variation of the threshold coupling strength with input beam ratio I_{40}/I_{2L}. The threshold value of the coupling strength is a minimum for equal intensity input beams. Unequal intensities of the two input beams require higher values of the coupling strength for threshold operation. For larger values of the coupling strength the product $gI_0L > 1$, and R and S reach their limiting values of I_{2L}/I_{40} and I_{40}/I_{2L} respectively in the absence of

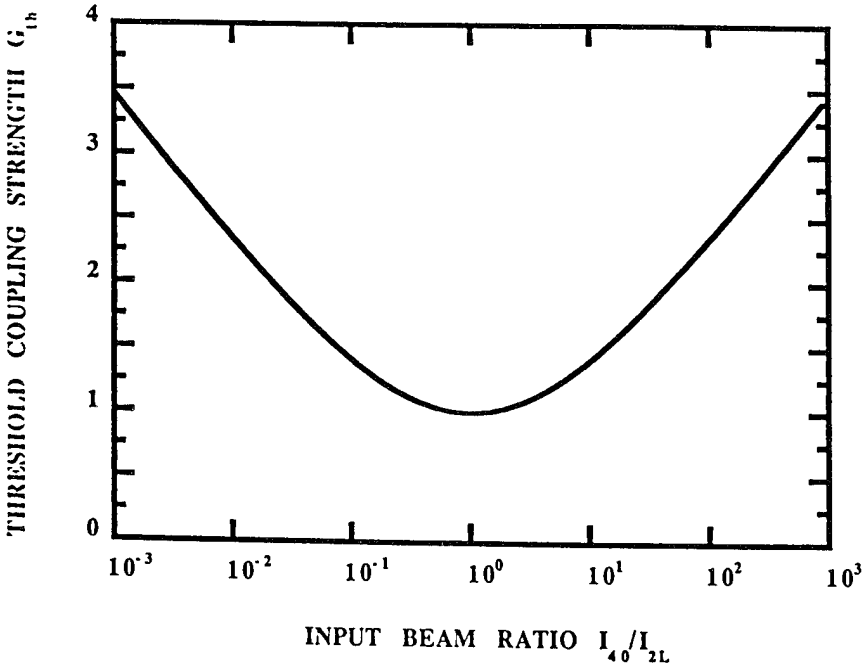

Fig. 2.10. Threshold coupling strength G_{th} as a function of input beam intensity ratio I_{40}/I_{2L}

absorption losses. Knowing $B_{12}(z)$ and $B_{34}(z)$, the intensities of the various beams as a function of the distance within the interaction volume may be calculated from the conservation laws:

$$I_1(z) = I_{12}(z)\frac{d_2 - d_1 I_{34}(z)}{1 - I_{12}(z)I_{34}(z)}, \qquad I_2(z) = \frac{d_2 - d_1 I_{34}(z)}{1 - I_{12}(z)I_{34}(z)},$$
$$I_3(z) = I_{34}(z)\frac{d_1 - d_2 I_{12}(z)}{1 - I_{12}(z)I_{34}(z)}, \qquad I_4(z) = \frac{d_1 - d_2 I_{12}(z)}{1 - I_{12}(z)I_{34}(z)}, \tag{2.54}$$

where $I_{12}(z) \equiv |B_{12}(z)|^2$ and $I_{34}(z) \equiv |B_{34}(z)|^2$. The known parameters for this problem are the net power flux Δ; the Kerr field coupling coefficient $2g$; and the interaction length L. We now discuss some numerical results obtained in our study of this problem.

2.4.2 Numerical Results

We consider CS_2 as a typical transparent Kerr medium with electrostrictive nonlinearity. The field Brillouin gain coefficient for backward SBS in CS_2 is about 0.1 cm/MW [2.22, 52], so that for a half-angle of $\theta \approx 10°$ in the forward direction, the amplitude Kerr coupling coefficient $2g$ is 2 cm/MW [2.48]. The Brillouin frequency of CS_2 near room temperature is $\Omega = 7.6$ GHz [2.52]. We choose an interaction length $L = 10$ cm. From (2.52) it follows that the threshold value of the total intensity I_0 is 0.1 MW/cm^2. Figure 2.11 is a plot of the

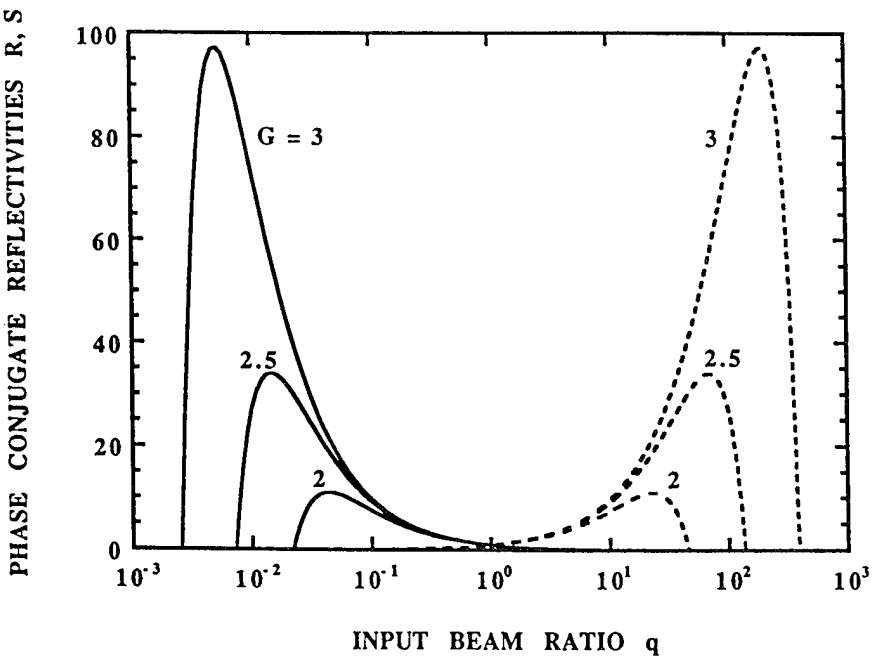

Fig. 2.11. Phase-conjugate reflectivities R (——) and S (– – –) in both the arms versus the input beam ratio

phase-conjugate intensity reflectivities R (solid curves) and S (dashed curves) in both the arms versus the ratio of the input beam intensities $q = I_{40}/I_{2L}$. For a given beam ratio, R and S are higher for a larger net Brillouin gain G since this leads to more coupling of beams. If the input intensity in one arm is much smaller than in the other, which in our study corresponds to $I_{40} \ll I_{2L}$ or $I_{2L} \ll I_{40}$, then the device can phase conjugate the weak beam with a very high reflection coefficient, much larger than unity (Fig. 2.11). The peak value of R corresponds to all of the power of the strong input beam I_{2L} being transferred to the diffracted beam 3, this intensity being further divided by the small input intensity of beam 4 to give the large value of the ratio R. A similar description is true for maximum S, with the roles of the input beams reversed. However, we expect that phase mismatch and linear absorption, which were neglected in obtaining the analytic results of previous section, will decrease the reflectivity appreciably. When R is high, S is correspondingly low: the diffraction of a weak beam is further scaled down by the large input intensity in that arm to give the ratio S. Hence S is appreciable only when R is negligible, much like a seesaw! Note that the harder the stronger arm is pumped, the smaller is the minimum intensity of the signal that can be phase conjugated in the other arm.

Figure 2.12 shows the same effect on a logarithmic scale, with a wider dynamic range of the phase conjugator for higher coupling strengths. Note that even a slight change in the total intensity, and hence in G, can change the minimum value of the weak beam intensity that can be phase conjugated by a few orders of magnitude. This is because the coupling-strength product appears in the argument of an exponential function in the transcendental equation,

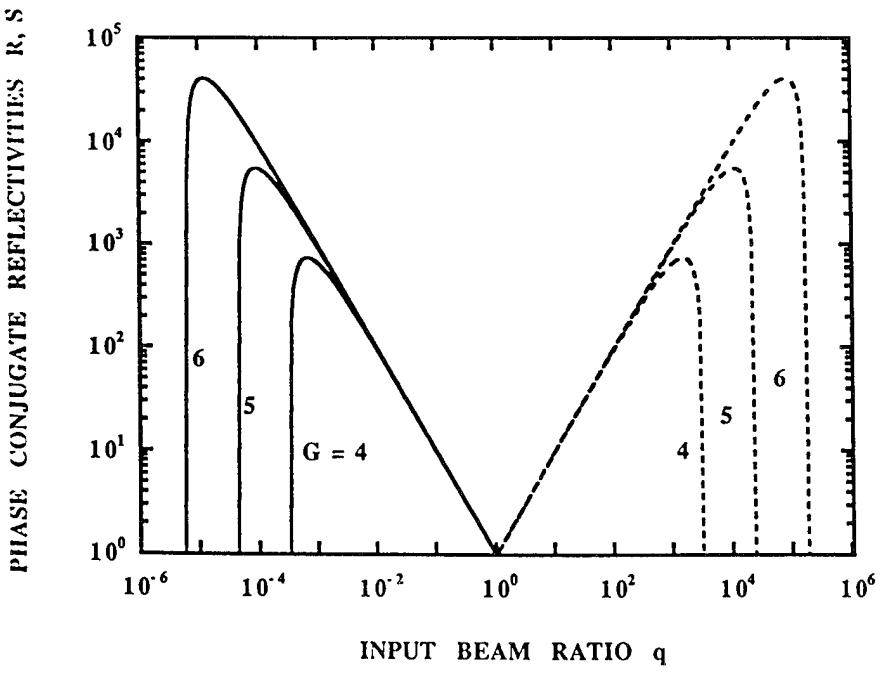

Fig. 2.12. Phase-conjugate reflectivities R (——) and S (– – –) in both the arms versus the input beam ratio

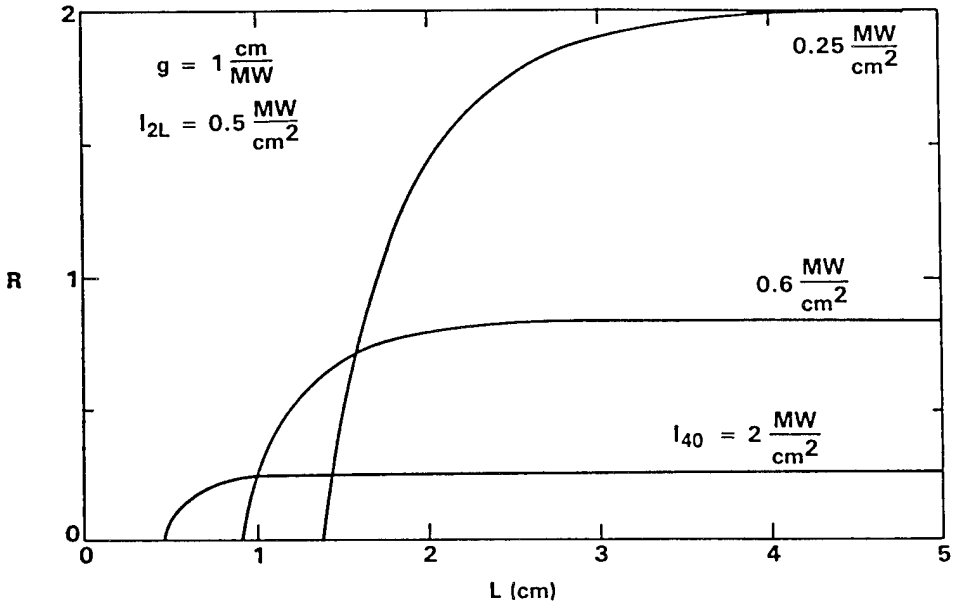

Fig. 2.13. Phase-conjugate reflectivity R in the left arm as a function of the interaction length

hence any slight variations in it will cause a large change in the results. The sensitivity of the MPPC device to weak input beam energy in one arm, and the rapid decrease in reflectivity in that arm with increasing probe strength, is similar to the experimental results recently reported by Lebow and Ackerman [2.51] for phase conjugation by BEFWM.

Figure 2.13 is a plot of R as a function of the interaction length for different values of I_{40}, keeping I_{2L} fixed. As expected from (2.52) a higher total input intensity requires a smaller interaction length to start the process. The interesting feature revealed in this graph is that once the threshold interaction length is crossed, it is not advantageous to use much longer lengths as the curves of R versus L remain pretty flat at longer lengths, this being more so at higher input intensities. The curves for different I_{40} cross because for a fixed I_{2L}, a smaller value of I_{40} leads to a higher phase-conjugate reflectivity, with larger interaction lengths required for the process to occur. Figure 2.14 is a similar graph for the phase-conjugate intensity reflectivity S in the other arm, the parameter values being the same as in the set of Fig. 2.13. In contrast to Fig. 2.13, S is higher for larger I_{40} because of the increased diffraction of beam 4 to create the phase-conjugated beam 1. A larger value of I_{40} also requires a smaller interaction length for observing the process, hence there is no crossing of the curves in Fig. 2.14 as is seen in Fig. 2.13.

The intensity distribution of the various beams within the interaction region is shown in Figs. 2.15–2.18. The Kerr coupling coefficient and the input intensities of beams 2 and 4 are kept fixed at 1 cm/MW, 0.5 MW/cm^2, and 0.6 MW/cm^2 respectively. Figure 2.15 is for an interaction length of 1 cm, and the coupling strength corresponding to this length is only slightly above the threshold value. Most of the energy remains in the incident beams, leading to low

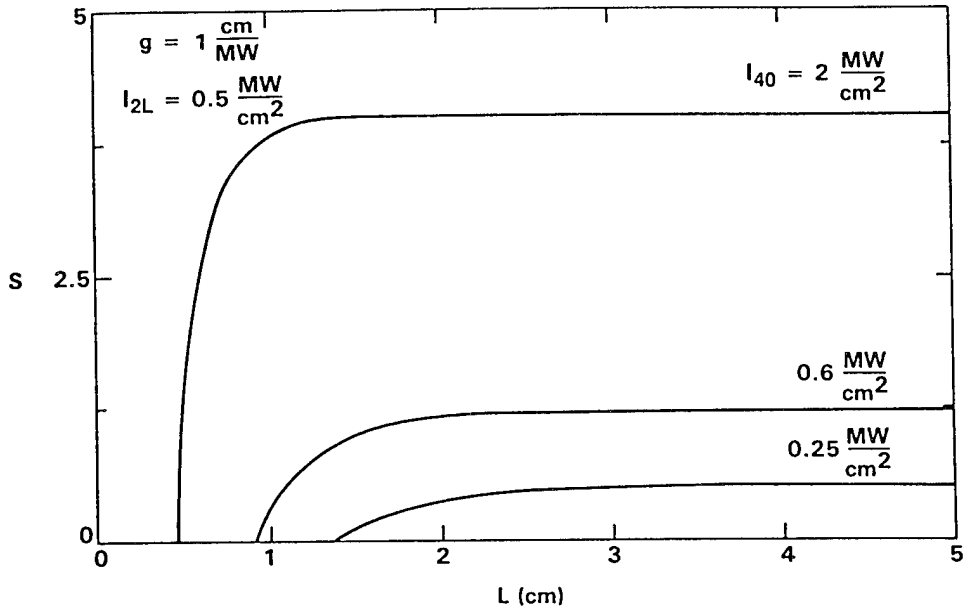

Fig. 2.14. Phase-conjugate reflectivity S in the right arm as a function of the interaction length

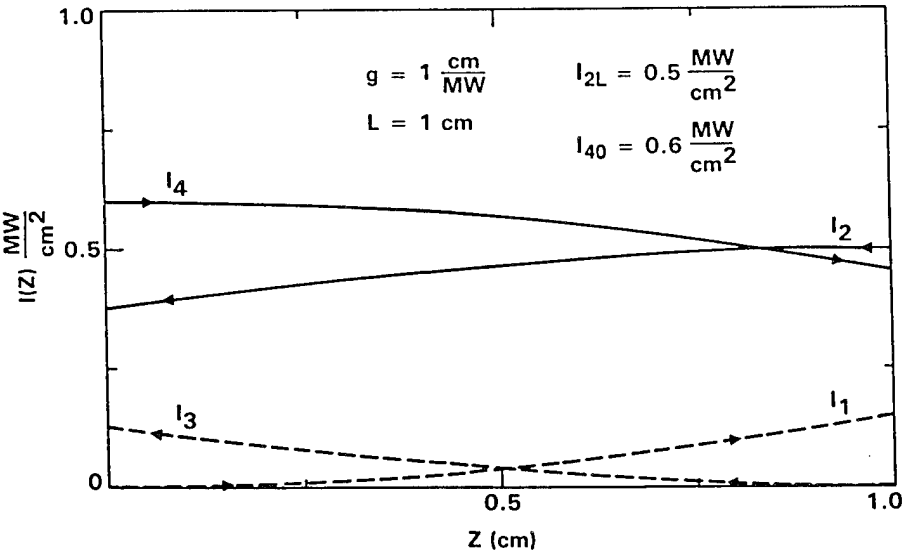

Fig. 2.15. Field distribution for MPPC inside the interaction region with $L = 1$ cm

phase-conjugate reflectivities in both arms. With an increase in the interaction length to 2 cm (Fig. 2.16), the phase-conjugate beams emerge with more energies at the output planes than in Fig. 2.15, and since the input beams are not totally depleted, R and S do not reach their maximum value. For $L = 4$ cm (Fig. 2.17) there is a complete transfer of energies from the incident beams to the phase-conjugate beams. Further increase in L causes the region where energy transfer occurs to shrink (see Fig. 2.18 for $L = 10$ cm), because now the process does not occur gradually throughout the interaction length. Instead, the intensities of the incident beams remain fairly constant for most of the distance traversed, there

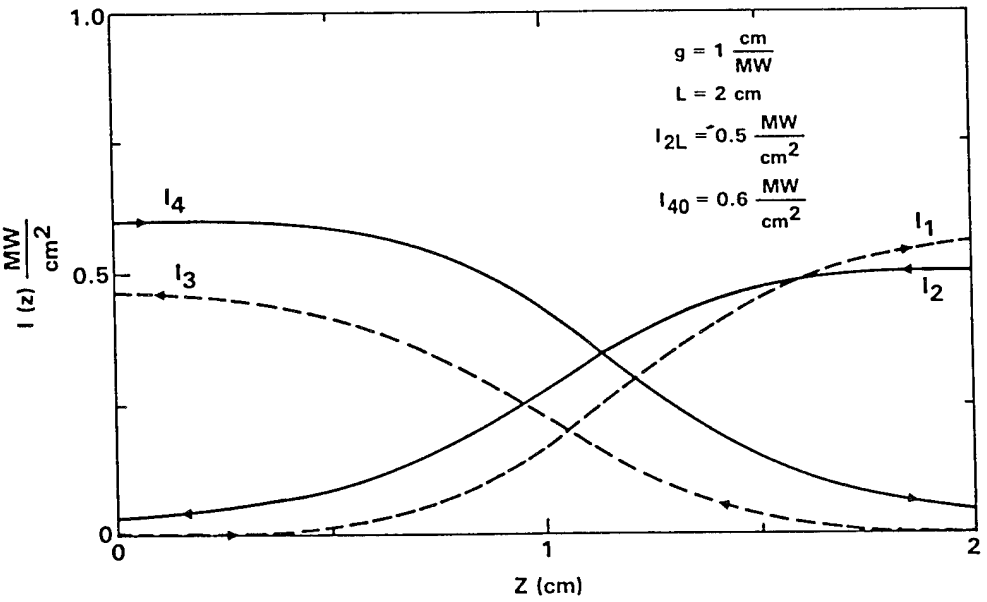

Fig. 2.16. Field distribution for MPPC inside the interaction region with $L = 2$ cm

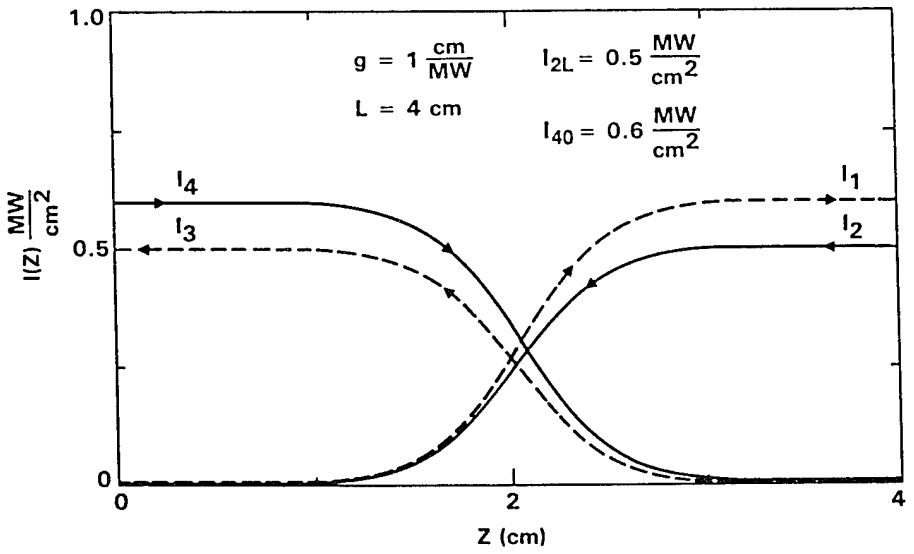

Fig. 2.17. Field distribution for MPPC inside the interaction region with $L = 4$ cm

being a sharp power transfer which is confined to a narrow region around the center of the interaction length. This behavior can be understood if we recall that beams 1 and 3 are zero at the $z = 0$ and $z = L$ planes respectively, so that there are no gratings to begin with at both the ends of the interaction length. The diffracted beams, and hence the gratings, slowly increase and are appreciable near the middle, where maximum interaction occurs. Complete depletion of the incident beams in this region once again results in the absence of the gratings, and hence the behavior shown in Fig. 2.18. An interesting outcome is that for MPPC in which two beam-pairs undergo acousto-optic Bragg scattering by

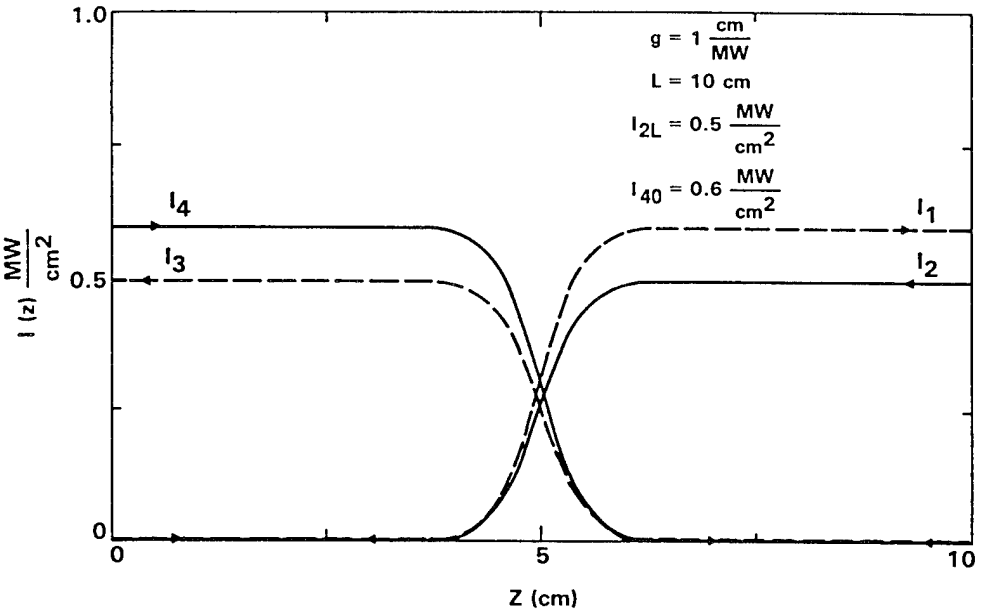

Fig. 2.18. Field distribution for MPPC inside the interaction region with $L = 10$ cm

a common sound wave, a complete energy transfer occurs for a finite thickness of the medium, in contrast to the infinite interaction region required for 100% efficiency for standard acousto-optic Bragg scattering of two beams.

2.5 Summary

We have described nonlinear optical phase conjugation by four-wave mixing in Kerr media. Analytic results are obtained for undepleted pumps and negligible linear absorption in the medium both for equal and different pump intensities. Pump depletion is accounted for in the transmission and reflection geometries separately. We have also considered mutually pumped phase conjugation in electrostrictive Kerr media.

Acknowledgement. Ragini Saxena would like to acknowledge a helpful technical discussion with Dr. Qi-Che He at the University of California at Santa Barbara regarding Sect. 2.3.2.

References

2.1 See, for example, A. Yariv, P. Yeh: *Optical Waves in Crystals* (Wiley, New York, 1984) Chap. 13

2.2 See, for example, B.Ya. Zel'dovich, N.F. Pilepetsky, V.V. Shkunov: *Principles of Phase Conjugation* Springer Ser. Opt. Sci. **42** (Springer, Berlin Heidelberg 1985)

2.3 See, for example, D.M. Pepper: Nonlinear Optical Phase Conjugation, in *Laser Handbook* 4 eds. M.L. Stitch, M. Bass (North-Holland, Amsterdam 1985) p. 333–486
2.4 See, for example, C.R. Giuliano: Physics Today, April (1981)
2.5 See, for example, *Optical Phase Conjugation* ed. R.A. Fisher (Academic, New York, 1983)
2.6 J. AuYeung, D. Fekete, D.M. Pepper, A. Yariv: IEEE J. Quantum Electron. **QE-15**, 1180 (1979)
2.7 A.E. Siegman, P.A. Belanger, A. Hardy: in Chap. 13 of [2.5] and the references therein; see also the Special Issue on Phase-Conjugate Resonators, J. Opt. Soc. Am. **73**, Number 5, May (1983)
2.8 I.M. Bel'dyugin, M.G. Galushkin, E.M. Zemskov: Sov. J. Quantum Electron. **5**, 1429 (1979); I.M. Bel'dyugin, B. Ya. Zel'dovich, M.V. Zolotarev, V.V. Shkunov: Sov. J. Quantum Electron. **15**, 1583 (1985)
2.9 N.G. Basov, I.G. Zubarev, A.B. Mironov, S.I. Mikhailov, A.Yu. Okulov: Sov. Phys. JETP **52**, 847 (1980)
2.10 F.A. Hopf: J. Opt. Soc. Am. **70**, 1320 (1980)
2.11 I. Bar-Joseph, A. Hardy, Y. Katzir, Y. Silberberg: Opt. Lett. **6**, 414 (1981)
2.12 J. Feinberg: Opt. Lett. **7**, 486 (1982); J. Feinberg: Opt. Lett. **8**, 569 (1983)
2.13 M.D. Ewbank, P. Yeh, M. Khoshnevisan, J. Feinberg: Opt. Lett. **10**, 282 (1985)
2.14 A.E.T. Chiou, P. Yeh: Opt. Lett. **11**, 306 (1986)
2.15 S.K. Kwong, G.A. Rakuljic, A. Yariv: Appl. Phys. Lett. **48**, 201 (1986)
2.16 J. Diels, I. McMichael: Opt. Lett. **6**, 219 (1981)
2.17 M. Tehrani: Proc. SPIE **412**, 186 (1983); P. Yeh, J. Tracy, M. Khoshnevisan: Proc. SPIE **412**, 240 (1983)
2.18 P. Yeh, M. Khoshnevisan, M.D. Ewbank, J. Tracy: Opt. Commun. **57**, 387 (1985)
2.19 P. Yeh, I. McMichael, M. Khoshnevisan: Appl. Optics **25**, 1029 (1986)
2.20 I. McMichael, P. Yeh: Opt. Lett. **11**, 686 (1986); I. McMichael, P. Beckwith, P. Yeh: Opt. Lett. **12**, 1023 (1987)
2.21 B. Ya. Zel'dovich, V.I. Popovichev, V.V. Ragul'skii, F.S. Faizullov: Sov. Phys. JETP **15**, 109 (1972)
2.22 W. Kaiser, M. Maier: Stimulated Rayleigh, Brillouin and Raman Spectroscopy, in *Laser Handbook* Vol. 2 eds. F.T. Arecchi, E.O. Schulz-Dubois (North-Holland, Amsterdam, 1972) Chap. E2; A. Yariv, P. Yeh: in Chap. 9 of [2.1]; Y.R. Shen: *Principles of Nonlinear Optics* (Wiley, New York, 1984) Chap. 11
2.23 John C. AuYeung: in Chap. 9 of [2.5] and the references therein
2.24 A. Yariv: Appl. Phys. Lett. **28**, 88 (1976); A. Yariv: Opt. Commun. **21**, 49 (1977)
2.25 R.W. Hellwarth: J. Opt. Soc. Am. **67**, 1 (1977)
2.26 A. Yariv, D.M. Pepper: Opt. Lett. **1**, 16 (1977); D.M. Pepper, A. Yariv: Optical Phase Conjugation Using Three-Wave and Four-Wave Mixing via Elastic Photon Scattering in Transparent Media, Chap. 2 of [2.5]
2.27 D.M. Bloom, G.C. Bjorklund: Appl. Phys. Lett. **31**, 592 (1977)
2.28 J.H. Marburger, J.F. Lam: Appl. Phys. Lett. **35**, 249 (1979); H.G. Winful, J.H. Marburger: Appl. Phys. Lett. **36**, 613 (1980)
2.29 A. Maruani: IEEE J. Quantum Electron. **QE-16**, 558 (1980)
2.30 K. Ujihara: Opt. Lett. **7**, 614 (1982)
2.31 S. Guha, P. Conner: Opt. Commun., **89**, 107 (1992).
2.32 A.E. Kaplan, C.T. Law: IEEE J. Quantum Electron. **QE-21**, 1529 (1985)
2.33 R. Lytel: J. Opt. Soc. Am B **3**, 1580 (1986)
2.34 D.M. Pepper, R.L. Abrams: Opt. Lett. **3**, 212 (1978)
2.35 M. Cronin-Golomb, B. Fischer, J.O. White, A. Yariv: IEEE J. Quantum Electron. **QE-20**, 12 (1984)
2.36 P. Yeh: Proceedings of the IEEE, **80**, 436 (1992)
2.37 Claire Gu, Pochi Yeh: Opt. Lett. **16**, 455 (1991)
2.38 A. Bledowski, W. Krolikowski, A. Kujawski: IEEE J. Quantum Electron. **QE-22**, 1547 (1986)
2.39 N.V. Kukhtarev, T.I. Semenets, K.H. Ringhofer, G. Tomberger: Appl. Phys. B **41**, 259 (1986)

2.40 S. Weiss, S. Sternklar, B. Fischer: Opt. Lett. **12**, 114 (1987); S. Sternklar, S. Weiss, B. Fischer: Opt. Eng. **26**, 423 (1987)
2.41 R.W. Eason, A.M.C. Smout: Opt. Lett. **12**, 51 (1987); A.M.C. Smout, R.W. Eason: Opt. Lett. **12**, 498 (1987)
2.42 M.D. Ewbank: Opt. Lett. **13**, 47 (1988)
2.43 D. Wang, Z. Zhang, Y. Zhiu, S. Zhang, P. Ye: Opt. Commun. **73**, 495 (1989)
2.44 M.D. Ewbank, R. Vazquez, R.R. Neurgaonkar, J. Feinberg: J. Opt. Soc. Am. B **7**, 2306 (1990)
2.45 P. Yeh, T.Y. Chang, M.D. Ewbank: J. Opt. Soc. Am. B **5**, 1743 (1988)
2.46 P. Yeh: Appl. Opt. **26**, 602 (1987)
2.47 R. Saxena, P. Yeh: J. Opt. Soc. Am. B **7**, 326 (1990)
2.48 P. Yeh, M. Khoshnevisan: J. Opt. Soc. Am. B **4**, 1954 (1987); P. Yeh: IEEE J. Quantum Electron. **QE-25**, 484 (1989)
2.49 N. Basov, I.G. Zubarev: Appl. Phys. **20**, 261 (1979)
2.50 A.M. Scott: Opt. Commun. **45**, 127 (1983); A.M. Scott, K.D. Ridley: IEEE J. Quantum Electron. **QE-25**, 438 (1989)
2.51 P.S. Lebow, J.R. Ackerman: Opt. Lett. **14**, 236 (1989)
2.52 M.K. Skeldon, P. Narum, R.W. Boyd: Opt. Lett. **12**, 343 (1987)

A.10

Diffraction properties of photorefractive gratings

Diffraction properties of photorefractive gratings

Ragini Saxena
Rockwell International Science Center
1049 Camino dos Rios, Thousand Oaks, CA 91360
(805) 373 - 4157

ABSTRACT

Volume phase gratings in photorefractive crystals have nonuniform amplitude and phase due to the energy exchanged by the writing beams within the material. Analytic expression is obtained for the diffraction efficiency of a weak reading beam that does not perturb the grating and has a different polarization from the write beams. For a read beam of arbitrary intensity, the diffraction efficiency is a nonlinear function of the read beam intensity and is nonreciprocal with respect to readout from the two input ports. These properties of photorefractive gratings are studied for arbitrary phase shifts of the index grating from the intensity pattern.

I. INTRODUCTION

The photorefractive crystal has proven to be an almost ideal holographic medium, demonstrating its ability to write efficient volume holograms at low levels of light without the need for special development procedures. The amplitude and phase of such holograms are nonuniform[1] within the crystal due to two-beam coupling effects[2] between the pair of coherent writing beams. Further, the read beam and its diffracted beam induce a new photorefractive grating that may be in or out of phase with the original grating being read.[3] The diffraction is therefore quite different from that of a simple Bragg scattering off a fixed thick grating, and the coupled wave theory of Kogelnik[4] must be modified to describe the diffraction efficiency η of such gratings. A recent study[5] examined diffraction efficiency of photorefractive gratings when polarization asymmetry occurs during writing and readout. The new photorefractive grating formed by the read beam and its diffracted component is ignored for a reading beam that is weak compared to the writing beams. For this case, η is independent of the read beam intensity, and the argument of the sine function in η is a nonlinear function of grating thickness, coupling constants during writing and readout, and input intensity ratio of writing beams. Inclusion of the effects arising from a read beam having an intensity comparable to that of the writing beams has shown η to be a nonlinear function of the read beam intensity and nonreciprocal with respect to readout from the two input ports.[6] Similar nonreciprocity with respect to direction of readout has been observed for fixed volume gratings in photorefractive media.[7] A theoretical explanation[8] of this effect was obtained by taking into account the new photoinduced grating formed by the read beam and its diffracted component, besides the fixed grating present initially. The nonlinear and nonreciprocal behavior of η has been examined for arbitrary phase shifts of the photorefractive grating from the intensity pattern.[9] Analytic expressions for the diffraction efficiency are obtained for limiting values of the phase shift between index change and fringe pattern.

II. THEORY

[A] Diffraction Efficiency of Fixed, Uniform Gratings

Periodic media with spatially varying conductivity σ are known as absorption gratings, while periodic media with spatially varying dielectric constant ε are known as phase gratings; when both σ and ε are periodically varying functions in space, then we have a "mixed" grating. An absorption grating is necessarily lossy because the nonzero conductivity of the medium leads to the decay of an incident light beam. An example of a 1-d phase grating with a sinusoidal index variation is given by

$$n(x) = n_0 + n_1 \cos Kx \quad , \tag{1}$$

where n_0 is the average index of refraction of the medium, n_1 is the uniform amplitude of the fixed index grating, K is the grating wave number equal to $2\pi/\Lambda$ (Λ being the grating spacing), and x is the spatial coordinate along the grating wave vector. The "thickness" of a grating is determined by the dimensionless parameter $Q = 2\pi\lambda L/n_0\Lambda^2$, where λ is the wavelength of light and L is the thickness of the grating in the direction of light propagation. A grating is planar or thin if $Q < 1$, and it is a thick volume grating if $Q \geq 10$. For grating spacing comparable to wavelength ($\Lambda \approx \lambda$), Q is less than or greater than unity depending on whether the grating thickness L is smaller or greater than $\Lambda \approx \lambda$. If the grating planes are perpendicular (parallel) to the grating surface, then we have unslanted transmission (reflection) gratings. The diffracted beam appears on the same side of the grating as the transmitted (reflected) read beam for a transmission (reflection) grating (Fig. 1). Table I by Kogelnik[10] summarizes the various diffraction orders and the maximum diffraction efficiency that can be obtained theoretically from uniform fixed gratings. Note that the diffraction efficiency of thin phase gratings is limited to about 34% in the first orders in the Raman–Nath regime. For volume phase gratings, maximum diffraction efficiency is 100% to the Bragg–matched first order, all higher orders being suppressed.

The fixed volume phase grating of Eq. (1) is formed by recording the interference pattern of two coherent writing beams I_{AW} and I_{BW}

$$I_W(x) = I_{0W} (1+m \cos Kx) \quad , \tag{2a}$$

where $I_{0W} = I_{AW} + I_{BW}$ is the sum of the intensities of the two writing beams, $m = 2\sqrt{I_{AW}I_{BW}} / (I_{AW}+I_{BW})$ is the modulation depth of the intensity pattern, and the subscript W indicates writing beams. If $\beta = I_{BW}/I_{AW}$ is the intensity ratio of the writing beams, then $m = 2\sqrt{\beta} / (1 + \beta)$. The recording medium (a photographic plate, for example) is exposed to the intensity pattern of Eq. (2a). After processing with a developer and a fixer, the plate is bleached to convert the recorded amplitude modulation into a phase modulation. Assuming a linear response of the photographic plate to the incident exposure, the refractive index is given by

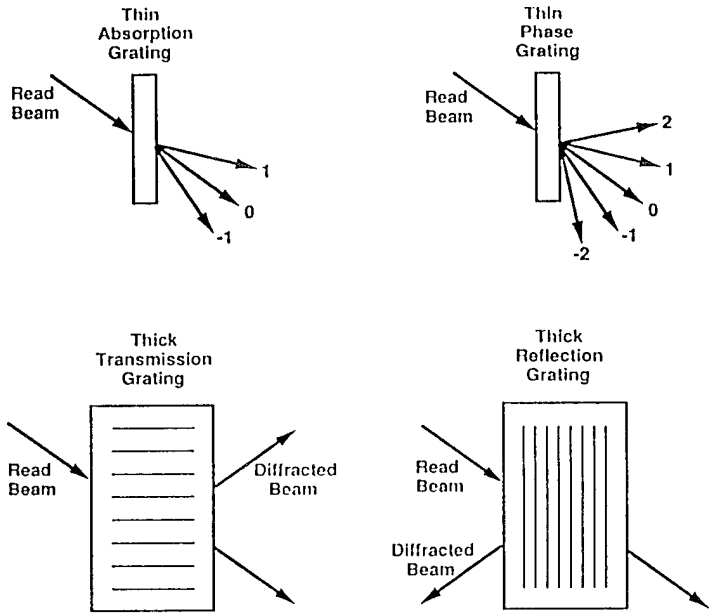

Fig. 1. Diffraction of a read beam from various types of fixed, uniform gratings.

Table I

Diffraction Properties of Various Gratings

$Q = \frac{2\pi\lambda L}{n_0\Lambda^2}$	Type	Geometry	Diffraction Orders	η_{max}
$Q < 1$ Thin	Absorption $\alpha(x)=\alpha(x+\Lambda)$	Transmission	Two: ± 1	6.25%
	Phase $n(x)=n(x+\Lambda)$	Transmission	Many	33.9% 1st-order
$Q > 1$ Thick	Absorption $\alpha(x)=\alpha(x+\Lambda)$	Transmission	One Bragg-Matched Order	3.7%
		Reflection		7.2%
	Phase $n(x)=n(x+\Lambda)$	Transmission		100%
		Reflection		100%

$$n(x) = n_o + n_{10}\, m \cos Kx = n_o + 2n_{10}\frac{\sqrt{\beta}}{1+\beta}\cos Kx \qquad (2b)$$

where n_{10} is a constant of proportionality that depends on the incident exposure and the recording medium.

To derive Kogelnik's formula[4] for diffraction efficiency of volume phase gratings with uniform amplitude, consider the transmission grating shown in Fig. 2 with an index of refraction given by Eq. (1). The electric field of the incident read beam and its diffracted component are described as plane waves

$$E_{AR}(\mathbf{r},t) = \frac{1}{2}\, A_R(z)\, \exp[i(\mathbf{k}_{AR}\cdot\mathbf{r} - \omega t)] + \text{c.c.}\ , \qquad (3)$$

where A_R is the complex amplitude of the read beam at steady-state, ω is the frequency and $\mathbf{k}_{AR}$ is the corresponding wave vector in the medium at an angle θ_{AR} with respect to the z-axis. To describe the diffracted beam, A is replaced by B. The subscript R denotes the read beam and its coherently generated diffracted beam. When the electric field of the

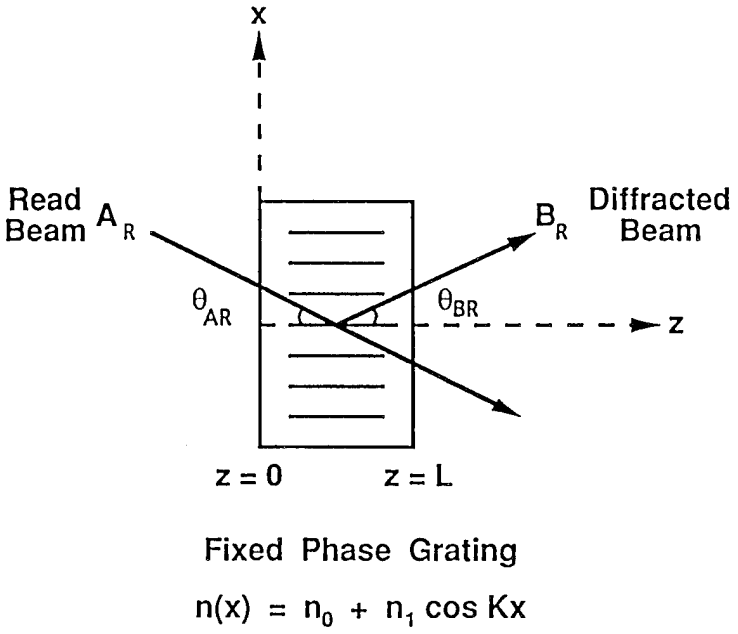

Fig. 2. The schematic representation of diffraction from a uniform phase grating.

optical wave is described by Eq. (3), then the intensity is equal to $\varepsilon_o n_o c|A_R(z)|^2/2$ in mks units,[11] where ε_o is the electric permittivity of free space and c is the velocity of light. Ignoring the multiplicative constant factor, $I_{AR}(z)\equiv|A_R(z)|^2/2$ is taken to represent the intensity of the beam in the rest of this paper. The z axis is taken normal to the surface of the medium, and the complex amplitudes are assumed to be functions of z due to absorption and diffraction. The amplitudes are independent of the transverse coordinate x because the grating is assumed to be infinite in that direction. To describe the propagation and coupling of the two waves at steady state in the thick transmission phase grating, we start with the scalar wave equation

$$\nabla^2 E + \frac{n^2\omega^2}{c^2} E = 0 \quad , \tag{4}$$

where $E = E_{AR} + E_{BR}$ is the total electric field. Substituting for n and E in the wave equation, using the slowly varying envelope approximation and ignoring phase-mismatched terms and terms that are quadratic in the index change, we arrive at the following coupled wave equations

$$\cos\theta_{AR} \frac{dA_R}{dz} = -\frac{\alpha_R}{2} A_R + i \frac{\pi n_1}{\lambda_R} B_R e^{i\Delta k_z z}$$

$$\cos\theta_{BR} \frac{dB_R}{dz} = -\frac{\alpha_R}{2} B_R + i \frac{\pi n_1}{\lambda_R} A_R e^{-i\Delta k_z z} , \tag{5a}$$

where

$$\Delta k_z = k(\cos\theta_{BR} - \cos\theta_{AR}) \quad , \quad k\sin\theta_{BR} + K = k\sin\theta_{AR} \quad , \tag{5b}$$

α_R is the intensity absorption coefficient of the grating at the reading wavelength that has been introduced phenomenologically to the coupled wave equations and Δk_z is the phase-mismatch along the z-direction. Integration of the coupled wave equations (5a) over the transverse coordinate x lead to the last relation expressed in Eq. (5b). For phase-matched readout, $\Delta k_z = 0$ (Fig. 3). Ignoring the trivial solution of $\theta_{BR} = \theta_{AR}$ which corresponds to the diffracted beam propagating along the read beam, the relevant solution is $\theta_{AR} = -\theta_{BR} \equiv \theta_R$ for $\Delta k_z = 0$ (Bragg-matched readout), with $\theta_R = \sin^{-1}(\lambda_R/2n_0\Lambda)$. Hence the Bragg–matched diffracted beam propagates at an angle to the grating planes that is equal and opposite to the reading beam angle. Using boundary conditions $A_R(0) = A_{R0}$ and $B_R(0) = 0$, the solutions for the beam amplitudes are given by

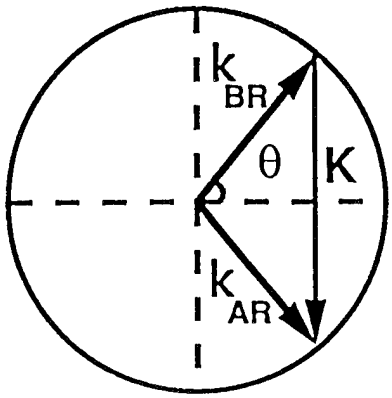

$$K = k_{AR} - k_{BR}$$

Fig. 3. Bragg–matched readout with $\Delta k_z = 0$.

$$A_R(z) = A_{R0} \exp(-\frac{\alpha_R z}{2\cos\theta_R}) \cos\kappa z ,$$

$$B_R(z) = i\, A_{R0} \exp(-\frac{\alpha_R z}{2\cos\theta_R}) \sin\kappa z, \qquad (6)$$

where $\kappa = \pi n_1/\lambda_R \cos\theta_R$, θ_R being the Bragg angle for the reading beam. Figure 4 shows the normalized beam intensities $|A_R(z)|^2/|A_{R0}|^2$ (solid curve) and $|B_R(z)|^2/|A_{R0}|^2$ (dashed curve) as a function of distance z into a lossless grating ($\alpha_R = 0$). At the beginning of the thick phase grating, there is no diffracted beam, and the normalized read beam intensity is unity. Periodic exchange of energy takes place between the read beam and its diffracted component. The ratio of the diffracted beam intensity at the output of the grating to the read beam intensity at the input of the grating determines the diffraction efficiency: $\eta = |B_R(L)|^2 / |A_{R0}|^2$. Substituting for κ, we arrive at Kogelnik"s formula[4]

$$\eta = \exp(-\frac{\alpha_R L}{\cos\theta_R}) \sin^2(\frac{\pi n_1 L}{\lambda_R \cos\theta_R}) \qquad . \qquad (7)$$

The argument of the sine function depends on the product of grating amplitude times its thickness and on the wavelength and Bragg angle at readout, but the argument is independent of the read beam intensity. For a lossless grating ($\alpha_R = 0$) and Bragg–matched readout ($\Delta k_z = 0$), diffraction efficiency is equal to unity whenever the argument of the sine function is an integral multiple of $\pi/2$, implying total transfer of the read beam energy to the diffracted beam. Substituting Eq. (2b) into Eq. (7), we obtain

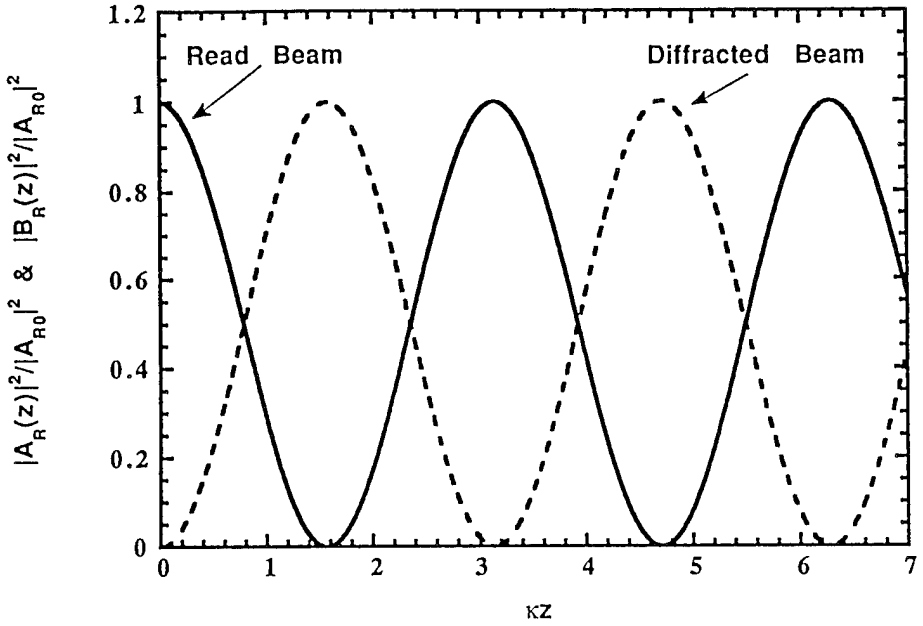

Fig. 4. Intensities of the read beam (solid curve) and the diffracted beam (dashed curve) as a function of normalized depth κz within the medium.

$$\eta = \exp(-\frac{\alpha_R L}{\cos\theta_R}) \sin^2 [\frac{\pi n_{10} L}{\lambda_R \cos\theta_R} \frac{2\sqrt{\beta}}{1+\beta}] . \quad (8)$$

The above equation illustrates the variation of the diffraction efficiency of uniform phase grating with the intensity ratio of the writing beams.

[B]. Photorefractive Gratings with Nonuniform Amplitude and Phase

Two coherent light beams intersect in a photorefractive crystal when writing a grating (Fig. 5); due to photorefractive two-beam coupling, one writing beam gains energy at the expense of the other writing beam. The nonreciprocal energy transfer between the two beams is due to Bragg scattering off the grating the beams themselves wrote. This phenomenon is known as "Self-Diffraction"[12], and the direction of energy transfer is determined by the orientation of the crystal and the nature of charge carriers (electrons or holes). Such an energy exchange is not found in most nonlinear materials because they respond locally to optical beams, with no phase shift between index grating and intensity pattern. We will now show that the amplitude and phase of the index modulation are no longer uniform due to the exchange of energy between the two writing beams in the photorefractive medium. Similar to the previous section, we describe the two writing beams as plane waves with complex amplitudes A_W and B_W. These two beams interfere to produce a sinusoidal intensity pattern given by

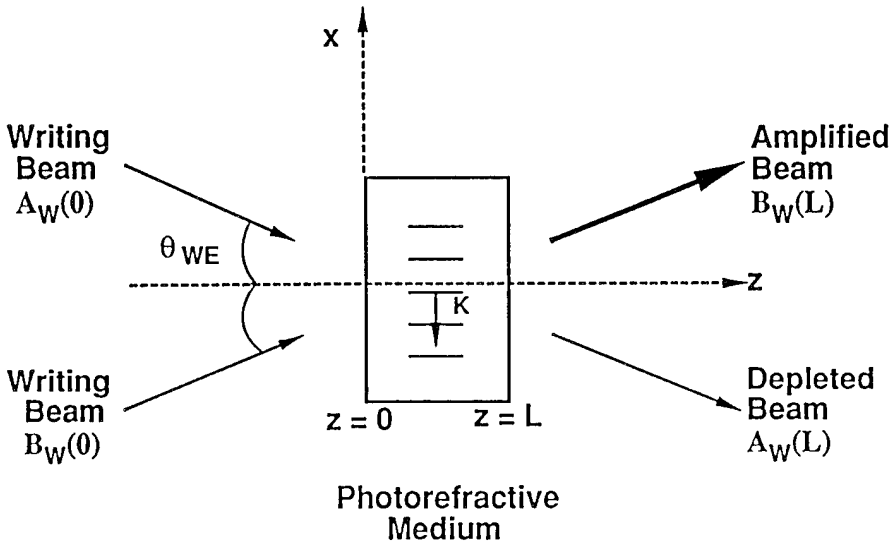

Fig. 5. Schematics of photorefractive two-beam coupling.

$$I_W(x,z) = I_{0W}(z)\left(1+\frac{m(z)}{2}\,e^{iKx}+\frac{m^*(z)}{2}\,e^{-iKx}\right) \quad , \tag{9}$$

where $I_{0W}(z)$ is the local sum of the two beam intensities: $I_{0W}(z) = I_{AW}(z)+I_{BW}(z) = [\,|A_W(z)|^2 + |B_W(z)|^2\,]/2$. K is the magnitude of the grating wavevector: $|K| = |k_{AW} - k_{BW}| = 2\pi/\Lambda$, Λ being the fringe separation equal to $\lambda_W/(2\sin\theta_{WE})$ when the two beams are symmetrically incident at an external angle of $2\theta_{WE}$ about the crystal face normal. λ_W is the wavelength of the two writing beams and x is the direction along the grating wave vector. m(z) is the local modulation depth of the incident intensity pattern: $m(z) = A_W(z)B_W^*(z)/I_0(z)$; it depends on the polarizations and intensity ratio of the two writing beams. The high intensity regions of the spatially periodic intensity pattern cause photoionization of the impurity levels in the bandgap. The mobile charges drift and diffuse before recombining and being trapped in regions of low intensity, leading to a separation of ionic charges inside the crystal. The resulting space-charge field produces a photorefractive index grating via the linear electro-optic effect.[12] Assuming electrons to be the charge carriers, the photorefractive index grating can be written as

$$n = n_b + \frac{n_{1W}}{2}\left[\,e^{i\phi}\,\frac{A_W B_W^*}{|A_W|^2+|B_W|^2}\,e^{iKx} + \text{c.c.}\right] \quad , \tag{10a}$$

where

$$n_{1W} = n_b^3 \, r_{eff,W} \, E_q \sqrt{\frac{E_0^2+E_d^2}{E_0^2+(E_d+E_q)^2}} \quad ,$$

$$\tan\phi = \frac{E_0^2+E_d(E_d+E_q)}{E_0 E_q} \quad . \tag{10b}$$

Here n_b is the background refractive index of the photorefractive medium in the absence of light, n_{1W} is the amplitude of the index grating at the fundamental harmonic of the grating vector and ϕ represents the spatial phase shift of the index gratings with respect to the light intensity pattern. $r_{eff,W}$ is an effective electro-optic coefficient that depends on the polarization of the writing beams, the orientation of the grating wave vector that is written, and the non-zero Pockels coefficients of the photorefractive medium. E_0 is the dc electric field applied to the photorefractive crystal, E_d is the characteristic electric field due to diffusion, and E_q is the saturation value of the space charge field. Substituting for n and E in the scalar wave Eq. (4), using the slowly varying envelope approximation and ignoring phase-mismatched terms and terms that are quadratic in the index change, we arrive at the following coupled wave equations

$$\frac{dA_W}{dz} = -\frac{\alpha_W}{2\cos\theta_{WI}} A_W + i c^{i\phi} \frac{\pi n_{1W}}{\lambda_W \cos\theta_{WI}} \frac{A_W B_W^*}{|A_W|^2 + |B_W|^2} B_W \quad ,$$

$$\frac{dB_W}{dz} = -\frac{\alpha_W}{2\cos\theta_{WI}} B_W + i c^{-i\phi} \frac{\pi n_{1W}}{\lambda_W \cos\theta_{WI}} \frac{A_W^* B_W}{|A_W|^2 + |B_W|^2} A_W \quad , \tag{11}$$

where α_W is the intensity absorption coefficient at the writing wavelegth and θ_{WI} is the half angle between the beams inside the crystal. Expressing the complex beam amplitudes in polar form: $A_W = \sqrt{2I_{AW}} \exp(i\psi_{AW})$, we obtain the following equations for beam intensities and phases

$$\frac{dI_{AW}}{dz} = -\frac{\alpha_W}{\cos\theta_{WI}} I_{AW} - \gamma \frac{I_{AW}I_{BW}}{I_{AW}+I_{BW}} \quad , \qquad \frac{d\psi_{AW}}{dz} = \zeta \frac{I_{BW}}{I_{AW}+I_{BW}} \quad ,$$

$$\frac{dI_{BW}}{dz} = -\frac{\alpha_W}{\cos\theta_{WI}} I_{BW} + \gamma \frac{I_{AW}I_{BW}}{I_{AW}+I_{BW}} \quad , \qquad \frac{d\psi_{BW}}{dz} = \zeta \frac{I_{AW}}{I_{AW}+I_{BW}} \quad , \tag{12a}$$

where

$$\gamma = \frac{2\pi n_{1W}\sin\phi}{\lambda_W \cos\theta_{WI}} \quad , \qquad \zeta = \frac{\pi n_{1W}\cos\phi}{\lambda_W \cos\theta_{WI}} \quad . \tag{12b}$$

The intensity equations and subsequently the phase equations can be solved as functions of distance z in the crystal

$$I_{AW}(z) = I_{AW}(0)\,\frac{1+\beta}{1+\beta\, e^{\gamma z}}\,\exp\left(-\frac{\alpha_W z}{\cos\theta_{WI}}\right) \quad ,$$

$$I_{BW}(z) = I_{BW}(0)\,\frac{1+\beta}{\beta+e^{-\gamma z}}\,\exp\left(-\frac{\alpha_W z}{\cos\theta_{WI}}\right) \quad , \tag{13a}$$

$$\psi_{AW}(z) - \psi_{BW}(z) = \psi_{AW}(0) - \psi_{BW}(0) - \zeta z + \frac{2\zeta}{\gamma}\ln\left[\frac{1+\beta e^{\gamma z}}{1+\beta}\right] \quad , \tag{13b}$$

where $\beta = I_{BW}(0)/I_{AW}(0)$ is the intensity ratio of the writing beams at the input. We find that the intensity of each beam at a distance z depends on the input intensities of **both** the beams, and there is an exponential dependence on the product γz. If the beam being amplified (≡ probe or writing beam B) is initially much weaker than the beam being depleted (≡ pump or writing beam A) such that $\beta \ll 1$, and $\beta \ll \exp(-\gamma L)$, we obtain an exponential buildup for the probe; while the pump is undepleted and remains constant at its input value in a lossless photorefractive medium: $I_{BW}(L) \approx I_{BW}(0)\, e^{\gamma L}$ and $I_{AW}(L) \approx I_{AW}(0)$. Substituting the solutions for the beam intensities and phases given by Eqs. (13) into the expression for the photorefractive index grating given by Eq. (10a), we arrive at the following expression

$$n(x,z) = n_b + \frac{n_{1W}}{\sqrt{\beta}\, e^{\gamma z/2} + \dfrac{e^{-\gamma z/2}}{\sqrt{\beta}}}\,\cos\left[Kx + \phi + \Delta\psi(0) - \zeta z + \frac{2\zeta}{\gamma}\ln\left(\frac{1+\beta e^{\gamma z}}{1+\beta}\right)\right]$$

$$\equiv n_b + n_{1eff}(z)\,\cos[Kx+\phi+\Delta\psi_{eff}(z)] \tag{14}$$

where $\Delta\psi = \psi_{AW} - \psi_{BW}$. This is the general expression for a photorefractive index grating using transmission geometry that is valid for arbitrary phase shift ϕ of index grating from the intensity pattern. In contrast to the fixed, volume phase grating with uniform amplitude and phase of Eq. (1), the photorefractive index grating in the above equation has an amplitude and phase that vary with the depth in the grating. Bending of the photorefractive hologram through the crystal thickness is caused by $\Delta\psi_{eff}(z)$ - there is no bending for $\phi = \pi/2$, and bending increases as ϕ shifts from $\pi/2$. Note that Eq. (14) is *independent of absorption losses* ($\propto \alpha_W$) in the medium at the writing wavelength. Without loss of generality, we arbitrarily set the relative phase between the two writing beams equal to zero at the input ($\Delta\psi(0) = 0$). Figure 6a is a plot of the nonuniform grating amplitude $2n_{1eff}(z)/n_{1W}$ and Fig. 6b is a plot of the nonuniform phase of the

grating $\Delta\psi_{eff}(z)$ as a function of depth z into the grating. The phase shift ϕ of the index grating from the intensity pattern is 0 (dashed curve), $\pi/6$ (dotted-dashed curve) and $\pi/2$ (solid curve), while $\beta = 0.01$ and $2\pi n_{1W} / (\lambda_W \cos\theta_{WI}) = 20\ cm^{-1}$. Note that $\Delta\psi_{eff}(z)$ changes sign in the bulk of the grating for $\phi = \pi/6$, so that the surfaces of equal index change are curved and tilted.[12]

For $\phi = 0$, there is no phase shift of the index grating from the intensity pattern, so that the intensity coupling constant γ between the writing beams is equal to zero, and the phase coupling constant ζ is equal to its maximum value of $\zeta_m = \pi n_1/\lambda_W \cos\theta_{WI}$. In this case, Eq. (14) simplifies to

$$n(x,z) = n_b + n_{1W} \frac{\sqrt{\beta}}{1+\beta} \cos(Kx - \zeta_m z) \quad , \tag{15a}$$

which is a grating with uniform amplitude and a spatial frequency that is modified by the phase coupling between the writing beams. The phase of the grating varies linearly with depth into the crystal, so that the grating planes are rotated to form slanted gratings. Maximum diffraction efficiency will occur at a read angle different from that during writing. Comparing with Eq. (2b), the amplitude n_{1W} of the photorefractive index grating given in Eq. (15a) must be replaced by $2n_{10}$ to yield the results of the uniform phase grating.

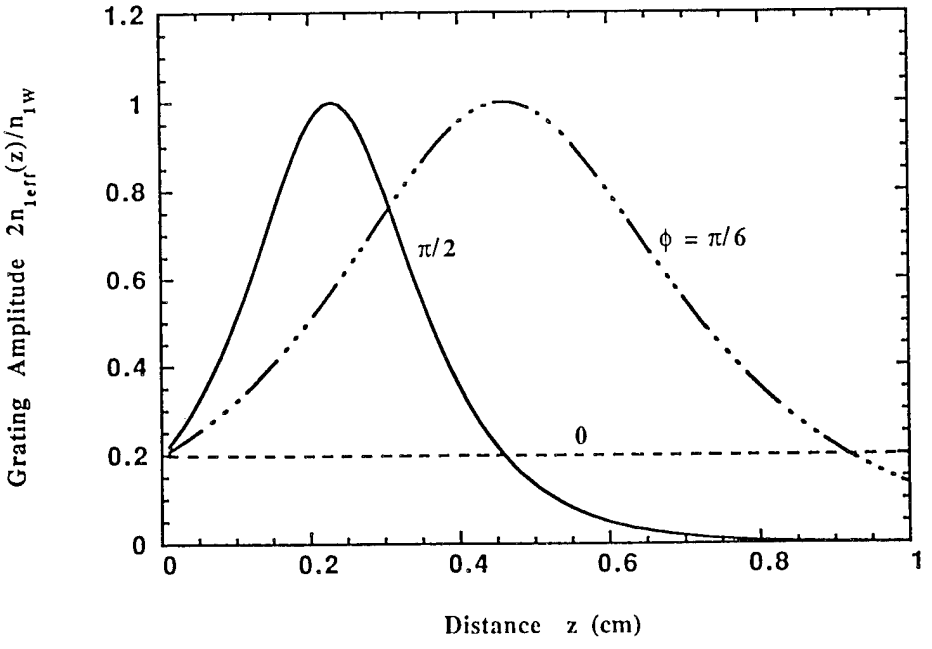

Fig. 6a. Nonuniform amplitude $2n_{1eff}(z)/n_{1W}$ of photorefractive grating for different values of phase shift ϕ of index grating from intensity pattern. The beam ratio β during writing is equal to 0.01, and $2\pi n_{1W}/\lambda_W \cos\theta_{WI}) = 20\ cm^{-1}$.

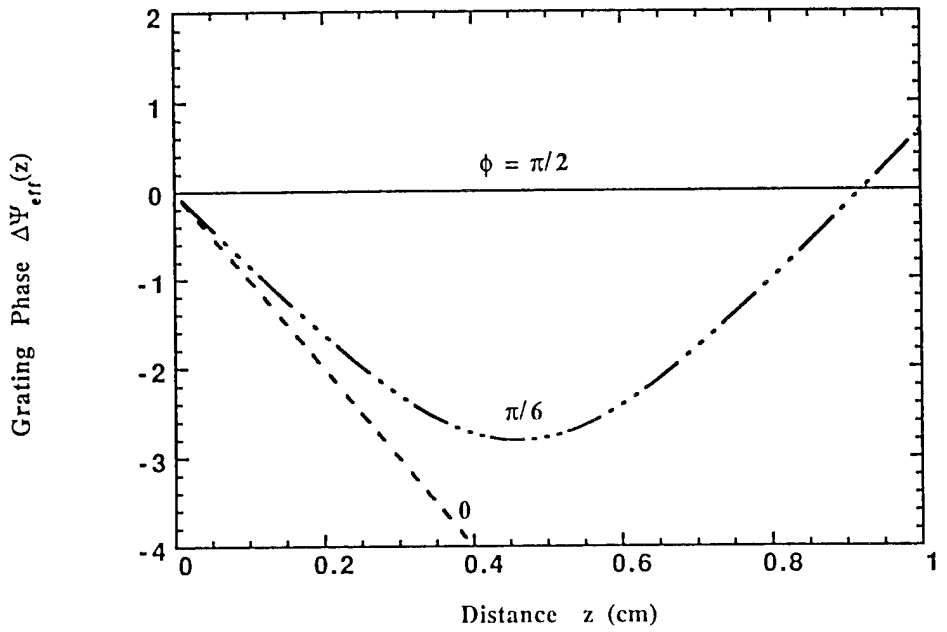

Fig. 6b. Nonuniform phase $\Delta\psi_{eff}(z)$ of photorefractive grating for different values of phase shift ϕ of index grating from intensity pattern. The other parameters are identical to Fig. 6a.

Similarly, if $\phi = \pi/2$, the phase coupling constant ζ is equal to zero and γ is equal to its maximum value of $\Gamma = 2\pi n_1/\lambda_W \cos\theta_{WI}$. In this case, Eq. (14) simplifies to

$$n(x,z) = n_b - n_{1W} \frac{1}{\sqrt{\beta}\, e^{\Gamma z/2} + \frac{e^{-\Gamma z/2}}{\sqrt{\beta}}} \sin Kx \,. \qquad (15b)$$

Hence the photorefractive index grating in the above equation has a uniform phase and an amplitude that varies with the depth in the grating and is spatially shifted by $\pi/2$ from the intensity pattern of Eq. (9). The nonuniformity $2n_{1eff}(z)/n_{1W}$ of the grating amplitude is a function of the input beam ratio β and the strength of the beam coupling Γ and is illustrated in Fig. 7 for Γ=20cm^{-1}, a coupling value easily achieved in single crystal $BaTiO_3$. The grating amplitude is maximum when the two writing beams have equal intensity; for $\beta = 1$ case, this occurs at the input plane itself, while for the $\beta = 0.01$ case, the two writing beams have equal intensity only after they have propagated some distance into the crystal and the weak probe has been amplified at the expense of the strong pump beam via photorefractive two-beam coupling. For $\beta = 100$, the probe is stronger than the pump to begin with, and two-beam coupling effects serve to further amplify the probe in the medium. Hence the optimum beam ratio is never achieved and the grating amplitude decreases monotonically in the medium. It is important to study the effects of this departure from uniformity of photorefractive index gratings on the diffraction efficiency of a weak reading beam. As we shall show in the next section, maximum diffraction efficiency occurs for $\beta = 0.01$, when the grating peaks near the middle of the interaction length.[12]

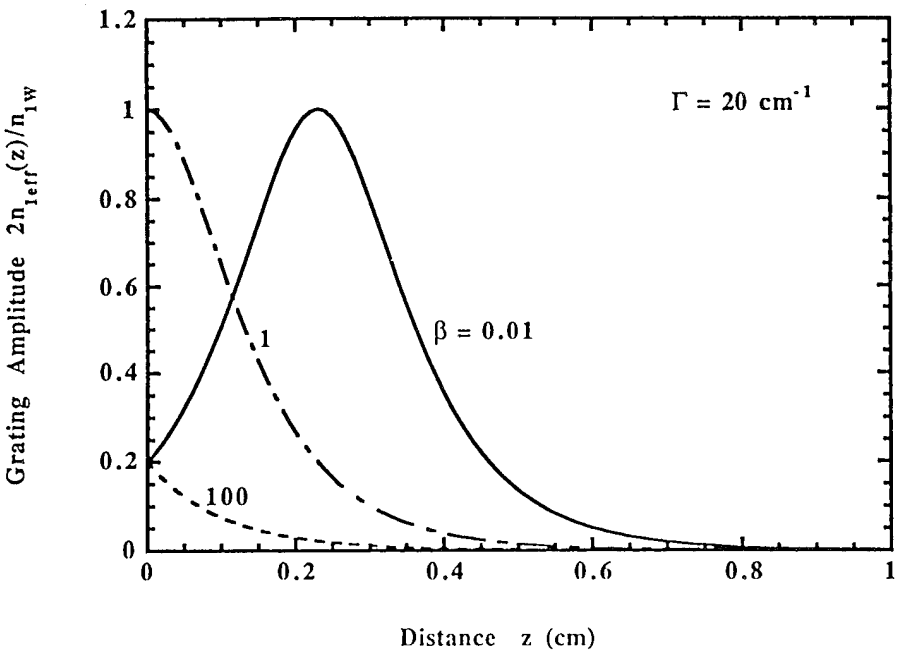

Fig. 7. Nonuniform amplitude $2n_{1eff}(z)/n_{1W}$ of photorefractive grating for different values of beam ratio β during writing. The two-beam coupling constant Γ is equal to 20 cm^{-1}.

[C]. Readout of $\pi/2$ Shifted Photorefractive Gratings with a Weak Incoherent Beam

The basic interaction geometry is illustrated in Fig. 8. A_W and B_W are the two coherent writing beams of wavelength λ_W that intersect within a photorefractive crystal of thickness L. The angle between the two beams is $2\theta_{WI}$ in the medium. The photorefractive grating induced by this pair of beams is read by an incoherent third beam A_R of wavelength λ_R that is incident at a different angle (θ_{RI} in the medium) for Bragg matched readout. A fourth beam B_R is generated by the diffraction of the read beam off this grating. The theoretical problem of interest is to find an expression for the diffraction efficiency of the photorefractive index grating when $\phi = \pi/2$, as given by Eq. (15b). The intensity of the read beam I_{AR} is assumed to be weaker than the writing beam intensities I_{AW}, I_{BW}, so that the readout process does not perturb the grating being read. Also, Bragg condition is satisfied during readout, so that $\mathbf{k}_{AR} - \mathbf{k}_{BR} = \mathbf{k}_{AW} - \mathbf{k}_{BW} = \mathbf{K}$. By following the methods used in the previous sections, we arrive at the coupled wave equations for the amplitudes of the read beam A_R and the diffracted beam B_R

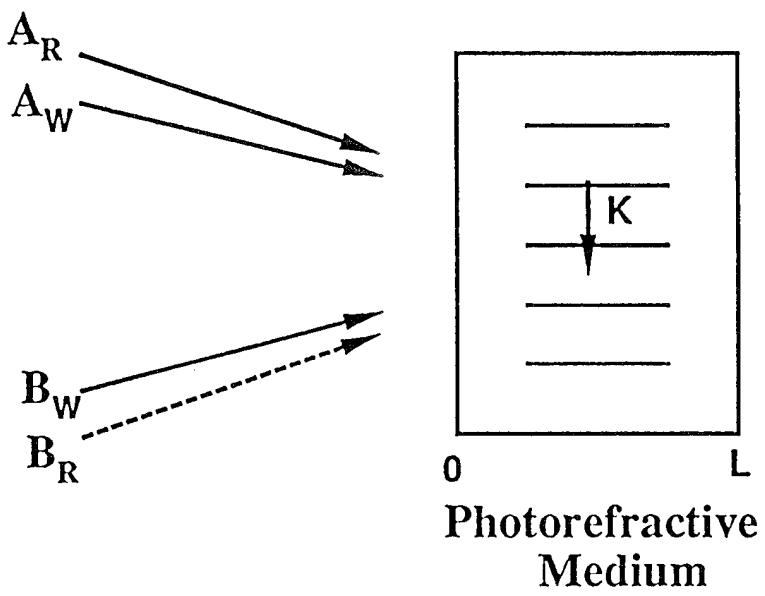

Fig. 8. Schematics of simultaneous writing and readout of photorefractive index grating.

$$\frac{dA_R}{dz} = -\frac{\alpha_R}{2\cos\theta_{RI}} A_R - \frac{\pi n_{1R}}{\lambda_R \cos\theta_{RI}} \frac{1}{\left(\sqrt{\beta}e^{\Gamma z/2} + \frac{e^{-\Gamma z/2}}{\sqrt{\beta}}\right)} B_R$$

$$\frac{dB_R}{dz} = -\frac{\alpha_R}{2\cos\theta_{RI}} B_R + \frac{\pi n_{1R}}{\lambda_R \cos\theta_{RI}} \frac{1}{\left(\sqrt{\beta}e^{\Gamma z/2} + \frac{e^{-\Gamma z/2}}{\sqrt{\beta}}\right)} A_R \quad . \qquad (16)$$

Since the read beam and its diffracted component can have a polarization different from that of the writing beams, r_{eff} at readout can be different from that during writing. Such a possibility is allowed for by distinguishing between the grating amplitudes n_1 during writing and readout, even though both the processes involve the same space charge grating with wave vector K. Using boundary conditions $A_R(0) = A_{R0}$, $B_R(0) = 0$, we obtain the following expression for the diffraction efficiency $(= |B_R(L)/A_{R0}|^2)$ of the hologram[5]

$$\eta = \exp\left(-\frac{\alpha_R L}{\cos\theta_{RI}}\right) \sin^2\left[\frac{2\kappa}{\Gamma}\left(\tan^{-1}(e^{\Gamma L/2}\sqrt{\beta}) - \tan^{-1}(\sqrt{\beta})\right)\right] , \qquad (17)$$

where $\kappa = \pi n_{1R}/\lambda_R \cos\theta_{RI}$ is the coupling constant during readout. κ and $\Gamma = 2\pi n_{1W}/\lambda_W \cos\theta_{WI}$ are related but can be quite different in value depending on the polarization states of the writing beams and that of the reading beam. Note that κ (Γ) is the amplitude (intensity) coupling constant, so that $2\kappa = \Gamma$ for identical polarization and wavelength during writing and readout. Then the expression (17) for diffraction efficiency simplifies to

$$\eta = \exp\left(-\frac{\alpha_R L}{\cos\theta_{RI}}\right) \frac{\beta}{1+\beta} \frac{[\exp(\Gamma L/2) - 1]^2}{1 + \beta \exp(\Gamma L)} , \qquad (18)$$

which is identical to the result obtained by Kukhtarev et al[12] for a lossless medium ($\alpha_R = 0$). In the limit of no coupling during writing ($\Gamma \to 0$, κ remains finite), Eq. (17) reduces to the Kogelnik result[4] given by Eq. (8) if we use the fact that n_{1R} is equal to $2n_{10}$ of the fixed, uniform grating; this limit can be achieved in noncubic photorefractive crystals by writing a grating that can be read out only by anisotropic diffraction. In particular, we examine the diffraction efficiency of holograms written in $BaTiO_3$ for the following two cases. In the first case, the writing beams at $\lambda_W = 514.5$ nm are extraordinary-polarized, resulting in strong two-beam coupling ($\Gamma_e = 20 cm^{-1}$). In such a case, the index modulation varies significantly over the thickness of the crystal because one beam is strongly amplified as the other strongly depletes. For the second case, the writing beams are ordinary-polarized for which the beam coupling constant is much smaller ($\Gamma_o = 1 cm^{-1}$). In both cases, the grating is read out by a weak beam at $\lambda_R = 633$ nm that is extraordinary-polarized ($\kappa = \Gamma_e/2 = 10 cm^{-1}$). Plots of the diffraction efficiency η as a function of medium thickness L, as given by Eq. (17), are shown in Fig. 9, where the beam ratio is taken to be 0.1 (absorption is neglected, for simplicity). Also plotted for comparison is the diffraction efficiency of a uniform hologram (with no coupling, corresponding to Eq. (8)), with the same reading beam coupling constant κ. Note that for the case of polarization asymmetry during writing/reading, the argument of the sine function in Eq. (17) can be quite large, allowing η to exhibit one complete cycle. Figure 10 is a plot of the diffraction efficiency η as a function of beam ratio β for L = 0.5 cm. The values of the coupling constants are the same as in Fig. 9. Note that writing with ordinary-polarized beams gives results similar to the Kogelnik case due to the smaller two-beam coupling effects. Corresponding to this choice of parameter values, the maximum diffraction efficiency occurs at an input intensity ratio of 0.01 for extraordinary-polarized writing beams, while the maxima occur at $\beta \sim 0.1$ and 8 for ordinary-polarized writing beams.

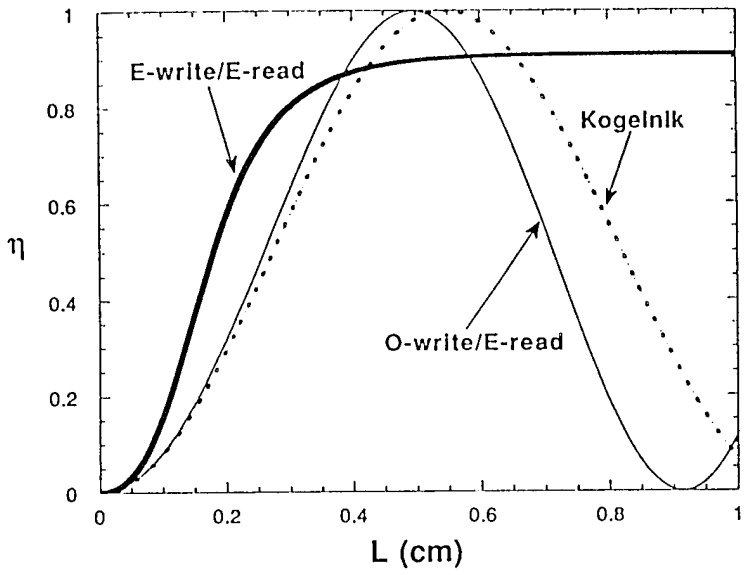

Fig. 9. Diffraction efficiency η as a function of medium thickness L. Input beam ratio β is equal to 0.1, and absorption effects are neglected (α = 0).

(i) $\Gamma = 2\kappa = 20\ cm^{-1}$ (E-write / E-read curve)
(ii) $\Gamma = 1\ cm^{-1}$, $2\kappa = 20\ cm^{-1}$ (O-write / E-read curve)
(iii) $\Gamma = 0$, $2\kappa = 20\ cm^{-1}$ (Kogelnik case)

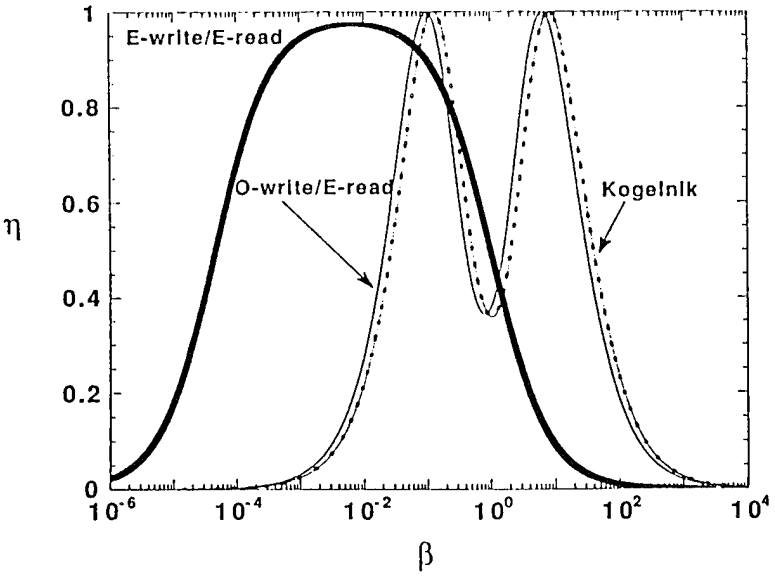

Fig. 10. Diffraction efficiency η as a function of beam ratio β during writing. Grating thickness L is equal to 0.5 cm. All other parameters are the same as in Fig. 9.

[D]. Readout of Photorefractive Gratings with a Strong Incoherent Beam

The basic interaction geometry is identical to that shown in Fig. 8, and the incoherent read beam intensity I_{AR} can be comparable to or larger than the intensities of the writing beams I_{AW}, I_{BW}. Hence the new grating formed by the read beam and its coherently generated diffracted beam must be taken into account, besides the grating being read. In this section, the diffraction efficiency of a photorefractive grating is examined for arbitrary phase shifts of the index grating from the intensity pattern. All the four waves are assumed to be plane waves with identical linear polarization, so that the grating amplitude n_1 is equal for the writing and readout beams. The total intensity is the sum of the intensity of all the four beams and the interference terms arising from the two pairs of coherent beams

$$I(\mathbf{r}) = \frac{1}{2}\sum_j \{|A_j|^2 + |B_j|^2 + [\, A_j B_j^* \exp(i\mathbf{K}_j\cdot\mathbf{r}) + \text{c.c.}\,]\} \quad , \tag{19}$$

where the grating vectors are defined by $\mathbf{K}_j \equiv \mathbf{k}_{Aj} - \mathbf{k}_{Bj}$, j = W, R. If Bragg condition is satisfied for the two coherent beam pairs: $\mathbf{K}_W = \mathbf{K}_R \equiv \mathbf{K}$, then the gratings formed by the two beam pairs combine to form a single grating that couples all the beams

$$n = n_b + \frac{n_1}{2}\left[e^{i\phi} \frac{A_W B_W^* + A_R B_R^*}{|A_W|^2 + |B_W|^2 + |A_R|^2 + |B_R|^2} \exp(i\mathbf{K}\cdot\mathbf{r}) + \text{c.c.}\right] \quad . \tag{20}$$

We can derive the following coupled wave equations by using the methods developed in the previous sections

$$\frac{dA_j}{dz} = \gamma \frac{A_W B_W^* + A_R B_R^*}{|A_W|^2 + |B_W|^2 + |A_R|^2 + |B_R|^2} B_j$$

$$\frac{dB_j}{dz} = -\gamma^* \frac{A_W^* B_W + A_R^* B_R}{|A_W|^2 + |B_W|^2 + |A_R|^2 + |B_R|^2} A_j, \tag{21}$$

where j = W, R, and γ is the complex field coupling coefficient defined as $\gamma = i\pi n_1 e^{i\phi}/(\lambda\cos\theta_I)$. In arriving at these equations, we have ignored the difference between the wavelengths ($\lambda_W \approx \lambda_R \equiv \lambda$) and angles ($\theta_{WI} \approx \theta_{RI} \equiv \theta_I$) of the writing and readout beams, so that the coupling constant is the same for both pairs of beams. For Bragg-matched readout, the frequencies of the various beam pairs can differ by a few tens of gigahertz and their angles differ by a few milliradians for typical values of 1 μm grating period and 1mm thickness of the photorefractive grating. The coupled wave equations (21) can be solved by using methods developed in Refs. 13–15: the constants of

integration associated with these equations are identified; two new variables $f \equiv A_R/A_W$ and $g \equiv B_R/B_W$ are defined and their equations are solved. The intensities of the four beams can then be expressed as the following functions of z[9]

$$|A_R(z)|^2 = \frac{c_W\,|f(z)g(z)|^2 - c_R\,|f(z)|^2}{|g(z)|^2 - |f(z)|^2}$$

$$|B_R(z)|^2 = \frac{c_R\,|g(z)|^2 - c_W\,|g(z)f(z)|^2}{|g(z)|^2 - |f(z)|^2}$$

$$|A_W(z)|^2 = \frac{c_W\,|g(z)|^2 - c_R}{|g(z)|^2 - |f(z)|^2}$$

$$|B_W(z)|^2 = \frac{c_R - c_W\,|f(z)|^2}{|g(z)|^2 - |f(z)|^2} \quad , \tag{22}$$

where

$$f(z) = \frac{sf_0 + (\sigma f_0 + 2b^*)\tanh \kappa z}{s - (\sigma - 2bf_0)\tanh \kappa z}$$

$$g(z) = \frac{sg_0 - (\sigma g_0 + 2b^*)\tanh \kappa^* z}{s + (\sigma - 2bg_0)\tanh \kappa^* z} \quad , \tag{23}$$

and $c_R = |A_R(0)|^2 + |B_R(0)|^2$, $c_W = |A_W(0)|^2 + |B_W(0)|^2$, $\sigma = c_R - c_W$, $b = A_R^*(0)A_W(0) + B_R^*(0)B_W(0)$, $s^2 = \sigma^2 + 4|b|^2$, $\kappa = s\gamma/4I_0$, $f_0 = A_R(0)/A_W(0)$, $g_0 = B_R(0)/B_W(0)$, $I_0 = [|A_R(0)|^2 + |B_R(0)|^2 + |A_W(0)|^2 + |B_W(0)|^2]/2$. The above equations are general solutions for forward four-wave mixing. For the problem at hand, we have the boundary conditions $B_R(0) = 0$, and $A_R(0)$, $A_W(0)$, and $B_W(0)$ are known quantities. The diffraction efficiency is then defined as $\eta \equiv |B_R(L)|^2 / |A_R(0)|^2$, where $|B_R(L)|^2$ can be calculated by evaluating the second equation of (22) at $z = L$. From the expressions for f(L) and g(L), it is obvious that η will be a function of $\tanh \kappa L$, where κ is a complex quantity for any general value of the spatial phase shift ϕ. Using mathematical identities, $\tanh \kappa L$ can be expressed in terms of $\tanh \kappa_r L$ and $\tan \kappa_i L$, where the subscripts r and i refer to the real and imaginary parts of a complex quantity, respectively. Hence we can expect η to exhibit both oscillatory and exponential behavior as a function of $|\kappa|L$.

[i] $\phi = \pi / 2$

γ is a real, negative quantity equal to $-\gamma_r$, with $\gamma_r = \pi n_1/(\lambda \cos\theta_I)$. The expression for η simplifies to[9]

$$\eta = \frac{16\, I_{AW}(0)\, I_{BW}(0) \tanh^2\kappa_r L}{s^2(1 + \tanh^2\kappa_r L) - 4\, s \tanh \kappa_r L\, [I_{AR}(0) + I_{AW}(0) - I_{BW}(0)]} \quad , \tag{24}$$

where $\kappa_r = s\gamma_r/4I_0$, $I_{Aj}(0) = |A_j(0)|^2/2$, etc. The expression for η involves only hyperbolic functions of $\kappa_r L$, and is asymmetric with respect to change in sign of κ_r, which implies unequal diffraction efficiencies for readout from the two input ports. A change in the sign of the coupling constant is equivalent to readout from the other input port. This is true for both equal and different intensity writing beams, except that the latter case would involve an interchange of the unequal intensities of the writing beams besides the change in read beam intensity to describe readout from the other input port.

For a weak reading beam [$I_{AR}(0) << I_{AW}(0), I_{BW}(0)$], the input intensities dependent factor $s/(2I_0)$ that is present in κ_r is equal to unity, so that $\kappa_r = \gamma_r/2$. Hence Eq. (24) simplifies to

$$\eta = \frac{\beta}{1+\beta} \frac{[\exp(\gamma_r L) - 1]^2}{1 + \beta \exp(2\gamma_r L)} \quad , \tag{25}$$

where β is the input beam ratio of the writing beams defined as: $\beta \equiv I_{BW}(0) / I_{AW}(0)$. This result is identical to the diffraction efficiency obtained in Eq. (18) if we neglect absorption and use $\Gamma = 2\gamma_r$. The same expression for η was obtained by Kukhtarev *et al.*[12] for a weak read beam and $\pi/2$ shifted photorefractive grating. For small coupling strengths, $\gamma_r L << 1$, and Eq. (25) reduces to $\eta \approx \beta\gamma_r^2 L^2 / [(1+\beta)^2]$. This expression is identical to Kogelnik's result (Eq. (8)) for small arguments of the sine function with $n_1 \equiv 2n_{10}$.

Figure 11 is a plot of the diffraction efficiency as a function of the read beam intensity, as given by Eq. (24). The equal intensity of the write beams is taken to be unity: $I_{AW}(0) = I_{BW}(0) = 1$. Note that the modulation depth can still be smaller than unity due to the read beam intensity in the denominator of the expression for m. For small coupling strengths ($\gamma_r L \approx 1$) and weak read beam ($I_{AR}(0) < I_{AW}(0), I_{BW}(0)$), the diffraction efficiency is independent of the read beam intensity. Increase of the read beam intensity above the write beam intensities serves to erase the grating being read, and the diffraction efficiency falls to zero. For strong coupling, the behavior of η is different—the diffraction efficiency is ~50% for weak read beams, and increases as the read beam becomes stronger than the write beams, reaches a broad maximum and eventually falls to zero when $I_{AR}(0) >> I_{AW}(0), I_{BW}(0)$. Enhancement of the diffraction efficiency occurs

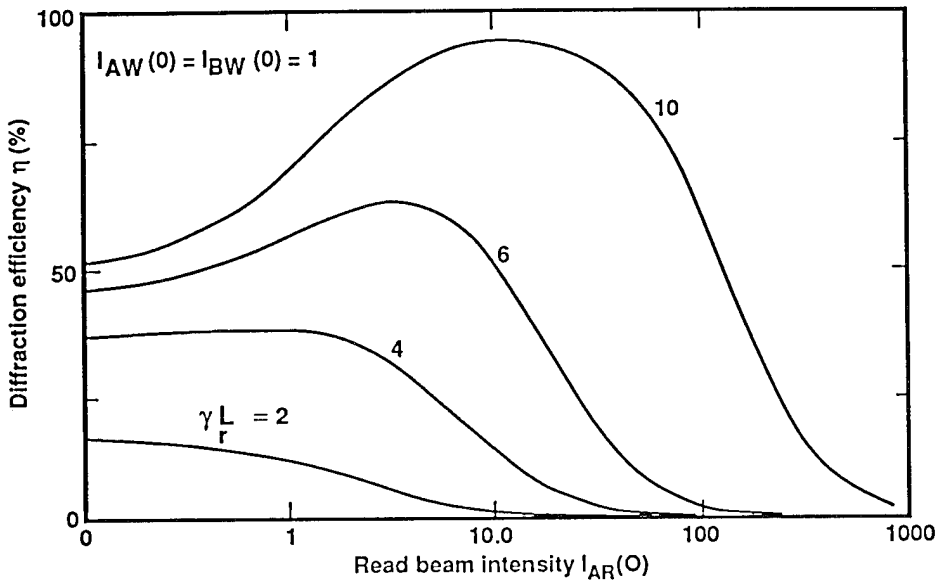

Fig. 11. Diffraction efficiency η as a function of read beam intensity $I_{AR}(0)$ for various coupling strengths $\gamma_r L$. The normalized, equal intensities of the write beams are unity: $I_{AW}(0) = I_{BW}(0) = 1$.

when the new grating formed by the read beam and its diffracted component is in phase with the grating being read. Figure 12 is the same set of curves as in Fig. 11 but for negative coupling constant γ_r, which corresponds to readout from the other input port. In this case, the two gratings are out of phase, so that there is no enhancement of the diffraction efficiency for any intensity of the read beam. As predicted by Eq. (24), the maximum diffraction efficiency is only 50% at large coupling strengths. Figure 13 is a plot of the diffraction efficiency η versus the normalized coupling strength $\gamma_r L$ for negligible absorption and equal intensity of write beams, $I_{AW}(0) = I_{BW}(0) = 1$. The asymmetry in η is negligible for a weak read beam and becomes appreciable only when $I_{AR}(0) > I_{AW}(0), I_{BW}(0)$.

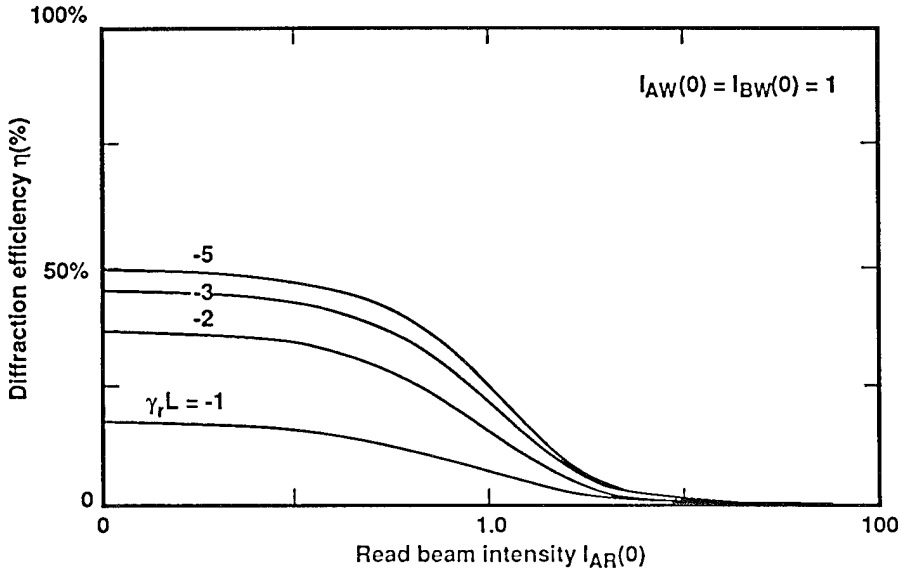

Fig. 12. Diffraction efficiency η as a function of read beam intensity $I_{AR}(0)$ for various negative coupling strengths $\gamma_r L$. The normalized, equal intensities of the write beams are unity: $I_{AW}(0) = I_{BW}(0) = 1$.

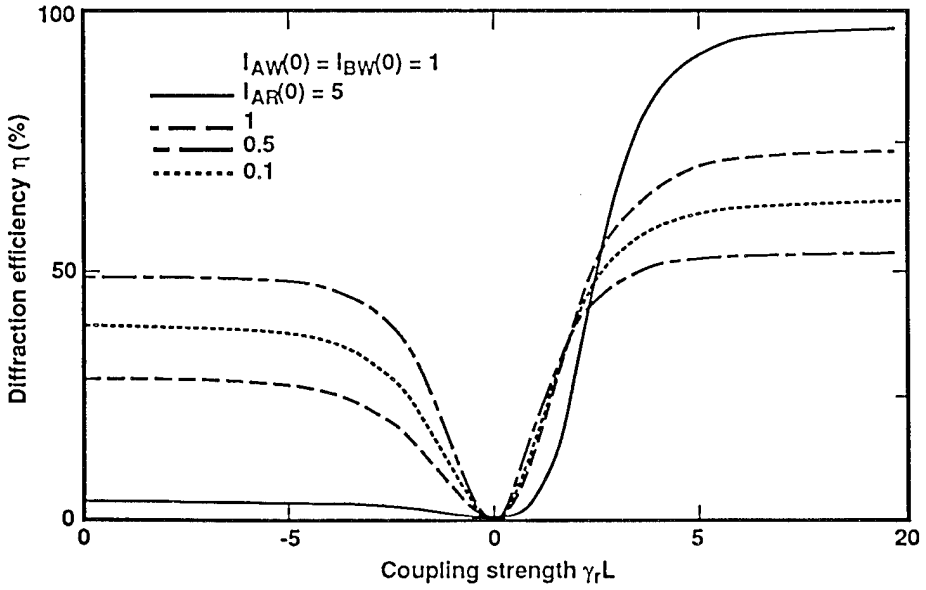

Fig. 13. Diffraction efficiency η as a function of coupling strength $\gamma_r L$ for various read beam intensities $I_{AR}(0)$. The normalized, equal intensities of the write beams are unity: $I_{AW}(0) = I_{BW}(0) = 1$.

[ii] $\phi = 0$

For the case of $\phi = 0$, which corresponds to a local index grating that follows the intensity pattern, γ (and hence κ) is a purely imaginary number that we take to be equal to $i\gamma_i(i\kappa_i)$. The expression for diffraction efficiency simplifies to[9]

$$\eta = \frac{4I_{AW}(0)I_{BW}(0)}{[I_{AR}(0) + I_{AW}(0) - I_{BW}(0)]^2 + 4I_{AW}(0)I_{BW}(0)} \sin^2 \kappa_i L \quad . \tag{26}$$

Apart from the multiplicative factor before the trignometric function and the read beam intensity dependence of κ_i, this result is reminiscent of Kogelnik's expression (Eq. (7)) for diffraction efficiency of uniform gratings. For a weak reading beam [$I_{AR}(0) << I_{AW}(0)$, $I_{BW}(0)$] and writing beams of comparable intensity [$I_{AW}(0) \approx I_{BW}(0)$], the multiplicative factor and the input intensities dependent factor $s/(2I_0)$ that is present in κ_i are both equal to unity. Hence Eq. (26) reduces to: $\eta = \sin^2(\gamma_i L/2)$, where $\gamma_i \equiv \pi n_1/(\lambda \cos\theta_i)$ is the amplitude coupling constant in Eqs. (21); this expression is identical to Kogelnik's formula (Eq. (7)) with $n_1 \equiv 2n_{10}$. If the writing beams have different intensities, then Eq. (26) simplifies to

$$\eta = \frac{4\beta}{(1+\beta)^2} \sin^2\left(\frac{\gamma_i L}{2}\right) \quad , \tag{27}$$

which is identical to the expression obtained by Kukhtarev *et al.*[12] for replay of a local photorefractive grating with a weak read beam. For small coupling strengths, $\gamma_i L << 1$, and Eq. (27) reduces to $\eta \approx \beta\gamma_i^2 L^2/[(1+\beta)^2]$, which is identical to Kogelnik's expression[4] for small arguments of the trignometric function. Increasing the read beam intensity serves to reduce the multiplicative factor in Eq. (26) until it is zero for a strong read beam [$I_{AR}(0) >> I_{AW}(0)$, $I_{BW}(0)$], implying erasure of the grating from readout. The $s/2I_0$ factor that is present in κ_i is not very sensitive to changes in read beam intensity and decreases slightly from unity as the intensity of the weak read beam is increased. Once $I_{AR}(0) > I_{AW}(0)$, $I_{BW}(0)$, the factor increases and is again equal to unity for a strong read. Note that η is symmetric with respect to change in sign of κ_i, which implies that there is no nonreciprocity in η for local photoinduced gratings, even when the read beam is intense.

For the general case of a nonzero spatial phase shift between photorefractive grating and fringe pattern and a read beam intensity comparable to that of the writing beams, the parameter dependence of diffraction efficiency is studied numerically. Figure 14 shows the nonlinear behavior of η as a function of the read beam intensity $I_{AR}(0)$ for various phase shifts ϕ. Note that the nonlinearity is more pronounced and that higher values of η are possible when $\phi = \pi / 6$. However, photorefractive gratings formed at $\phi = \pi / 2$ are more difficult to erase. The curve for $\phi = \pi/2$ is identical to that shown in

Fig. 11. For $\phi = 0$ case, both the multiplicative factor and $s/2I_0$ in κ_i decrease as the reading beam intensity is increased, and the decrease of the first function is more rapid. The coupling strength $\gamma_i L$ is equal to 10 in the calculations, so that for an initial read beam intensity of 0.1, $\kappa_i L$ is equal to 2.38. This is considerably more than $\pi/2$ at which a sine function peaks, so even though the argument of the sine function is decreasing from the initial value of 2.38 with increasing read beam intensity, η still increases with $I_{AR}(0)$ until the factor $s/2I_0$ in κ_i reduces to $2\pi/(\gamma_i L) = 0.63$. Beyond that value, η starts decreasing mainly due to the rapidly falling values of the multiplicative factor with $I_{AR}(0)$. The curve for $\phi = \pi/6$ in Fig. 14 represents a combination of effects present in $\phi = \pi/2$ and $\phi = 0$ cases. Figure 15 shows the nonreciprocal behavior of η with respect to direction of readout for various phase shifts ϕ and a read beam intensity equal to that of the writing beams. For equal intensity writing beams, a change in the sign of the coupling constant is equivalent to readout from the other input port. Note that $\phi = 0$ ($\phi = \pi/2$) gives oscillatory (exponential) behavior of η as a function of $|\gamma|L$, while $\phi = \pi/6$ exhibits a combination of both behaviors, with decaying oscillations. The nonreciprocity is enhanced for $\phi = \pi/6$, while $\phi = 0$ case is symmetric with respect to readout from either input port even when the read beam is as intense as the write beams. Figure 16 is a plot of η versus $|\gamma|L$ for a weak reading beam ($I_{AR}(0) = 0.01$). The

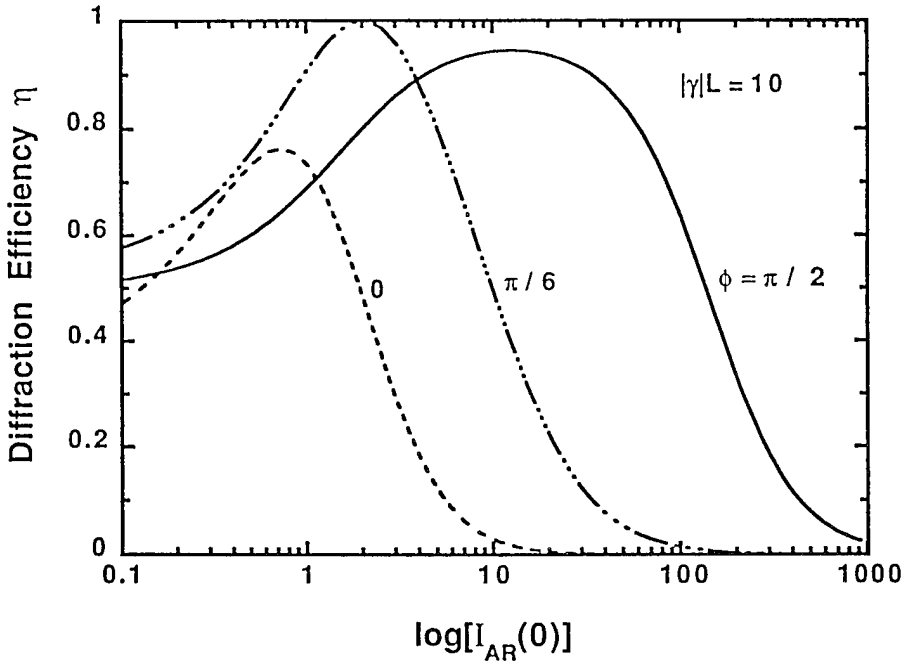

Fig. 14. Diffraction efficiency η as a function of read beam intensity $I_{AR}(0)$ for various values of spatial phase shift ϕ. The modulus of the coupling strength, $|\gamma|L$, is chosen to be 10, and the writing beams are taken to be equal; i.e., $I_{AW}(0) = I_{BW}(0) = 1$.

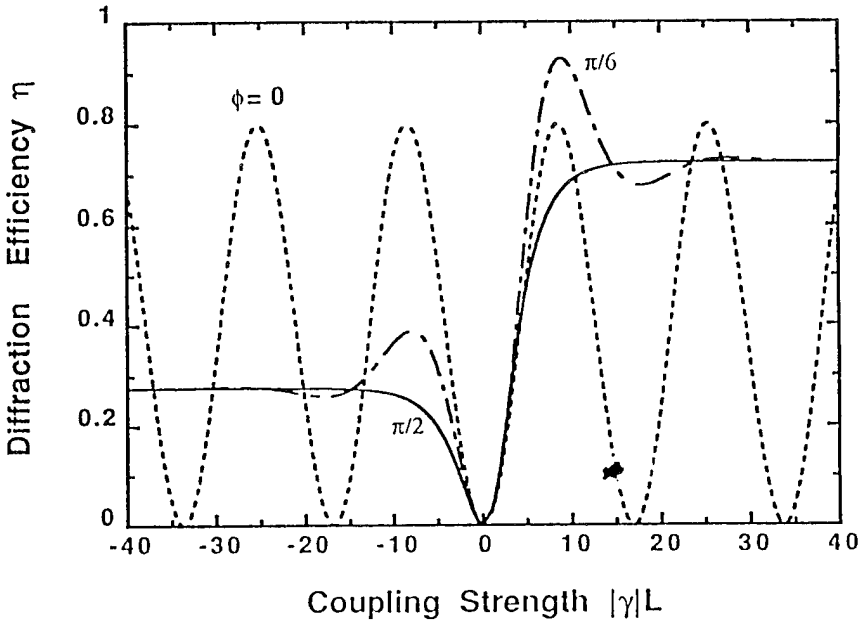

Fig. 15. Diffraction efficiency η as a function of coupling strength |γ|L for various values of spatial phase shift φ. The read beam is taken to be equal to the writing beams; i.e., $I_{AR}(0) = I_{AW}(0) = I_{BW}(0) = 1$.

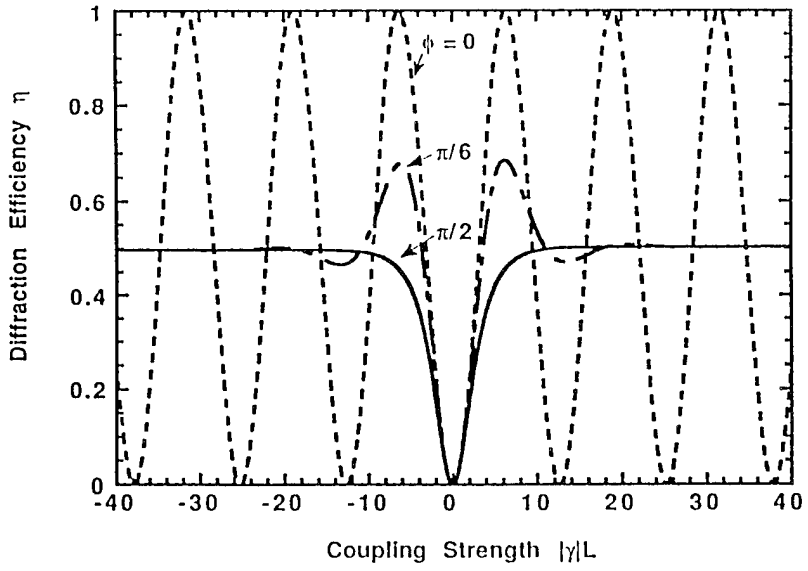

Fig. 16. Same as in Fig. 15, but for $I_{AR}(0) = 0.01$.

diffraction efficiency is now a symmetric function of coupling constant for all values of ϕ, and the oscillatory behavior for $\phi = 0$ reaches a peak value of unity, as expected from Eq. (26)—for the choice of parameters in this figure, the slant of the gratings is zero, leading to a Bragg matched readout with 100% maximum diffraction efficiency.

III. SUMMARY

Kogelnik's formula for diffraction efficiency of a volume phase grating is derived for Bragg matched readout. The differences between a photorefractive index grating and a thick phase grating of uniform amplitude and phase are outlined. For a weak read beam and polarization asymmetry during writing and readout, the diffraction efficiency of a photorefractive grating is independent of the read beam intensity; it is a function of grating thickness, coupling constants during writing and readout, and input intensity ratio of writing beams. For a strong read beam, the diffraction efficiency is a nonlinear function of the read beam intensity. The diffraction efficiency is also nonreciprocal with respect to readout from the two input ports. The nonlinear and nonreciprocal properties of diffraction efficiency are enhanced when the phase shift has a value lying between 0 and $\pi/2$.

ACKNOWLEDGEMENT

This research is supported in part by the U. S. Air Force Office of Scientific Research under contract F49620-92-C-0023.

REFERENCES

1. J.M. Heaton, P.A. Mills, E.G.S. Paige, L. Solymar and T. Wilson, *Optica Acta* **31**, 885 (1984).

2. P. Yeh, *IEEE J. Quant. Electron.* **QE- 25**, 484 (1989).

3. D.L. Staebler and J.J. Amodei, *J. Appl. Phys.* **43**, 1042 (1972).

4. H. Kogelnik, *Bell Syst. Tech. J.* **48**, 2909 (1969).

5. J. Hong and R. Saxena, *Opt. Lett.* **16**, 180 (1991).

6. R. Saxena, F. Vachss, I. McMichael and P. Yeh, *J. Opt. Soc. of Am.* B **7**, 1210 (1990).

7. N.A. Vaines, S.L. Chapman and R.W. Eason, *Appl. Opt.* **28**, 4381 (1989).

8. Claire Gu and Pochi Yeh, *J. Opt. Soc. of Am.* B **7**, 2339 (1990).

9. R. Saxena, C. Gu and P. Yeh, J. Opt. Soc. of Am. B **8**, 1047 (1991).

10. H. Kogelnik, *Laser Technology—November issue*, 68 (1967).

11. A. Yariv and R.A. Fisher, "Optical Phase Conjugation," ed., R.A. Fisher (Academic, New York, 1983), Chap. 1

12. N.V. Kukhtarev, V.B. Markov, S.G. Odulov, M.S. Soskin, and V.L. Vinetskii, *Ferroelectrics* **22**, 949 (1979).

13. B. Fischer, J.O. White, M. Cronin-Golomb, and A. Yariv, *Opt. Lett.* **11**, 239 (1986).

14. P. Yeh, *J. Opt. Soc. Am.* **B4**, 1382 (1987).

15. K.H. Ringhofer and L. Solymar, *Appl. Phys.* **B48**, 395 (1989); D.C. Jones and L. Solymar, *Appl. Phys.* **B50**, 355 (1990).